Dissertation

Submitted to the
Combined Faculties for the Natural Sciences and for
Mathematics of the Ruperto-Carola University of Heidelberg
for the degree of
Doctor of Natural Sciences

presented by

MSc Felix Oppel

Born in Berlin, Germany

Oral-examination: 02.10.2013

Clonal Dynamics and Phenotypic Plasticity within the Pancreatic Tumor Initiating Cell Compartment

Referees: Prof. Dr. Andreas Trumpp

Prof. Dr. Hanno Glimm

Summary

In pancreatic cancer and other solid tumor entities subpopulations of cancer stem cells (CSCs) or tumor initiating cells (TIC) have recently been identified. These cells were described to be tumorigenic in immunodeficient mice and give rise to the whole heterogeneity of the patient`s tumor. Besides those phenotypic markerspreviously associated with TIC function, little is known about pancreatic TIC. This thesis project unravels the clonal dynamics of long-term tumor growth in pancreatic cancer, and explores the phenotypic diversity within the pancreatic TIC population.

Primary patient tumor samples were xenografted in immunodeficient NOD.Cg-Prkdc^{scid}Il2rg^{tm1Wjl}/SzJ (NSG) mice to remove benign human cells and receive sufficient amounts of tissue. Adherent cultures were established from xenograft tumor tissue in serum-free medium simulated with growth factors. These culture conditions allowed the enrichment of pancreatic TIC without restriction to a certain phenotype. These cultures grew as three-dimensional epithelial colonies with tight cell-cell contacts, and reliably initiated tumors in NSG mice. In order to induce TIC differentiation, culture conditions were changed to 10% FBS containing medium and withdrawal of cytokines. Subsequently, the cells lost three-dimensional growth, formed monolayers and showed irregular morphology. This was accompanied by a down-regulation of markers previously described for pancreatic TIC, stem cells of various entities or normal pancreatic progenitors. However, despite this differentiation-like phenotype, tumor initiation in serial transplantation was not substantially affected. Moreover, sorted CD133^{-} cells formed equally efficient tumors as the CD133^{+} cell fraction and contained a similar proportion of CD133^{+} cells *in vivo*. In sum, these data indicate that pancreatic TIC are diverse with respect to marker expression, and exhibit an previously unknown phenotypic plasticity.

To determine the clonal kinetics of individual TIC *in* vivo early passage serum-free cultures from 3 patients were lentivirally marked and serially transplanted over 3 generations in NSG mice. In primary mice, 0.003-0.113% of all transduced cells were detected to contribute significantly to tumor formation. However, the second and third generation tumor formation was predominantly driven by distinct TIC clones that were not detected in earlier generations, but recruited later to participate in tumor

formation. Mathematical modeling indicated profound changes in the proliferation of individual TIC that produced mainly non-tumorigenic progeny with limited capacity of self-renewal. These data indicate that in pancreatic cancer long-term tumor growth is driven by the succession of transiently active TIC generating tumor tissue in temporally restricted bursts. The recruitment of inactive TIC clones to tumor formation after serial transplantation indicates a context-dependent switch between a quiescent and an active status.

A clonal relation between tumorassociated fibroblast-like cells and neoplastic cells has been described in breast cancer. To investigate whether pancreatic TIC also give rise to fibroblast-like cell types xenograft tumors were analyzed in detail for their stromal compartment. Xenograft tumors contained no human stroma and attracted murine fibroblast-like cells instead. Human stroma cells were only found in xenograft tumors when these were co-transplanted with tumor cells, but engrafted with very low efficacy. Thus, due to the instability of human stroma cells in xenograft tumors grown in NSG mice, a possible clonal relation between fibroblast-like cells and neoplastic cells could not be investigated conclusively.

In total, this study describes a previously unknown phenotypic and functional plasticity of pancreatic TIC. Its data show that TIC in pancreatic cancer have to be defined functionally level *in vivo* and that this cannot be replaced by the examination of phenotypic markers. Understanding the molecular mechanisms that regulate the activation and quiescence of pancreatic TIC might be important for future therapy approaches against pancreatic cancer.

Zusammenfassung

In den letzten Jahren wurden im Pankreaskarzinom und in anderen soliden Tumorarten Subpopulationen von Krebsstammzellen (CSCs) oder Tumor-initiierenden Zellen (TIC) identifiziert. Diese Zellen sind in der Lage in immundefizienten Mäusen Tumore zu bilden und können die gesamte Heterogenität des ursprünglichen Patiententumors hervorbringen. Außer phänotypischen Markern, die mit TIC Funktion assoziiert wurden, ist wenig über TIC im Pankreaskarzinom bekannt. In diesem Forschungsprojekt soll die klonale Dynamik der TIC untersucht werden, die das Tumorwachstum im Pankreaskarzinom langfristig unterhält, sowie die phänotypische Diversität innerhalb des TIC-Kompartiments.

Aus primärem Patientenmaterial wurden Xenograft-Tumore in immundefizienten NOD.Cg-Prkdc^{scid}Il2rg^{tm1Wjl}/SzJ (NSG) Mäusen initiiert. Durch diesen Prozess wurde das Gewebe expandiert und benigne menschliche Gewebearten entfernt. Aus dem Xenograft-Tumorgewebe wurden adhärente Zellkulturen mit Hilfe von serum-freien Kulturbedingungen und der Stimulation mit Wachstumsfaktoren etabliert, so dass TIC ohne Beschränkung auf einen bestimmten Phänotyp angereichert wurden. Diese Kulturen wuchsen als dreidimensionale epitheliale Kolonien mit dichten Zell-Zell-Kontakten und bildeten zuverlässig Tumore in NSG Mäusen. Um TIC zu differenzieren wurden den Zellen die Wachstumsfaktoren entzogen und die Kulturbedingungen auf 10% FBS-haltiges Medium umgestellt. Daraufhin verloren die Zellen ihr dreidimensionales Wachstum, wuchsen einzelschichtig und zeigten irreguläre Morphologie. Gleichzeitig wurden viele Marker-Proteine runterreguliert, die für Pankreas-TIC, Stammzellen verschiedener Entitäten oder normale Vorläuferzellen im Pankreas beschrieben sind. Trotz diesem differenzierungs-ähnlichen Phänotyp war das Tumor-initiierende Potential der Zellen in serieller Transplantation in NSG Mäusen nicht substantiell verändert. Weiterhin bildeten sortierte CD133$^-$ Tumorzellenfraktionen gleichermaßen Tumore in NSG Mäusen wie CD133$^+$ Kontrollzellen und regenerierten die CD133$^+$ Population *in vivo*. Insgesamt zeigen diese Daten, dass TIC im humanen Pankreaskarzinom diverse Phänotypen haben können und eine unerwartete phänotypische Plastizität aufweisen.

Um die klonale Dynamik einzelner TIC *in vivo* zu untersuchen wurden frühe Passagen serum-freier Kulturen von 3 Patienten lentiviral markiert und seriell über drei Generationen in NSG Mäuse transplantiert. In primären Mäusen trugen 0,003-0,113% aller transduzierten Zellen nachweislich zum Tumorwachstum bei. Die Bildung von sekundären und tertiären Tumoren wurde jedoch dann hauptsächlich von TIC-Klonen bestimmt, die in vorhergehenden Generationen nicht nachgewiesen werden konnten, aber später zum Tumorwachstum rekrutiert wurden. Mathematische Berechnungen zeigten hierbei starke Veränderungen der Proliferationsraten individueller TIC-Klone, die bei der Tumorbildung hauptsächlich nicht tumorigene Nachkommenzellen hervorbrachten. Diese Daten zeigen, dass im Pankreaskarzinom das langfristige Tumorwachstum durch die Abfolge kurzzeitig aktiver TIC-Klone unterhalten wird, die neues Tumorgewebe in temporären Impulsen hervorbringen. Die Rekrutierung inaktiver TIC-Klone nach serieller Transplantation weist auf einen vom Umfeld abhängigen Wechsel zwischen aktivem und inaktivem Status hin.

Beim humanen Brustkrebs wurde gezeigt, dass Tumor-assoziierte Fibroblasten-ähnliche Zellen von Krebszellen gebildet werden können. Um zu untersuchen, ob dies auch im Pankreaskarzinom passiert, wurde das Stroma-Kompartiment der Xenograft-Tumore detailliert untersucht. In Xenograft-Tumoren konnte kein humanes Stroma nachgewiesen werden. Stattdessen wanderten murine Fibroblasten-ähnliche Zellen in die Tumore ein und bildeten eine desmoplastische Reaktion. Humane Stromazellen wurden nur nach Kotransplantation nachgewiesen, jedoch fügten sich nur mit sehr geringer Frequenz in die Xenograft-Tumore ein. Daher scheinen humane Stromazellen in Xenograft-Tumoren so instabil zu sein, dass eine klonale Verbindung zum neoplastischen Kompartiment in diesem Model nicht nachweisbar ist.

Insgesamt zeigt diese Studie, dass TIC im Pankreaskarzinom eine unerwartete phänotypische und funktionelle Plastizität haben. Die Daten zeigen, dass in dieser Tumorentität TIC durch ihre Funktion in Mäusen Tumore zu bilden definiert werden müssen und nicht durch die Expression phänotypischer Marker. Die molekularen Mechanismen, welche die Aktivität und Ruhe von TIC im Pankreaskarzinom regulieren, könnten für die Entwicklung neuer Therapien von Bedeutung sein.

Table of Contents

List of Figures

List of Tables

List of Abbreviations

ALDH	Aldehyde dehydrogenase
AML	Acute myeloid leukemia
AmpR	Ampicillin resistance
APC	Allophycocyanine
APC-H7	Allophycocyanine-H7
ATP	Adenosine-5'-triphosphate
bio	Biotinylated
BSA	Bovine serum albumin
CD	Cluster of differentiation
CML	Chronic myeloid leukemia
CMV	Cytomegalovirus
CSC	Cancer stem cell
CXCR	C-X-C chemokine receptor
DMSO	Dimethylsulfoxide
DNA	Desoxyribonucleic acid
dNTPs	Deoxynucleosidetriphosphates
ds	Double stranded
ECM	Extracellular matrix
EGF	Epidermal growth factor
emPCR	Emulsion-based clonal amplification PCR
EMT	Epithelial-to-mesenchymal transition
env	Envelope
FACS	Fluorescence activated cell sorting
FGF	Fibroblast growth factor
FLC	Fibroblast-like cell
GTP	Guanosine-5'-triphosphate
GDP	Guanosine-5'-diphosphate
HBSS	Hank`s balanced salt solution
HGF	Hepatocyte growth factor
HIV	Human immunodeficiency virus

HSC	Hematopoietic stem cell
HT	High-throughput
IGF	Insulin-like growth factor
IgG	Immunoglobulin G
LAM	Linear amplification mediated
LC	Linker cassette
LT	Long-term
LTR	Long terminal repeat
LT-TIC	Long-term tumor-initiating cell(s)
LV	Lentivirus
MID	Multiplex identifier
MMP	Matrix methalloproteinase
MOI	Multiplicity of infection
MPC	Multipotent progenitor cell
NOD	Non-obese diabetic
NSC	Neural stem cell
NSG	NOD.Cg-Prkdc^{scid}Il2rg^{tm1Wjl}/SzJ
PBS	Phosphate buffered saline
PCR	Polymerase chain reaction
PDAC	Pancreatic ductal adenocarcinoma
PDGF	Platelet-derived growth factor
PE	Phycoerythrine
PEI	Polyethylenimine
PGK	Phosphoglycerate kinase
PTC	Pancreatic tumor colony
RNA	Ribonucleic acid
RSV	Rous sarcoma virus
RT	Room temperature
SCID	Severe combined immunodeficiency
SDF1	Stromal derived factor 1
SIN	Self-inactivating
ss	Single stranded

SSC	Side scatter
TIC	Tumor-initiating cell(s)
TIMPs	Tissue inhibitors of metalloproteinases
TNFα	Tumor necrosis factor alpha
T-TAC	Transiently amplifying cell(s)
VSV-G	Vesicular stromatitis virus glycoprotein
αSMA	Alpha smooth muscle actin

1. Introduction

1.1 The Pancreas

1.1.1 Structure

The pancreas is an organ required for digestion and sugar metabolism in vertebrates and is divided into the exocrine and the endocrine pancreas (figure 1).

The endocrine part of the pancreas produces hormones and disseminates them into the blood stream. It comprises of four main cell types organized in clusters called Islets of Langerhans. Alpha-cells secrete glucagon, beta-cells secrete insulin, gamma-cells secrete pancreatic polypeptide and delta-cells secrete somatostatin into the blood stream. Insulin and glucagon are partners in regulating the blood glucose level. Whereas glucagon stimulates the release of glucose into the bloodstream, insulin triggers the uptake of glucose into liver, skeletal muscle and fat tissue.

The exocrine pancreas produces digestive enzymes and secretes them into the duodenum. The development and regenerative maintenance of the exocrine pancreas is a complex interplay of different cell types within regulated by the specific activity or silence of signaling pathways and soluble factors (reviewed by [1]).The production of enzymes like amylase (AMY2A), lipase (PNLIP) and trypsin (PRSS1-3) is executed by the acinar cells which form the acinar glands [1]. The acinar-specific expression of these enzymes is regulated by the transcription factor Ptf1a [2, 3].

The duct epithelium is responsible for the transportation of the digestive enzyme solution. It secretes a bicarbonate-rich fluid which dilutes and pH-buffers the acinar secretion and builds up the ductal tree, a channel network leading from small structures at the acinar glands (terminal ducts) over structures with increasing diameter (intra- and interlobular ducts) to the pancreatic main, duct which leads into the intestine. Markers of duct cells are Cytokeratin 7 (Krt7), Krt19, EpCam, Mucin 1 (MUC1) and carbonic anhydrase II (CA2) (reviewed by [4]).

The third cell type within the exocrine pancreas includes centroacinar cells residing at the border between the terminal ducts and the acinar glands. Centroacinar cells also differ from acinar and duct cells regarding their morphology. These cells have a small

main diameter of 10µm and have cytoplasmic protrusions connecting them to adjacent centroacinar, acinar and islet cells [5, 6]. The developmental origin of these cells remains unknown and the cellular heterogeneity within the centroacinar cell compartment is poorly understood [1].

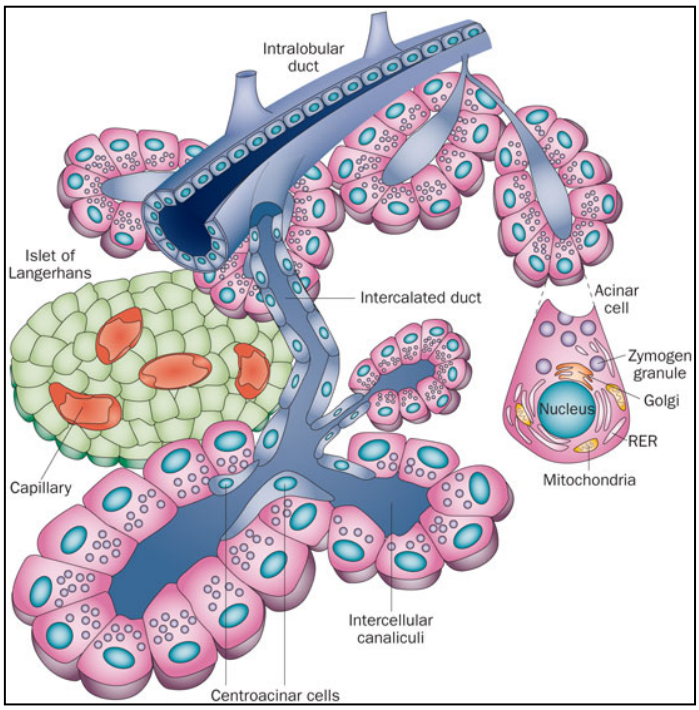

Figure 1: Cellular structure of the pancreas. The exocrine part of the pancreas secretes digestive enzymes into the duodenum, whereas the endocrine part supplies hormones into the blood stream. The exocrine part of the pancreas is composed of acinar glands that produce and secrete digestive enzymes and the ducts that pH-buffer and transport the enzyme mix to the gut. The endocrine part is organized as the Islets of Langerhans that are mainly composed of α-, β-, γ- and δ-cells. Figure modified from reference [7].

1.1.2 Development

During mammalian endoderm development, the pancreas forms from the dorsal and ventral pancreatic buds growing out from the duodenum. The growth of the emerging exocrine pancreas is supported by of soluble factors secreted by the adjacent mesenchyme (reviewed by [1, 8, 9]). Without that stimulation, pancreatic multipotent progenitor cells (MPCs) follow the endocrine lineage and fail to yield exocrine acini [10]. FGF2, FGF7 and FGF10 promote pancreatic development and differentiation towards the exocrine lineage [11-13]. FGF10 activates Notch signaling in epithelial cells thereby promoting a population of undifferentiated MPCs that give rise to the

developing duct epithelium [13-15]. Within the exocrine lineage, the choice between ductal and acinar differentiation can be regulated by retinoids. 9-*cis* retinoic acid (9cRA) induces ductal differentiation by promoting laminin-1 expression in the mesenchyme [16]. By contrast, acinar differentiation of pancreatic MPCs can be induced by all-trans retinoic acid (atRA) [16-18].

At day 11.5 of embryonic pancreas development (E11.5), all MPCs commonly share the set of transcription factors Hnf1β, Hes1, Nkx6.1, Nkx6.2, Pdx1, Ptf1a, and Sox9 [19-23]. The first spatial discrimination of populations restricted to ductal, acinar or endocrine lineages arises at E12.5, when the pancreatic bud splits into trunks and tips. Besides Pdx1 and Sox9, which are expressed in both regions, the trunks are characterized by ongoing Hnf1β, Nkx6.1, Nkx6.2 and acquired Hnf6 expression and active Notch signaling [23-25]. From E13.5 on, trunk progenitor cells give rise to endocrine and duct cells. Inactivation of Notch signaling thereby promotes endocrine fate, whereas prolonged Notch activity induces ductal differentiation. In contrast, acinar cells are generated by progenitors located in the tips which display inactive Notch signaling [21, 26, 27]. Acinar differentiation becomes fixed from E13.5 on, by the expression of Ptf1a, Rbpjl, Mist1 and Nr5a2 [28-32].

1.1.3 Regeneration

Centroacinar cells were discussed to be a possible multipotent progenitor cell (MPC) population in pancreatic regeneration. This was due to the expression of genes involved in pancreatic development including Notch and its target gene Hes1, Sox9 and ALDH1 enzyme [6, 21, 33, 34]. On the functional level it has been demonstrated that centroacinar cells strongly proliferate following partial pancreas resection or chemically induced damage and can be converted rapidly into acinar cells upon artificial disruption of Notch signaling [35]. However, without extrinsic intervention centroacinar cells normally do not function as MPCs in the adult uninjured pancreas and do not give rise to acinar or β-cells [21].

Observation has shown that regeneration in the exocrine pancreas in response to tissue damage was performed by surviving acinar cells that transiently

dedifferentiate. In this process, these cells lose their mature acinar cell markers like digestive enzymes or Ptf1a, and express factors involved in pancreatic development such as Sox9, Pdx1 and the Notch target Hes1 [36]. Besides Notch, Wnt-signaling becomes activated, and the cells transiently acquire the ability to give rise to new acinar tissue [37, 38]. In that state, the cells resemble morphologically the duct epithelium, so that this process has been termed acinar to ductal metaplasia (AMD). After closure of the lesion, the cells regain their acinar differentiation and execute a specialized function in the adult organ. In summary, these data indicate that in the pancreas transient progenitors are made upon damage. Thus, regeneration of the adult pancreas appears different from what is described for other organs which have a permanent, hierarchically organized adult stem cell compartment like the colon epithelium [39-43], the brain [44-46] or the blood system [47-50].

1.2 Pancreatic Cancer

The most common type of pancreatic cancer is the pancreatic ductal adeno-carcinoma (PDAC), representing about 95% of all diagnosed tumors in the pancreas. This type of cancer arises from the exocrine pancreas and is characterized by pseudo-glandular structures formed by the tumor cells.

1.2.1 Epidemiology

PDAC is a highly malignant disease. According to the Robert-Koch-Institute in Hamburg, in 2008 PDAC represented the 9th leading cause of new incidences of male cancer and the 7th leading cause for women in Germany (www.krebsdaten.de). In Germany and the United States, it represents the fourth leading cause of cancer related death (www.rki.de, [51]).

PDAC is characterized by high metastatic activity to the liver, lung, lymph nodes, and the peritoneum. Standard therapy approaches involve surgery, chemotherapy and radiation. The most common therapeutic agents used to treat PDAC in clinics are gemcitabine and erlotinib, which have been described to be most effective in

combination [52]. However, such treatment cannot prevent the poor prognosis with a 5-year survival rate remaining below 10%. Since symptoms of pancreatic cancer are unspecific, the disease is often diagnosed at advanced stage, so that most patients die within one year after diagnosis (www.krebsdaten.de, [51, 53-57]).

1.2.2 Molecular Pathology of Pancreatic Cancer

1.2.2.1 Common Genetic Alterations

The most frequent oncogene in pancreatic cancer is mutant KRAS, which is mutated in about 95% of all patients [58-65]. KRAS encodes a member of the Ras GTPase family and acts in many signaling pathways, affecting cell proliferation, survival, cytoskeleton dynamics and motility. Normal Kras protein can switch between an activated and an inactivated status. Active Kras is bound to GTP and executes its signaling function. Upon hydrolysis of GTP to GDP triggered by GTPase-activating-proteins (GAPs), Kras activity is shut off. In pancreatic cancer, the mutant KRAS oncogene has an inoperative GTPase domain resulting in constantly active signaling [66, 67]. So far, no effective treatment strategy has been developed to inhibit mutant Kras protein. Kras signaling enhances endogenous expression of the epidermal growth factor receptor (EGFR) and it has been shown that inhibition of this receptor diminishes KRAS-mediated pancreatic tumorigenesis [68]. Jones et al. revealed by global genome analyses that besides KRAS mutation the signaling pathways Wnt, Notch, Hedgehog, TGF-β and JNK are affected frequently by genetic alterations driving PDAC malignancy [69]. Mutations also change cellular processes like apoptosis, invasion, cell adhesion, cell division or DNA damage control [69, 70]. Moreover, inactivating or deleting mutations of the tumor suppressors TP53, p16/CDKN2A and SMAD4 were detected in the majority of patients [65].

1.2.2.2 Tumor Initiation and Genetic Evolution

The primary event for PDAC initiation is the mutation of KRAS producing a constantly active form of that molecule. Experimental mouse models have shown that under

constantly active Kras signaling, damage induced acinar-to-ductal-metaplasia (ADM) develops to a precursor lesion of PDAC called pancreatic intraepithelial neoplasm (PanIN) [71-75] from fully differentiated acinar cells. This process is accelerated by chronic pancreatitis [72] which has been proposed as a risk factor for pancreatic cancer formation [76-78]. In a genetically engineered *in vivo* model of pancreatic carcinogenesis using a mouse strain expressing mutant Kras, researchers demonstrated that ADM prior to PanIN formation differs from the AMD process during acinar cell dedifferentiation in normal exocrine pancreas regeneration [37]. In carcinogenesis, the ADM is persistent and not transient as in the normal situation (see section 1.1.2.3). In both cases, acinar markers are down-regulated, cells acquire a duct-like appearance and activate factors involved in pancreatic development [36-38]. The expression of the pancreatic development gene, Sox9, has recently been proposed as a particular driver of acinar-derived PanIN formation [22]. However, in contrast to regeneration, where wnt-signaling is required, in carcinogenesis β-catenin signaling inhibits ADM and is shut off during this process (figure 2) [37].

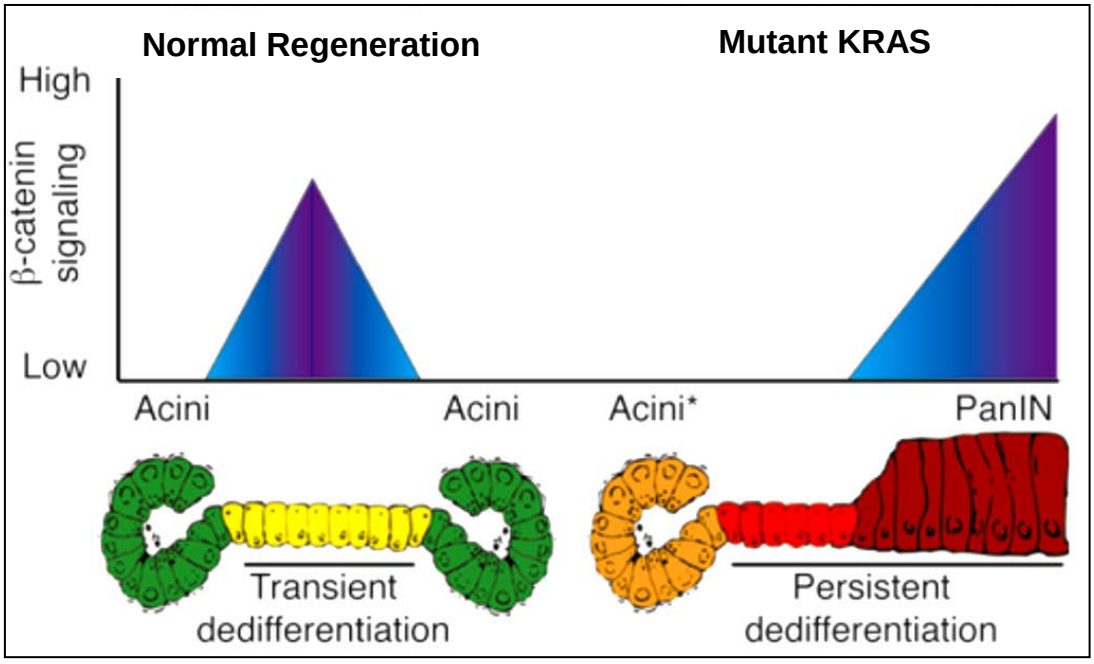

Figure 2: Wnt-signaling in normal acinar regeneration and mutant KRAS induced PanIN formation. Transient acinar dedifferentiation in normal regeneration is supported by canonical wnt-signaling. After closure of the lesion cells regain acinar differentiation and wnt-signaling stops. In contrast, active β-catenin inhibits mutant KRAS induced persistent dedifferentiation and is turned on after PanIN formation. Figure modified from [37].

Based on their degree of architectural and cellular abnormality, PanIN precursor lesions are categorized according to three sequential stadia called PanIN-1, PanIN-2 and PanIN-3. After Kras mediated PanIN-1 formation, PanIN-2 was described to develop upon additional mutational loss of p16/CDKN2A function. In later PanIN-3 structures, additional hits in TP53, SMAD4 and BRCA2 tumor suppressor genes are frequently found (figure 3; reviewed by [79], [61]). Genetic progression from PanIN precursor lesions to malignant metastatic cancer was examined by Yachida et al. [80], who compared the mutations of primary tumors and metastases of 7 patients subjected to warm autopsy. Here, the whole mutational heterogeneity of the metastases was also found within the primary tumor. So, metastases were initiated by tumor cell clones that genetically evolved from the parental non-metastatic clone. Moreover, the time frame of PDAC progression from the initial mutation to the metastatic disease was estimated to exceed 10 years and to be therefore comparable to other kinds of solid tumors.

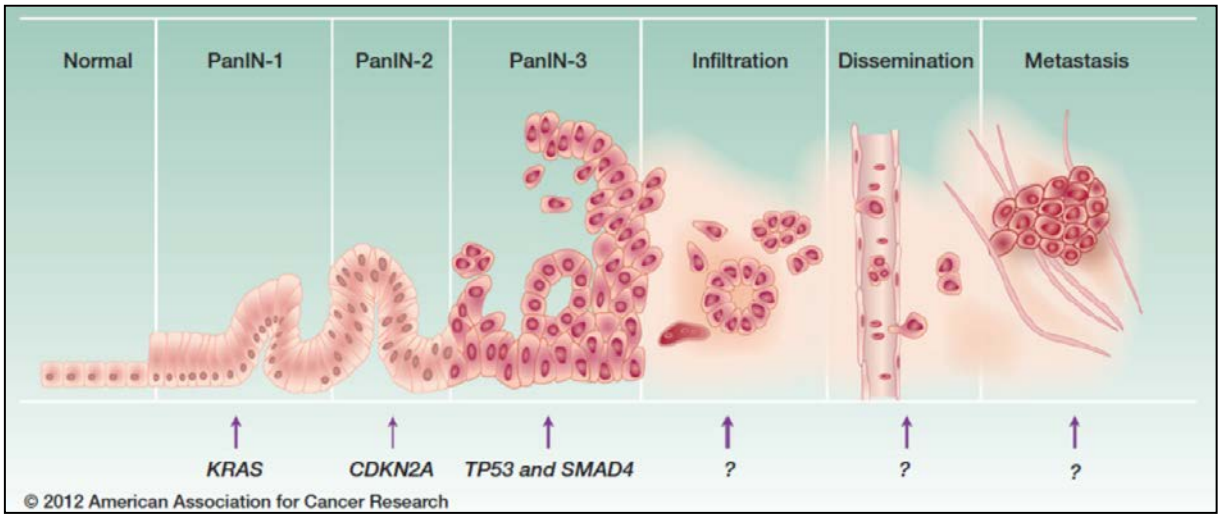

Figure 3: Model of pancreatic cancer progression by sequential gain of mutations. Normal cell gain a mutational constant activation of KRAS oncogene and form an initial pancreatic intraepithelial neoplasm (PanIN-1), the earliest precursor lesion of pancreatic ductal adenocarcinoma (PDAC). An additional mutation in p16/CDKN2A tumor suppressor gene leads to PanIN-2 formation, whereas later acquired mutational inactivation of tumor suppressors TP53 and SMAD4 induces PanIN-3 formation. The genetic progression following PanIN-3 to metastatic PDAC is to date not finally understood. Figure modified from reference [61].

1.2.3 The Role of Tumor-associated Stroma in Pancreatic Cancer

Pancreatic cancer growth and progression is characterized by the formation of intense desmoplatic reaction surrounding islands of neoplastic cells [81-83]. This so-called stroma mainly consists of extracellular matrix (ECM) components and tumor-associated fibroblast-like cells (FLCs) that express mesenchymal markers like vimentin and α-smooth-muscle actin (αSMA). In literature, stromal FLCs are described as fibroblasts, myofibroblasts or pancreatic stellate cells [84-86]. FLCs enhance the tumorigenic potential of pancreatic cancer cells in co-xeno-transplantation experiments [87]. Tumor cells and FLCs stimulate one another by secreting signaling molecules, which enhances the proliferation of both cell compartments and facilitates cancer invasion (figure 4) [88-99]. Factors that stimulate stromal FLCs are mainly secreted by cancer cells and immune cells invading the tumor. The best described factors are platelet-derived growth factor (PDGF), sonic hedgehog (Shh), transforming growth factor β (TGFβ), and tumor necrosis factor α (TNFα). These factors also stimulate the stromal fibroblast-like cells to proliferate and produce extracellular matrix (ECM) components and ECM modulatory factors like matrix metallo proteinases (MMPs) and their inhibitors (TIMPs). That leads to an ECM remodeling and facilitates tumor cell invasion. Moreover, stromal FLCs secrete stromal derived factor 1 (SDF1), insulin-like growth factor 1 (IGF1) and hepatocyte growth factor (HGF). These promote tumor cell proliferation, survival and motility. Fujita *et al.* [100] described that stromal FLCs activate Notch signaling in pancreatic tumor cells by direct cell-cell contacts *in vitro*.

The clonal origin of the pancreatic-cancer-associated stroma is still poorly understood. Existing studies propose a tumor independent mesenchymal origin [100-102]. Epithelial-to-mesenchymal transition (EMT) is another potential source for carcinoma-associated fibroblasts-like cell types in pancreatic cancer and other human neoplasms [100, 103-106]. However, so far the production of non-tumorigenic FLC types by EMT of solid tumor cells has only been described for breast cancer [104]. Even though EMT frequently occurs in PC migration and invasion [107, 108], it remains unclear whether pancreatic carcinoma cells can produce their own stroma by EMT.

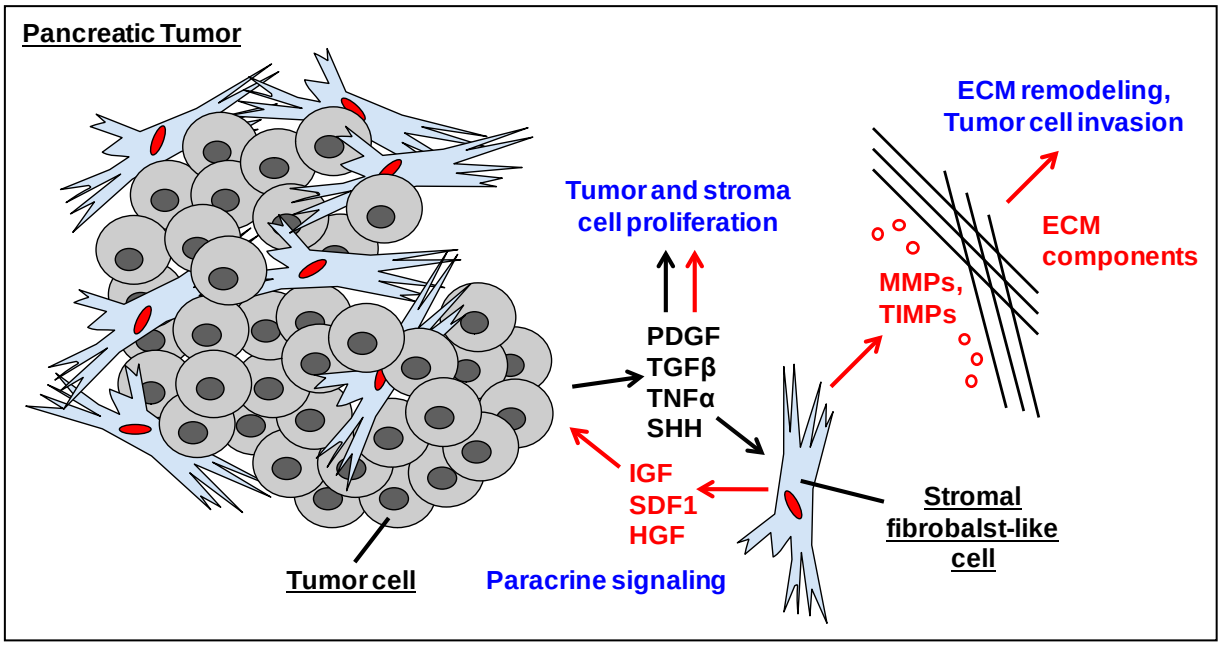

Figure 4: Interactions between tumor and stroma cells facilitate pancreatic cancer progression. Tumor cells and stromal fibroblast-like cell types (FLCs) stimulate each other by paracrine signaling which leads to enhanced proliferation in both compartments. Factors secreted by tumor cells (black) stimulate the secretion of extracellular matrix (ECM) components, matrix remodeling enzymes like matrix-metalloproteases and their inhibitors (TIMPs) by FLCs. Matrix remodeling supports tumor cell invasion and metastasis formation.

1.3 Tumor-Initiating Cells

In recent decades cancer researchers have increasingly focused on the functional heterogeneity of neoplastic cells within a tumor and its metastases. In that regard, subpopulations of tumor initiating cells (TIC), also referred as cancer stem cells (CSCs), have attracted attention. As a tool investigate human tumor cells *in vivo*, researchers made use of highly immunodeficient mice developed by genomic engineering. TIC are defined by their ability to form tumors upon transplantation into immunodeficient and to give rise to the whole heterogeneity of the original patient`s tumor, whereas bulk tumor cells are non-tumorigenic [109-112]. Within that, the capacity of xenograft tumor cells to initiate tumors in serial transplantation became the “gold standard” to prove their potential to maintain long-term tumor growth. However, single cell based assays or clonal marking are required to define the long-term self-renewing potential of individual TIC, as recently used to describe a subpopulation of long-term TIC (LT-TIC) in human colon cancer [113].

The “hierarchical model” of long-term tumor growth claims that self-renewing TIC give rise to tumorigenic cells with abolished self-renewing and limited proliferation capacity which then turn into non-tumorigenic bulk tumor cells (figure 5, reviewed by [48], [114] and [115]). By contrast with the hierarchical model, the “stochastic model” considers each tumor cell as equipotent. In that model, functional heterogeneity is not caused by functional differentiation of an individual TIC clone`s progeny, but rather exclusively by genetic/epigenetic differences between single tumor cell clones induced by genetic evolution, and the sequence of random variations in the cell division interval determining by chance the dominance of the one clone and the regression of the other (figure 5) [115-120]. Both concepts remain controversially discussed.

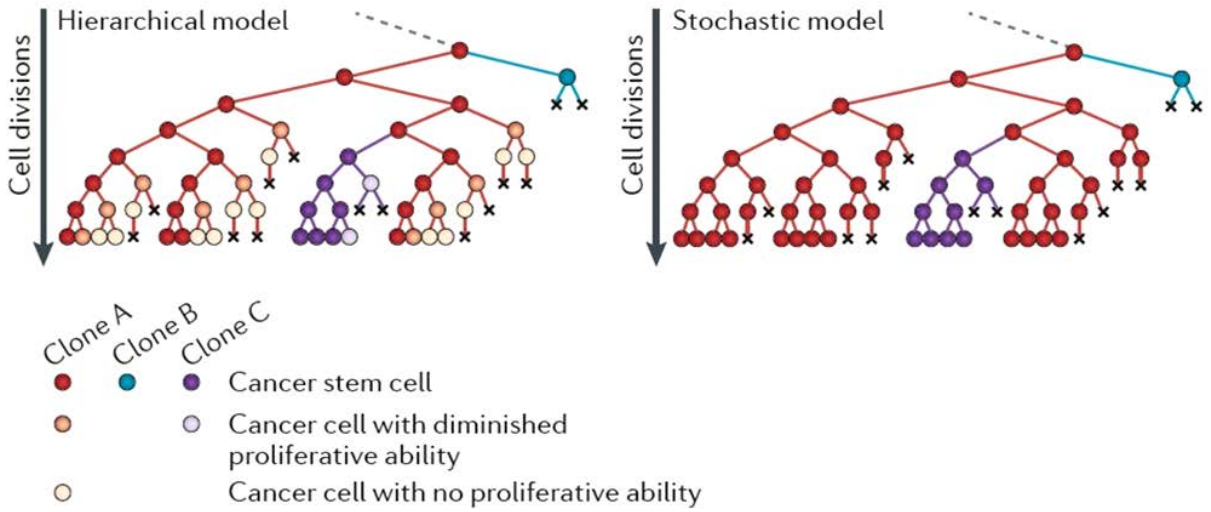

Figure 5: The hierarchical and the stochastic model of cancer stem cells (CSCs). In the hierarchical model self-renewing CSCs give rise to non-self-renewing cells with limited proliferation capacity that subsequently turn into bulk tumor cell showing no proliferation. Thereby, heterogeneity is derived from the functional differentiation of self-renewing CSCs. In contrast, the stochastic model considers all tumor cells as equally tumorigenic, where the dominance of one clone over the other arises from random intrinsic and extrinsic determinants. However, in both models the genetic and epigenetic differences between individual CSCs can cause the positive or negative selection of clones. Figure modified from reference [115].

1.3.1 Tumor Initiating Cells and Stem Cells Share Functional Characteristics

Very early, in 1907, a connection between cancer and stem cells was initially postulated when similarities in pathology were observed between embryonic and cancerous tissue [121]. Later, in the 1960s to 1980s researchers found evidence for stem cells in teratomas, and proposed cancer growth as a caricature of the healthy tissue development where malignant cells differentiated into non-tumorigenic or benign bulk tumor cells [122-126]. Later, the TIC compartment in human leukemia and colon cancer was found to be hierarchically organized from self-renewing long-term TIC to non-self-renewing, short-term tumorigenic, transiently amplifying cells (T-TAC), that thereby reflected the clonal dynamics of their healthy organs regeneration [109, 111, 113, 127-130]. For colon cancer, this finding was supported by the observation that the architecture of the cancerous tissue in well differentiated tumors reflected the normal colon epithelium [43]. Here, an intestinal stem cell-like population was found at the bottom of the irregular crypts of colorectal tumors.

1.3.2 Identification of Tumor Initiating Cells

Due to the presumed connection between TIC function and an undifferentiated cell status, surface markers of normal stem cells were investigated for the possibility that they might also mark malignant “stem cells”. CD133, a marker of normal adult neuroglial [46], hematopoietic [131, 132], prostate epithelium [133] and skeletal muscle [134] stem cells was examined by fluorescence-activated cell sorting (FACS) and subsequent transplantation of negative and positive fractions from primary patient tumor material into immunodeficient mice. With these experiments $CD133^{+}$ TIC were described for example in malignant gliomas [135, 136], colon cancer [137] or Ewing´s sarcoma [138]. Further, Al-Hajj and colleagues provided initial evidence of a $CD44^{+}/CD24^{-/low}/lineage^{-}$ subpopulation highly enriched for TIC in human breast cancer [139]. However, drawbacks regarding the potential use of TIC markers in clinics were found through the later identification of CD133-negative TIC in gliomas [140] and colon cancer [141]. Thus, to date TIC surface markers remain controversial in the field of cancer research.

Subpopulations of TIC for pancreatic ductal adenocarcinoma (PDAC) have also been described. Also in this tumor entity defined markers were postulated to associate with *in vivo* tumorigenicity (table 1; recently reviewed by [142]). In 2007, Li et al. identified CD44/CD24/EpCam triple-positive TIC from primary patient-derived PDAC tissue which represented 0.2-0.8% of the purified tumor cells and gave rise to tumors in immunodeficient mice with a much higher frequency than the vast majority of triple-negative cells [143]. Additionally, using patient-derived tumor tissue, Hermann et al. postulated in 2007 a subpopulation of $CD133^+$ pancreatic TIC comprising less than 3% of the purified cells, and showed tumor-initiating potential in immunodeficient mice upon transplantation of $5x10^2$ cells compared to 10^6 $CD133^-$ cells that were not tumorigenic [144]. The $CD133^+$ population was further subdivided into two subpopulations based on the expression of the chemotaxis and SDF1 receptor CXCR4. Only $CXCR4^+$ cells formed metastases, and the authors claimed that $CXCR4^-$ cells could not transfer into $CXCR4^+$ cells. The $CD133^+$ population was also described as more resistant to gemcitabine treatment than $CD133^-$ cells. In a later study, the authors described the Nodal/Activin pathway as a regulator of pancreatic TIC self-renewal [145].

Besides phenotypic surface markers, functional characteristics of normal stem cells like aldehyde dehydrogenase (ALDH) expression have also been associated with TIC function in various malignancies [146-148]. ALDH superfamily members were hypothesized to play a role for stem cell function in tissue repair and development based on their ability to oxidize retinaldehyde to retinoic acids which influence the lineage decision of undifferentiated cells (reviewed by [149]). For example, inhibition of ALDH function was shown to delay the differentiation of hematopoietic stem cells (HSCs) by diminished retinoic acid production [150, 151]. ALDH activity was described to mark undifferentiated cell populations displaying stem or progenitor cell potential in the blood system [152], skeletal muscle [153, 154], mammary epithelium [146] or prostate epithelium [155]. Also in pancreatic cancer $ALDH^+$ cells were described to be highly tumorigenic compared to $ALDH^-$ cells, to have a higher resistance to gemcitabine and to be more invasive [147, 148].

Another connection between TIC and an undifferentiated cell status involved the concept of “migrating cancer stem cells” [156]. Here, the expression of markers

characteristic of the process of epithelial-to-mesenchymal transition (EMT) was correlated with the expression of stem cell associated genes. EMT has been observed to facilitate cancer progression and metastasis as a functional pro-migratory cellular program [157-160]. In particular, Wellner et al. showed that the EMT inducer Zeb1 promotes the tumor-initiating potential of pancreatic and colon cancer cells [161]. Their results indicated that Zeb1 represses the microRNA200 family, which induces epithelial differentiation by repressing stem cell associated factors like Sox2 and Klf4. Together with Oct4 and c-myc, Sox2 and Klf4 have been described to reprogram fully differentiated cells into a pluripotent status ([162]; recently reviewed by Adachi and Schöler, [163]).

Long-term self-renewing TIC were also associated with the formation of distant metastases [113, 156]. The receptor tyrosine family member c-Met was identified to enhance growth and invasion in pancreatic cancer [164-166]. In xenograft tumors established from primary human pancreatic cancer tissue, researchers found that c-Met marks a highly tumorigenic TIC population [167]. Those cells, which co-expressed CD44 representing 0.5%-5% of all tumor cells, were shown to have the highest TIC potential. Administration of the c-Met inhibitor XL184 retarded tumor growth and prevented metastasis formation *in vivo*. Thus, the authors proposed the HGF/c-Met pathway as a suitable therapy target for pancreatic cancer.

Table 1: Phenotypes and properties of described TIC populations in pancreatic cancer.

Study	Phenotype	Properties
Li et al., 2007, [143]	CD44+/CD24+/EpCam+	Increased Sonic Hedgehog expression
Herman et al., 2007, [144]	CD133+	Chemoresistant, CD133+CXCR4+ respocible for metastasis
Rasheed et al., 2010, [148]	ALDH+	TIC associated with overall survival; TIC exhibit mesenhymal features and are frequently found in metastatic lesions
Li et al., 2011, [167]	CD44+/c-Met+	Highly metastatic

Table modified from reference [142].

1.4 High-Sensitive LAM-PCR for Clonal Tracking *in Vivo*

Linear amplification-mediated polymerase chain reaction (LAM-PCR) is a method to analyze the genomic integration sites (IS) of viral vectors in mammalian cells and to use such integration sites as clonal mark to identify the progeny of individual cells in highly polyclonal samples [168]. LAM-PCR is highly sensitive with a resolution of a single DNA copy in 1µg of genomic DNA [169].

In this thesis project LAM-PCR was used to track the clonal dynamics of pancreatic tumor initiating cells (TIC) that were stably marked by transduction with lentiviral vector particles originating from the human immunodeficiency virus (HIV) [170, 171]. By comparison to other systems, lentiviral vectors have the advantage of efficiently marking cells in the G_1/G_0 phase of the cell cycle, thereby marking non-dividing cells [171-173]. The integration of lentiviral vectors into the genome occurs in a semi-random manner. This means that vectors prefer certain regions of the genome, whereas the exact site of integration remains random. Thus, the sequence of the genomic DNA flanking the lentiviral long terminal repeats (LTRs) is different for each integration event, so that individual cell clones harbor unique genomic marks after transduction.

By LAM-PCR procedure [168] a linear amplification of the genomic DNA flanking the viral LTR is mediated by PCR-primers annealing in the known LTR sequence. The linear PCR product is subsequently transferred to a double stranded DNA, so that it can be subjected to a restriction digest. Since the sequence of the DNA is random, for each cell clone a different fragment length is created by digestion. These fragments can be visualized in a gel electrophoresis (figure 6). Moreover, since two clones can randomly have a similar fragment size, high-throughput sequencing is applied to identify the exact vector-genome junction and thereby the specific clone.

Using this method in a serial xenograft-tumor transplantation line employing lentivirally marked primary human colon cancer cells, our group has recently discovered that the colon cancer TIC compartment is hierarchically organized [113].

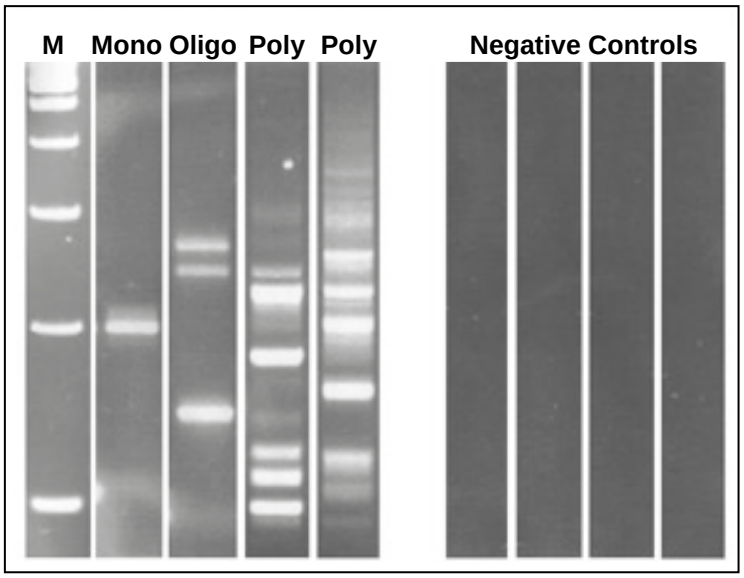

Figure 6: Linear amplification mediated PCR (LAM-PCR) allows detection of genomic viral integration sites (IS). IS of individual cell virally marked clones can be identified from mono-, oligo- and polyclonal samples as DNA fragments of clone specific size in gel electrophoresis. Figure modified from reference [168].

1.5 Thesis objectives

New therapeutic approaches are urgently needed to treat pancreatic cancer. Besides information on certain markers that were postulated to mark functional TIC populations, little is known about the clonal dynamics within the pancreatic TIC compartment. To understand the long-term tumor growth in pancreatic cancer on a clonal level might be important for the development of future therapy approaches specifically targeting the TIC population.

Thus, the clonal composition of the pancreatic TIC compartment was analyzed to see if it is homogenously organized, or if subpopulations of TIC differ in their ability to maintain long-term tumor growth. This investigation was performed by serial transplantation of lentivirally marked cultured TIC in immunodeficient mice and subsequent highly-sensitive LAM-PCR. Using the same method, Dieter et al. [113] recently described the hierarchical organization of the human colon cancer TIC compartment. Thereby, this thesis was also meant to draw conclusions about similarities and differences between the clonal dynamics maintaining long-term tumor growth in distinct solid tumor entities.

Aberrant cellular differentiation has been implicated in cancer biology. Pancreatic TIC were described to be enriched in populations displaying phenotypic similarities to normal adult stem cell populations [144]. The differentiation potential pancreatic TIC, however, has so far only been investigated on a phenotypic level *in vitro*, but not yet on a functional level *in vivo*. In this thesis, previously described differentiating culture conditions and xenotransplantation experiments were used to simultaneously monitor TIC differentiation both on a phenotypic and a functional level. By this method was examined whether pancreatic TIC can be functionally differentiated by such treatment and whether TIC function is predictable by the expression of phenotypic markers. The focus of this part of the project was to find out how phenotypically diverse or even plastic pancreatic TIC are.

The desmoplastic reaction in pancreatic cancer which is mainly composed of tumor-associated fibroblast-like cells was described to influence the biology of the neoplastic compartment and support tumor progression. This work thirdly aimed to unravel a possible clonal relation between tumor-associated fibroblasts and the

neoplastic cell as previously shown for breast cancer. For this reason, the stroma compartment of xenograft tumors grown in NSG mice was characterized in detail using dissociated cells and outgrowth cultures.

This study was designed to obtain information about the phenotypic and functional heterogeneity of pancreatic TIC. This information will be important for the development of future therapeutic approaches targeting this malignancy. Controlling TIC activity and self-renewal might lead to the specific elimination of TIC from pancreatic tumors, and to related clinical applications.

2 Materials and Methods

2.1 Materials

2.1.1 Laboratory Equipment

Agarose gel documentation	Peqlab, Erlangen
Agarose gel electrophoresis chamber	Biometra Göttingen
Analytical balance TE124S	Satorius, Göttingen
BD™ LSRII flow cytometer	BD Biosciences, Heidelberg
Biofuge® pico	Heraeus, Hanau
Centrifuge inserts	Kendro, Langenselbold
Centrifuge Multifuge® 3SR	Heraeus, Hanau
Confocal microscope SP5	Leica, Wetzlar
Cryobox Nalgene	Thermo Fisher Scientific, Schwerte
Electrophoresis power supply	Elchrom Schientific, Cham
FACS Aria™ cell sorter	BD Biosciences, Heidelberg
Fluorescence Mircoscope Axiovert 2000	Zeiss, Oberkochen
Freezer -20°C	Liebherr, Biberach a.d.Riss
Freezer -80°C	Sanyo, Hamburg
Fridge 4°C	Liebherr, Biberach a.d.Riss
Incubator Heraeus® 150	Thermo Fisher Scientific, Schwerte
iPhone 4 camera	Apple, Cupertino
Isoflurane vaporizer Vapor 19.3	Dräger, Lübeck
Junior GS sequencer	Roche, Mannheim
Light microscope for cell culture	Zeiss, Oberkochen
Magnet MPC-96	Invitrogen, Darmstadt
Magnet DynaMag™-96 side skirted	Invitrogen, Darmstadt
Microtome HM 340-E	Thermo Fisher Scientific, Schwerte
Microwave	Bartscher, Salzkotten
Mr. Frosty freezing container	Thermo Fisher Scientific, Schwerte
NanoDrop® Spectrophotometer ND1000	Peqlab, Erlangen
Neubauer cell counting chamber	Marienfeld, Lauda-Königshofen
Nitrogen cryo-system	German-Cryo, Jüchen

Pap peb	Kisker, Steinfurt
PCR-Thermocycler	Landgraf, Langenhagen
Pipetboys acu	Integra Biosciences, Fernwald
Pipettes Research® (10µl, 20µl, 200µl, 1ml)	Eppendorf, Hamburg
Precision balance TE3102S	Satorius, Göttingen
Rotator Reax2	Heidolph, Schwabach
Safety cabinet Herasafe® KS	Thermo Fisher Scientific, Schwerte
Shaking incubator	Axon, Kaiserslautern
Submerged Gel Electrophoresis Device SEA 2000®	Elchrom Schientific, Cham
Thermo cycler TPersonal	Biometra, Göttingen
Thermo mixer comfort	Eppendorf, Hamburg
Tissue-Tek® TEC™ embedding system	Sakura Finetek, Tokyo
Transilluminator	Biotec-Fischer, Reiskirchen
Ultracentrifuge L8-M + rotor SW27	Beckman Coulter, Krefeld
Vacuum pump	Merck, Darmstadt
Vortexer MS1	IKA, Staufen

2.1.2 Disposable Materials

BD™ Falcon™ FACS tube, round bottom (5ml)	BD Biosciences, Heidelberg
BD™ Falcon™ tube conical-bottom (15ml, 50ml)	BD Biosciences, Heidelberg
Cell culture flasks, EasyFlask™ (25cm^2, 75cm^2, 175cm^2)	Nunc (Thermo Fisher Scientific), Schwerte
Cell culture well-plates (6-,12-, 96-well)	BD Biosciences, Heidelberg
Cell strainer (100µm and 40µm pore size)	BD Biosciences, Heidelberg
Cotton swabs	Noba, Wetter
Cover slips Ø 20mm	Menzel, Braunschweig
Cryotubes	Corning, Kaiserslautern
Embedding cassettes	Sanowa, Leimen
Glass slides SuperFrost®	Menzel, Braunschweig

HumanHT-12 v4 Expression BeadChips	Illumina, München
Injection needle (23G-26G)	BD Biosciences, Heidelberg
Injection needle, blunt (18G)	BD Biosciences, Heidelberg
Lab gloves nitril	Microflex, Reno
Microcon®-30 centrifuge filter device	Merck, Darmstadt
Multi-well plate 0.3ml	Roche, Mannheim
Parafilm	Pechiney, Chicago
Pasteur pipettes	WU Mainz, Bamberg
PCR reaction tube (200µl)	Genaxxon, Ulm
Petri dish (5cm, 10cm)	Genaxxon, Ulm
Petri dish (15cm)	Thermo Electron, Langenselbold
Pipettes (2ml, 5ml, 10ml, 25ml, 50ml)	Genaxxon, Ulm
Pipette tips (10µl, 20µl, 200µl, 1ml)	Starlab, Hamburg
Safe-Lock Tubes™ (0.5ml, 1.5ml, 2ml)	Eppendorf, Hamburg
Scalpels	Feather Safety, Osaka
Sterile filters (0.22µm, 0.45µm pore size)	Merck, Darmstadt
Stericup vacuum filters (0.45µm pore size)	Merck, Darmstadt
Syringe Omnifix® Solo (1ml, 5ml, 10ml, 20ml, 50ml)	B. Braun, Melsungen
Twin.tec PCR plate 96-well	Eppendorf, Hamburg
Ultra low attachment plates/flasks	Corning, Kaiserslautern
Ultracentrifugation tubes	Beranek, Weinheim

2.1.3 Chemicals and Reagents

Adenosine-triphosphate (ATP) 10mM	Epicentre Biotech., Madison
Agar	Sigma-Aldrich, München
Agarose	Serva, Heidelberg
AMPure® XP beads	Beckman Coulter, Krefeld
Aqua ad injectabila (H_2O_{dd})	B. Braun, Melsungen
Baytril®	Bayer, Leverkusen
Bovine serum albumin (BSA)	Sigma-Aldrich, München

Bromphenol blue	Sigma-Aldrich, München
Calcium chloride ($CaCl_2$)	Sigma-Aldrich, München
Citric acid ($C_6H_8O_7$)	Sigma-Aldrich, München
Dimetylsulfoxide (DMSO)	Sigma-Aldrich, München
Disodium-EDTA	Sigma-Aldrich, München
Desoxy-Nucleotides (dNTPs) (10mM)	Genaxxon, Ulm
DNA ladder (100bp, 1kb)	Invitrogen, Darmstadt
Dynabeads® M280 streptavidin	Invitrogen, Darmstadt
Eosin	Merck, Darmstadt
Ethanol	Sigma-Aldrich, München
Ethanol, denatured	DKFZ, Heidelberg
Ethidiumbromide (0.07%)	AppliChem, Darmstadt
Ethylendiaminetetraacedic acid (EDTA) 0.5M, pH=8	AppliChem, Darmstadt
Formalin solution, pH=7.4 (10%)	Sigma-Aldrich, München
Genomic DNA, human	Roche, Mannheim
Glycerol	Serva, Heidelberg
Hematoxylin	Merck, Darmstadt
Hexanucleotide mix (10x)	Roche, Mannheim
Hoechst 33342	Invitrogen, Darmstadt
Isopropanol	Sigma-Aldrich, München
Lithium chloride	Sigma-Aldrich, München
Loading buffer (5x)	Elchrom Schientific, Cham
Mounting medium, Anti-Fade Reagent	PromoCell, Heidelberg
Nuclease-free water	Ambion, Darmstadt
PCR buffer (10x)	Invitrogen, Darmstadt
Phalloidin-PF647 (200U/ml)	PromoCell, Heidelberg
Propidium iodide solution (1mg/ml)	Invitrogen, Darmstadt
Sodium chloride (NaCl)	VWR, Wien
Sodium citrate ($C_6H_5Na_3O_7 \cdot 2H_2O$)	Sigma-Aldrich, München
Sodium hydroxide (NaOH)	Sigma-Aldrich, München
Spreadex® gels, type EL1200	Elchrom Schientific, Cham

Tris-acetate-EDTA (TAE) buffer (40x)	Elchrom Schientific, Cham
Tris-borate-EDTA (TBE) buffer (40x)	Genaxxon, Ulm
Tris HCL, pH 7.5 (1M)	US Biological, Swampscott
Triton X-100	AppliChem, Darmstadt
Trypane Blue 0.04%	Invitrogen, Darmstadt
Xylol	VWR, Wien
β-Mercaptoethanol	Sigma-Aldrich, München

2.1.4 Enzymes

Collagenase IV	Invitrogen, Darmstadt
Klenow polymerase	Roche, Mannheim
Restriction enzymes + buffer	New England Biolabs, Frankfurt/Main
T4-DNA-Ligase + buffer	New England Biolabs, Frankfurt/Main
Taq-DNA-Polymerase	Invitrogen, Darmstadt

2.1.5 Antibodies

2.1.5.1 Antibodies for Flow Cytometry

For flow cytometry staining, the antibodies used were directly conjugated with fluorochromes allophycocyanine (APC), allophycocyanine-H7 (APC-H7) or phycoerythrine (PE).

Antigen	Clone	Isotype	Fluorochrome	Dilution	Supplier
CD133	AC133	Mouse IgG1	PE	1:10-1:20	Miltenyi, Bergisch-Gl
CD133	293C3	Mouse IgG2b	PE	1:10-1:20	Miltenyi, Bergisch-Gl.
CD44	G44-26	Mouse IgG2b	APC	1:10	BD Biosc., Heidelberg
CD44	27-35	Mouse IgG2b	APC-H7	1:200	BD Biosc., Heidelberg

CD24	ML5	Mouse IgG2a	PE	1:20	BD Biosc., Heidelberg
EpCam	EBA-1	Mouse IgG1	APC	1:20	BD Biosc., Heidelberg
Thy1	5E10	Mouse IgG1	PE	1:200	BD Biosc., Heidelberg
Thy1.2	53-2.1	Rat IgG2a	PE	1:50	BD Biosc., Heidelberg

2.1.5.2 Antibodies for Indirect Immunofluorescence

Primary antibodies

Raised in	Clonality	Antigen	Clone	Dilution	Supplier
Goat	polyclonal	Sox2		1:100	R&D Systems, Wiesbaden
Rabbit	polyclonal	Oct4		1:100	Abcam, Cambridge
Mouse	monoclonal	Klf4	56CT5.1.6	1:100	Abgent, Oxfordshire
Mouse	monoclonal	Nestin	10c2	1:100	Santa Cruz, Heidelberg
Mouse	monoclonal	Desmin	D33	1:100	Santa Cruz, Heidelberg
Mouse	monoclonal	Krt7	OV-TL 12/30	1:100	Dako Systems, Hamburg
Rabbit	polyclonal	Krt7		1:200	Abcam, Cambridge
Goat	polyclonal	Ptf1a		1:50	R&D Systems, Wiesbaden
Rabbit	polyclonal	α-Amylase		1:100	Sigma-Aldrich, München

Mouse	monoclonal	αSMA	1A4	1:200	Sigma-Aldrich, München
Mouse	monoclonal	Vimentin	V9	1:100	Santa Cruz, Heidelberg
Mouse	monoclonal	Thy1	AS02	1:100	Dianova, Hamburg
Rat	monoclonal	Thy1.2	53-2.1	1:100	BD Biosc., Heidelberg

Secondary antibodies

Secondary antibodies for indirect immunofluorescence were conjugated with fluorochromes for detection in fluorescence or confocal microscopy.

PF: PromoFluor®; DyL: DyLight®; AF: AlexaFluor®

Raised in	**Antigen**	**Fluorochrome**	**Dilution**	**Supplier**
Goat	Mouse IgG	PF-555	1:200	PromoCell, Heidelberg
Goat	Rabbit IgG	PF-488	1:200	PromoCell, Heidelberg
Goat	Rabbit IgG	PF-647	1:200	PromoCell, Heidelberg
Donkey	Mouse IgG	DyL-649	1:200	Jackson IR, Suffolk
Donkey	Rabbit IgG	DyL-549	1:200	Jackson IR, Suffolk
Donkey	Goat IgG	DyL-488	1:200	Jackson IR, Suffolk
Donkey	Rat IgG	AF-680	1:200	Invitrogen, Darmstadt

2.1.6 Plasmids

Plasmid	Encodes for	Supplier
pMDL gag pol (p101)	Viral gag, pol	Naldini Lab, Milan
pRSV rev (p102)	Viral rev	Naldini Lab, Milan
pMD2.VSVG (p103)	VSVG protein	Naldini Lab, Milan
pCCLsincPPT.PGK-eGFP.WPRE (p106)	EGFP	Naldini Lab, Milan

All plasmids further encode an ampicillin resistance gene (AmpR) for amplification in bacteria.

2.1.7 Oligonucleotides

All oligonucleotides were purchased from Eurofins MWG Operon, Ebersberg.

LC: Linker cassette; LTR: Long terminal repeat; bio: biotinylated; MID: Multiplex Identifier

Denomination	Sequence (5`-3`)
LC1	GACCCGGGAGATCTGAATTCAGTGGCACAGCAGTTAGG
LC3-1	AATTCCTAACTGCTGTGCCACTGAATTCAGATC
LC3-2	TACCTAACTGCTGTGCCACTGAATTCAGATC
LCI	GACCCGGGAGATCTGAATTC
LCIII	GATCTGAATTCAGTGGCACAG
LTRI	GACCCGGGAGATCTGAATTC
LTRII	GATCTGAATTCAGTGGCACAG
SK LTR 1 bio	GAGCTCTCTGGCTAACTAGG
SK LTR 2 bio	GAACCCACTGCTTAAGCCTC
SK LTR 3 bio	AGCTTGCCTTGAGTGCTTCA
SK LTR 4 bio	AGTAGTGTGTGCCCGTCTGT
SK LTR 5 bio	GTGTGACTCTGGTAACTAGAG
454-Titanium primer	CCATCTCATCCCTGCGTGTCTCCGACTCAG-MID-GATCCCT CAGACCCTTTTAGTC
454-Titanium linker	5'Bio-CCTATCCCCTGTGTGCCTTGGCAGTCTCAGAGTGGCAC AGCAGTTAGG

2.1.8 Materials and Tools for Experimental Surgery

Alcohol pads	B. Braun, Melsungen
Braunoderm® iodine solution	B. Braun, Melsungen
BD Matrigel™ Growth Factor Reduced	BD Biosciences, Heidelberg
Bepanthen® eye and nose lotion	Bayer, Leverkusen
Cotton swabs	Noba, Wetter
Earmarker	FST, Heidelberg
Epidural cannula 18G	BD Biosciences, Heidelberg
Forceps, delicate	FST, Heidelberg
Forceps, standard strong	FST, Heidelberg
Heat Pad	Thermolux, Murrhardt
Hemostat standard	FST, Heidelberg
Isoflurane	Abbott, Ludwigshafen
Reflex Wound Clip System	FST, Heidelberg
Rimadyl (carprofen), 50mg/ml	Pfizer, Karlsruhe
Scissors, artery, ball tip	FST, Heidelberg
Scissors, standard	FST, Heidelberg
Thread PGA Resorba 4-0	Resorba, Nürnberg
Tuberculin syringe 0.5ml, 27G	BD Biosciences, Heidelberg

2.1.9 Commercial Kits

DNeasy® Blood & Tissue Kit	Quiagen, Hilden
EndoFree Plasmid Maxi Kit	Quiagen, Hilden
Fast-Link™ DNA Ligation Kit	Epicentre Biotech., Madison
GS Junior Titanium emPCR Kit (Lib-L)	Roche, Mannheim
GS Junior Titanium PicoTiterPlate Kit	Roche, Mannheim
GS Junior Titanium Sequencing Kit	Roche, Mannheim
PicoGreen dsDNA Assay Kit	Invitrogen, Darmstadt
RNeasy® Mini Kit	Quiagen, Hilden

2.1.10 Cell Lines

HEK 293T	ATCC, Wesel
HeLa	ATCC, Wesel

2.1.11 Bacterial Strain

One Shot® TOP10 chemically competent Escherichia coli (E. coli)	Invitrogen, Darmstadt

2.1.12 Mouse Strain

NOD.Cg-Prkdc^{scid}Il2rg^{tm1Wjl}/SzJ (NSG) mice	The Jackson Laboratory, Bar Habor

2.1.13 Cell Culture

2.1.13.1 Cell Culture Media and Reagents

Advanced Dulbecco`s Modified Eagel Medium F-12 (DMEM/F12)	Gibco (Invitrogen), Darmstadt
Roswell Park Memorial Institute (RPMI) 1640 Medium	Gibco (Invitrogen), Darmstadt
Dulbecco`s Modified Eagel Medium (DMEM)	Gibco (Invitrogen), Darmstadt
Iscove`s Modified Dulbecco`s Medium (IMDM)	Gibco (Invitrogen), Darmstadt
Medium 199	Gibco (Invitrogen), Darmstadt
Accutase enzyme mix	PAA, Cölbe
Dulbecco`s Phosphate Buffered Saline (PBS)	Gibco (Invitrogen), Darmstadt
Hank`s Balanced Salt Solution (HBSS)	Sigma-Aldrich, München

2.1.13.2 Media Additives

Fetal Bovine Serum (FBS)	PAN Biotechnology
FGF-basic (FGF2)	R&D Systems, Wiesbaden
FGF10	R&D Systems, Wiesbaden

Glucose	Invitrogen, Darmstadt
Heparin	Sigma-Aldrich, München
HEPES buffer	Sigma-Aldrich, München
L-glutamine (200mM)	Invitrogen, Darmstadt
Nodal	R&D Systems, Wiesbaden
Penicillin/streptomycin (200mM)	Invitrogen, Darmstadt

2.1.13.3 Bacterial Media and additives

Ampicillin sodium salt	Sigma-Aldrich, München
LB (lysogeny broth) medium	Invitrogen, Darmstadt
SOC medium	Invitrogen, Darmstadt

2.1.13.4 Buffers and Media Compositions

Medium	Composition
Cancer stem cells medium new (CSCN medium)	Advanced DMEM/F12 Glucose (0.6%) Heparin 12µg/ml HEPES buffer (5mM) L-glutamine (2mM) Penicillin/streptomycin (2mM) 10ml B27-supplement (1x) FGF-basic (10ng/ml) FGF10 (20ng/ml) Nodal (20ng/ml)
Differentiation medium (RPMI medium)	RPMI1640 medium FBS (10%) L-glutamine (2mM) Penicillin/streptomycin (2mM)

HeLa medium	DMEM FBS (10%) L-glutamine (2mM) Penicillin/streptomycin (2mM)
293T medium	IMDM FBS (10%) L-glutamine (2mM) Penicillin/streptomycin (2mM)
Freezing solution	11ml RPMI medium 6ml FBS 3ml DMSO
Thawing solution	10ml RPMI medium 10ml FBS
Tumor purification mix	Medium 199 (without additives) Collagenase IV (2mg/ml) $CaCl_2$ (3mM)
LB liquid medium	1L H_2O_{dd} 25g LB powder
LB agar	1L H_2O_{dd} 25g LB powder 12.5g Agar Ampicillin (100µg/ml)
Loading buffer blue run (5x)	Tris-HCl (pH=7, 25mM) EDTA (pH=8, 150mM) Bromphenole blue (0.05%) Glycerol (25%)
3M LiCl solution	Tris-HCl (pH=7.5, 10mM) EDTA (1mM) LiCl (3M)
6M LiCl solution	Tris-HCl (pH=7.5, 10mM) EDTA (1mM) LiCl (3M)

Fixation solution	PBS Paraformaldehyde (4%)
Permeabilization buffer	PBS Triton X-100 (0.1%) Sodium citrate (0.1%)
Blocking buffer	PBS BSA (0.1%)
HF	HBSS FBS (2%)
HFPI	HBSS FBS (2%) Propidium iodide (200ng/ml)
Unmasking buffer	H_2Odd Citric acid (1.8mM) Sodium citrate (8.2mM) pH 6

2.1.14 Primary Material

Primary patient-derived tumor material was provided by the department for surgery of the Heidelberg University Hospital (study groups of Prof. Dr. Jürgen Weitz and Prof. Dr. Jens Werner). All experiments with human material were done in accordance with the guidelines of the declaration of Helsinki. Each patient agreed to tissue donation. Experiments were performed as permitted by the University Ethics Review Board.

2.1.15 Computer Software

Axiovision (release 4.8)	Zeiss, Oberkochen
BLAST-like alignment tool (BLAT)	http://genome.ucsc.edu
Chipster	Kallio et al., 2011, reference [174]
Endnote X6	Thompson Reuters, New York
FACS Diva Software (version 6.1.3)	BD Biosciences, Heidelberg

GraphPad Prism 6	Graph Pad, La Jolla
GS Junior Sequencer software V2.5	Roche, Mannheim
GS Run Processor V2.5	Roche, Mannheim
IS Over Time	In house software
Leica Application Suite Advanced Fluorescence (LAS AF) Lite	Leica, Wetzlar
Office 2007/2010	Microsoft, Redmond
Photoshop CS2	Adobe, Dublin

2.2 Methods

2.2.1 Tumor Cell Dissociation

Tumor tissue was minced into small pieces (<2mm) and washed two times in PBS. Centrifugations were performed at 900rpm for 5min (4°C). Tissue pieces were digested in tumor purification mix for 2.5 hours at 37°C in a rotating incubator. Subsequently, the digestion mix was filtered once though a 100µm cell strainer, and then twice through a 40µm cell strainer, to yield a single cell suspension. After each filtering step cells were centrifuged at 1000rpm for 10min (4°C). The dissociated single cell suspensions was taken into culture, analyzed by flow cytometry or transplanted further as described below.

2.2.2 Cell Culture Methods

All cell cultures used in this thesis were incubated under sterile conditions at 37°C, and 5% CO_2 in a humidified atmosphere.

2.2.2.1 Establishment of Spheroid Cultures

For serum-free culture conditions CSCN medium was used. Cytokines FGF-basic, FGF10 and nodal were added every 3-4 days. To establish spheroid cultures,

dissociated single cell suspensions were drawn up into CSCN medium in ultra-low attachment plates.

2.2.2.2 Establishment of Adherent Colony Cultures

For adherent culture establishment, undigested whole tumor pieces (1-2mm size) were plated into normal cell culture flasks to allow the attachment of tumor cells by the outgrowth method [175]. For adherent colonies CSCN medium was used. Cytokines FGF-basic, FGF10 and nodal were added every 3-4 days.

2.2.2.3 Splitting of Cell Cultures

For the splitting of adherent cultures, the cell layer was washed once with 5-10ml PBS and then incubated with 2.5-5ml accutase for 5-45min at 37°C. The incubation time was variable for every distinct cell culture. After all cells had fully detached, cells were centrifuged down at 1000rpm for 10min (4°C). Cells were then resuspended in new CSCN medium.

For splitting of spheroid cultures the cells were centrifuged down at 800rpm for 5min (4°C) in 50ml Falcon tubes, and washed once with 20ml PBS. After repeated centrifugation, the spheroids were resuspended in 5ml accutase and incubated for 10min at 37°C in the water bath. After that spheroids were vortexed gently at low intensity and incubated again for 5min followed by additional vortexing. The process of incubation and vortexing was repeated until no more clumps were visible in suspension. Subsequently, cells were centrifuged at 1000rpm for 10min (4°C), washed once with PBS and resuspended in CSCN medium.

2.2.2.4 Cryoconservation of Cells

For long-term viable storage of cultured cells or tumor pieces, cryoconservation was used. Cell or tumor piece suspensions were centrifuged down at 1000rpm for 10min (4°C). $1x10^5$ to $1x10^7$ were resuspended in 700µl RPMI medium and mixed with

700µl freezing medium in a 1.5ml tube. Cells were immediately placed in an isopropanol-filled Mr. Frosty container and frozen at -80°C. In this step, the container mediates a slow 1°C/h cooling of the cell which is protective due to lower ice crystal formation. After 24h cells were transferred into -120°C liquid nitrogen tanks.

Cryoconserved cells were thawed rapidly in a water bath and transferred into a 50ml tube. 1ml of thawing medium was used to clean the freezing tube and added slowly over the course of 1 minute. Next, 5ml and 20ml of thawing medium were added within a time span of 1 minute each, to dilute the DMSO of the freezing medium. Cells were centrifuged down at 1000rpm for 10min and washed once with 25ml PBS to remove remaining DMSO. Cell were centrifuged repeatedly and resuspended in culture medium for later cultivation.

2.2.2.5 Differentiation of Adherent Colony Cultures

For differentiation, freshly established adherent colony culture cells were detached by accutase and re-plated half in CSCN and half in RPMI medium. Serum-free and serum cultures were passaged in parallel up to 12 times. Cultures were split at 50-90% confluence between 1:1 and 1:5. For monitoring changes in cell biology at passages 3 and 8 comparative gene expression profiling and indirect immunofluorescence were performed. Both cultures were analyzed by flow cytometry for surface marker expression at each passage.

2.2.2.6 Outgrowth Cultures for Xenograft Tumor Analysis

In order to characterize xenograft tumor cell populations *in vitro* for morphology and marker expression cell cultures were established by the outgrowth method [175] in RPMI medium by placing 1-2mm tumor pieces into 6-well plates containing autoclaved Ø20mm cover slips. Cells were cultured until outgrowth of desired cell populations and subsequently fixated and stained by indirect immunofluorescence as described below.

2.2.3 Xenotransplantation Experiments

In this study, primary human tumor cells or whole tumor pieces were transplanted. All animal experiments were executed using immunodeficient NSG mice as permitted by the Regional Commission in Karlsruhe. Mice were purchased from Jackson Laboratory and kept in a specific-pathogen-free animal facility according to German laws and with the permission of the institutional ethic committee. Mice were sacrificed by cervical dislocation 3-26 weeks after transplantation when tumors reached the size of maximum 1cm^3 or whenever initial signs of suffering of the animals became obvious. Mice were anesthetized on a 37°C heating pad with 1.75% isofluran in the breathing air. As painkiller, 4ng Rimadyl (carprofen) were applied per gram of body weight. Drinking water provided for the mice contained 0.5mg/ml Baytril®. All animal experiments were performed under a laminar airflow cabinet using sterile materials.

2.2.3.1 Transplantation of Tumor Pieces

To expand primary patient-derived tumor tissue, whole tumor sections were transplanted subcutaneously or under the kidney capsule of NSG mice. For that purpose, tumor material was minced into small pieces and washed twice in PBS containing 2mM penicillin/streptomycin. Mice were anesthetized and shaved at the left mid abdominal site using a scalpel or an electric razor. The shaved side was disinfected using alcohol pads and iodine solution and in perpendicular direction to the spine, a 1cm incision was made into the skin. The tumor pieces were applied as described below. After transplantation, the wound was clipped and resterilized with iodine solution. Clips were removed after 7 to 10 days.

2.2.3.1.1 Subcutaneous Application of Tumor Pieces

After incision, the skin was mobilized and tumor pieces of up to 0.5cm^3 size were pushed under the skin using a hemostat.

2.2.3.1.2 Application of Tumor Pieces under the Kidney Capsule

After incision into the skin, the peritoneum was cut above the kidney. By applying gentle pressure, the kidney was moved through the cut and stabilized with a cotton swab. The kidney was kept moist with PBS using a cotton swab. Carefully, using a delicate forceps, the kidney capsule was opened slightly to insert the epidural cannula containing <2mm tumor pieces. The cannula was pushed gently for 5mm into the cranial direction. Subsequently, the tumor pieces were carefully injected and the cannula was removed from the kidney. Next, the kidney was pushed back into the abdomen, and the peritoneum was stitched using self-resorbing thread.

2.2.3.2 Transplantation of Cells

For *in vivo* experiments, cultured or purified tumor or stroma cells were transplanted subcutaneously, under the kidney capsule or into the pancreas of NSG mice.

2.2.3.2.1 Preparation of Cell/Matrigel Mix

Single cell suspensions were centrifuged for 10min at 1000rpm (4°C). After removal of the supernatant, the cells were resuspended in 1ml culture medium and transferred to a 1.5ml reaction tube. Next, the cells were centrifuged for 5min at 2000rpm (RT). The supernatant was removed except for 200µl. The pellet was resuspended in the remaining supernatant and transferred into a 0.5ml reaction tube. The cells were again centrifuged for 5min at 2000rpm (RT). The supernatant was removed leaving 20-50µl medium covering the cell pellet. The cells were mixed with an equal amount of matrigel and transferred into a 0.5ml tuberculin syringe (27G). The syringes were then cooled on ice until transplantation as described below.

2.2.3.2.2 Subcutaneous Transplantation of Cells

For subcutaneous transplantation, mice were anaesthetized as described above. The left or right mid abdominal site was disinfected using alcohol pads and iodine

solution. The disinfected skin was pulled up with a forceps to inject the cell/matrigel mix (prepared as described above) into the skin folding. To compare the growth characteristics of tumor initiated by differentially treated cell cultures, both flanks of an individual mouse were used to transplant two different cell entities.

2.2.3.2.3 Transplantation of Cells under the Kidney Capsule

Kidney capsule transplantation was performed as described for tumor pieces (2.2.3.1.2). Instead of injecting tumor pieces from an epidural cannula, a cell/matrigel mix prepared as described above was injected with a tuberculin syringe.

2.2.3.2.4 Transplantation of Cells in the Pancreas

Mice were anaesthetized, disinfected and shaved as described above. A 2cm skin incision was made in a ventral direction. The peritoneum was opened about 5mm above the spleen to expose the pancreas by gentle pressure. Using PBS soaked cotton swabs the pancreas was moistened and spread out on the peritoneum in a ventral direction. Coming from the spine a tuberculin syringe was pushed into the pancreas to inject the cell/matrigel mix prepared as described above. Subsequently, the pancreas was pushed back into the abdomen and the peritoneum was stitched using self-resorbing thread. The skin was closed with wound clips and disinfected again with iodine solution. Clips were removed after 7-10 days.

2.2.3.3 Harvesting of Xenograft Tumors

Mice were sacrificed by cervical dislocation. The legs were pulled away from the abdomen and fixed with needles. The mice were disinfected with 70% ethanol and their abdomens were opened with surgical scissors in cranial direction. The skin was mobilized from the flanks and fixed with needles. Peritoneum and sternum were cut in a cranial direction. Tumors were excised using surgical instruments and transferred into sterile PBS. Organs were examined visually for metastases. Liver,

spleen and lung were removed and fixed in 10% formalin for histopathological examination as described below (2.2.12).

2.2.4 Molecular Biology Methods

2.2.4.1 Isolation of RNA from Cell Cultures

Cultured cells were washed with PBS and centrifuged down at 1000rpm for 10min (4°C). After the supernatant was discarded, the pellet was frozen at -80°C. For RNA isolation cells were thawed on ice. Subsequently RNA was isolated using the RNeasy Mini Kit according to supplier instructions and eluted in 30µl RNAse-free water. DNA was digested on the column. RNA concentration and purity was determined using the NanoDrop ND1000 device. RNA was aliquoted and stored at -80°C.

2.2.4.2 Isolation of DNA from Cells or Tumor Tissue

DNA from suspension cells or <2mm tumor pieces was isolated. After washing in PBS, cells or tumor pieces were centrifuged down at 1000rpm for 10min at 4°C. The supernatant was discarded, and pellets were frozen at -80°C until DNA isolation using the DNeasy® Blood & Tissue Kit following manual instructions. The concentration and purity of DNA was determined using the NanoDrop ND1000 device. DNA was stored at -20°C.

2.2.5 Gene Expression Profiling

Comparative gene expression profiling was performed in cooperation with the Core Facility for Genomics & Proteomics of the German Cancer Research Center Heidelberg, using HumanHT-12 v4 Expression BeadChips. For that purpose, 10µl of minimum 50ng/µl RNA solution were provided. Quality check of the RNA was performed by the Core Facility. RIN values show the integrity of the RNA, where a value of 10 represents fully intact undegraded RNA. For expression profiling, only

RNA with RIN values between 7.5 and 10 was used. Normalization and processing of raw data was performed using chipster software [174].

Global gene expression profiles were analyzed using Microsoft Excel. Gene expression values of control cells were subtracted from those of the experimental cells obtaining the fold change (FC). FC values were used to calculate the fold expression (FE) compared to the control samples. In a log2-scale, FC values represent FE values as the power of base 2 ($FE=2^{FC}$). A fold change of 1 represents twice the gene expression exhibited by the controls (FE=2), whereas -1 represents half the expression (FE=0.5). A FE value ≥2 was considered an up-regulation and a FE value ≤0.5 a down-regulation of the respective gene.

2.2.6 Lentiviral Vector Production

In order to mark primary pancreatic tumor cells by genomic integration sites, lentiviral vector particles were produced encoding the enhanced green fluorescent protein (EGFP) marker gene as described previously [176]. Self-inactivating (SIN) lentiviral vectors of the 3rd generation based on the human immunodeficiency virus (HIV) were used. Due to a deletion in the 3` long terminal repeat (LTR) these virus particles cannot replicate after infection of a cell, and are thus suitable for the safe use in scientific and clinical applications.

The system required four distinct DNA plasmids: pMDL gag pol (p101) encodes for viral enzymes integrase, protease and reverse transcriptase (pol) and the HIV matrix, capsid and nucleocapsid porteins (gag) under control of a CMV promoter; pRSV rev (p102) encodes for the RSV U3 promoter driven “regulator of expression of virion proteins” (rev) which is required for viral replication; pMD2.VSVG (p103) encodes CMV promoter controlled for the glycoprotein of the vesicular stromatitis virus (VSVG) that is introduced to the viral surface for pseudotyping, which enables HIV to infect a broad range of human cell types; pCCLsincPPT.PGK-eGFP.WPRE (p106) represents the lentiviral expression vector encoding the EGFP marker gene under the control of the human phosphoglycerate kinase (PGK) promoter.

Lentiviral vector particles were produced in HEK 293T cells. For that purpose, $1x10^7$ cells were seeded in 15cm petri dishes in 15ml 293T medium. The next day, medium was changed 2h prior to transfection to a volume of 10ml fresh medium per dish. Polyethylenimine (PEI) served as transfection reagent, and was used in a DNA:PEI ratio of 1:3. For each dish, 179.25µl of a 1mg/ml PEI solution were diluted in 320.25µl IMDM medium without additives (∑ 500µl) in 1.5ml reaction tubes.

For each dish, a DNA mix was prepared containing the following amounts of plasmid DNA:

Plasmid	**Amount per dish**
p101	12.5µg
p102	6.25µg
p103	9µg
p106	32µg

DNA was diluted in IMDM medium without additives to a total volume of 500µl per dish in 1.5ml reaction tubes. The 500µl PEI mix and the 500µl DNA mix were combined to a 1ml DNA/PEI solution and incubated for 1h at RT. Next, 1ml of DNA/PEI solution was added to each dish followed by gentle shaking. After 12h of incubation, the medium was changed to 15ml fresh 293T medium. After 24h of incubation the virus supernatant was harvested and centrifuged at 800rpm for 5min to remove residual HEK 293T cells. Next, the supernatant was sterile filtered using Stericup vacuum filters (0.45µm pore size) and transferred into ultracentrifugation tubes (35ml/tube). Ultracentrifugation was performed at 20,000rpm for 2h at 20°C to pellet lentiviral particles for concentration. Subsequently the supernatant was discarded by turning the tubes upside down. Residual medium was removed with cotton swabs. To the bottom of the ultracentrifugation tubes 70µl of PBS were given and incubated for 30min at RT. To avoid drying, the tubes were covered with parafilm during this 30min incubation period. Next, the PBS was pipetted over the bottom of the ultracentrifugation tubes for 20 times to resolve the viral pellet. The PBS of all tubes was collected in one 1.5ml reaction tube and shaken for 20min at RT. After that, the virus supernatant was distributed into 5-20µl aliquots and stored at -80°C.

To determine the functional titer of lentiviral supernatants, HeLa cell were transduced *in vitro* using serial dilutions of the harvested virus suspension. HeLa cells grown in IMDM medium were seeded into a 6-well plate at a density of $5x10^4$ cells per well. After 24 incubation, the cells of one well were detached by accutase treatment and counted to determine the cell number per well. The virus was diluted in a 24-well plate by adding 1µl virus supernatant into 1ml IMDM medium. This virus suspension was serially diluted at a 1:10 ratio by transferring 100µl of one dilution into 900µl of fresh IMDM medium. This was performed until five serial dilutions were prepared. The culture medium in the 6-well plate was replaced by 500µl IMDM-medium containing 16µg/ml polybrene. Next, 500µl virus dilution were added into each well to transduce adherent HeLa cells. By this further 1:2 dilution step, cells were transduced at a dilution range between 10^{-3} and 10^{-7} of the original virus supernatant. After 72h incubation the transduction efficiency of the cells in each well was determined by flow cytometry. The functional virus titer (transduction unit/ml) was calculated from the well that has received the lowest virus dilution showing a transduction of 1-25% of all living cells using the formula:

Transduction unit/ml = Cell number *x* dilution factor *x* % $EGFP^+$ cells/100

2.2.7 Lentiviral Marking

For lentiviral marking, cultured cells were detached by accutase treatment and centrifuged for 10min at 1000rpm. $1x10^5$ to $2x10^6$ cells were resuspended in 2ml CSCN medium and mixed with lentiviral vector particles at an MOI of 1 to 40 by gentle vortexing. Cells were subsequently incubated overnight and transplanted into NSG mice within 24 hours for *in vivo* experiments. On day 3 after transduction, transduction efficiency was measured by flow cytometry or by counting the proportion of $EGFP^+$ cells under the fluorescence microscope. For flow cytometry, dead cells were excluded by staining with propidium iodide. Thus, cells were washed once with HFPI and centrifuged down at 1200rpm for 5min at 4°C. Samples were measured using a LSRII flow cytometer and FACS Diva software. The gate for $EGFP^+$ cells was adjusted to an $EGFP^-$ control.

2.2.8 Linear Amplification Mediated PCR (LAM-PCR)

LAM-PCR was used to detect lentiviral integration sites (IS) in the genome of primary pancreatic cancer cells as described previously [113, 168]. The method facilitates the amplification of the genomic DNA flanking IS and thereby the identification of the specific IS locus. Through the use of biotinylated primers designed to bind in the 3`-region of the lentiviral LTR (3`-LAM-PCR) a linear PCR was performed and resulting products were captured on a solid phase (streptavidin coated Dynabeads). From linear amplicons, dsDNA was synthesized which subsequently was digested by restriction enzymes. To increase the IS coverage, each experiment employing LAM-PCR was performed in duplicates either using TSP509I or MSEI for restriction digest. A linker cassette was ligated to the DNA fragments in order to add a known DNA sequence to the LAM-amplicon which enabled amplification of the DNA fragments by exponential PCR steps. The single steps of the LAM-PCR procedure are visualized in figure 7.

LAM-PCR was performed using DNA isolated from purified cells of serially transplanted tumors in NSG mice. For that purpose 1/3 to 1/2 of all purified tumor cells were used for DNA isolation, 1/3 to 1/2 were transplanted into next generation mice (same proportion as used for DNA isolation) and the rest was used for flow cytometry analysis of EGFP expression or was cryoconserved. In case of an incomplete digestion of the tumor tissue, left over tumor pieces were additionally subjected to DNA isolation and LAM-PCR.

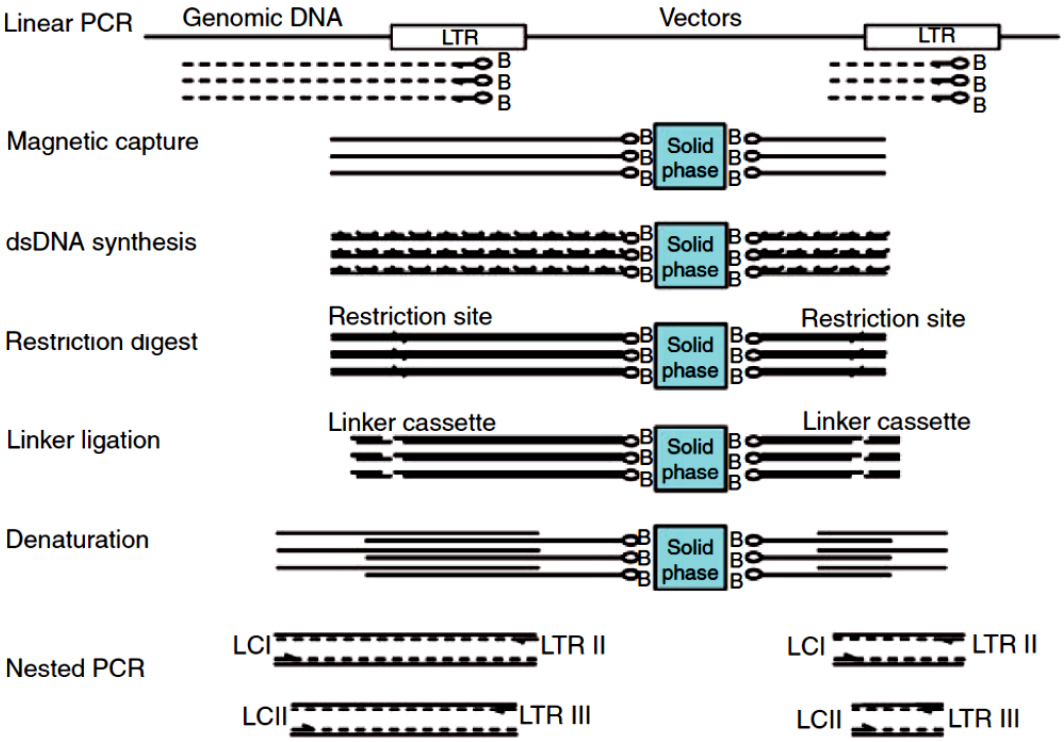

Figure 7: Stepwise experimental procedure of LAM-PCR. LC: Linker cassette; LTR: Long terminal repeat. Figure modified from [168].

2.2.8.1 Generation of Linker Cassette

The linker cassette was needed to exponentially amplify the LAM-PCR products by adding the known sequence of the linker to the unknown sequence of the DNA fragment. For each restriction enzyme used in LAM-PCR procedure a different overhanging DNA was required for ligation based on the varying DNA overhangs produced by restriction at different recognition sites. The linker cassette was generated by annealing the oligonucleotides LC1 and LC3-1 when TSP509I was used for the restriction digest, and in case of MSEI digestion, by annealing of LC1 and LC3-2.

Annealing of linker cassette:

Reagent	Volume
LC1 (100µM)	40µl
LC3-1/LC3-2 (100µM)	40µl
$MgCl_2$ (100mM)	10µl
Tris (250mM)	110µl
∑	200µl

Oligonucleotides were mixed and incubated at 95°C for 5min in a heating block. The heating block was then turned off to allow slow cooling of the nucleotide mix overnight. Subsequently 300µl water was added and the mix was applied on a Micrcon-30 column. After centrifugation at 12600rpm for 12min at RT, the flow through was discarded, and the column was placed upside down into a new collection tube. By centrifugation at 3600rpm for 3min at RT, the DNA was harvested and diluted with water to 80µl total volume. The linker cassette was aliquotted and stored at -20°C until use.

2.2.8.2 Linear PCR

The linear PCR was performed using a 96-well plate. Each well contained 50µl of the following PCR mix:

Reagent	Volume
10x PCR-buffer	5µl
dNTPs (10mM)	1µl
Taq DNA polymerase (5U/µl)	0.5µl
Primer SK LTR 1 bio (0.167pmol/µl)	0.25µl
Primer SK LTR 2 bio (0.167pmol/µl)	0.25µl
DNA	Xµl
H_2Odd	Ad 50µl

For each linear PCR, 1µg of DNA was used and amplified running the following PCR-program:

Denaturation	95°C	2min	
Denaturation	95°C	45s	100 cycles
Annealing	60°C	45s	
Elongation	72°C	1min	
Termination	72°C	5min	

After 50 cycles, another 1µl of Taq DNA polymerase (5U/µl) was added. The PCR was then continued for additional 50 cycles.

2.2.8.3 Magnetic Capture

The linear PCR products were captured using streptavidin-conjugated magnetic beads. The magnetic beads were washed twice with 40µl PBS + 0.1% BSA, and one time with 20µl 3M LiCl. The wash supernatant was removed by stabilizing the beads by exposition to a MPC-96 magnet. After that the beads were resuspended in 50µl 6M LiCl. Subsequently, the 50µl PCR product solution was mixed with the 50µl bead suspension and incubated at RT overnight on a rotator with 300rpm.

2.2.8.4 dsDNA Synthesis

Next, the single stranded linear PCR product bound to the magnetic beads was processed to a double stranded DNA. For that purpose, samples in the 96-well plate were exposed to a DynaMag^{TM} magnet for 96-well plates so that the supernatant could be removed without loss of the beads.

The bead-coupled DNA was washed with 100µl water and subsequently incubated in 10µl of the following reaction mix for 1h at 37°C:

Reagent	Volume
H_2Odd	8.25µl
10x Hexanucleotide mix	1µl
Klenow polymerase	0.5µl
dNTPs (10mM)	0.25µl
∑	10µl

2.2.8.5 Restriction Digest

After dsDNA was synthesized, 80µl of DNA was added to the reaction mix. By exposure to a magnetic field, beads were stabilized to remove the supernatant. After that, beads were washed with 100µl water and resuspended in 10µl of the following restriction digest mix:

Reagent	Volume
H_2Odd	8.8µl
10x NEB 1-buffer	1µl
Restriction enzyme (5U/µl)	0.2µl
∑	10µl

The restriction digest was performed using either TSP509I or MSEI as restriction enzyme. The digest mix was incubated for 1h at 65°C for TSP509I or at 37°C for MSEI.

2.2.8.6 Linker Ligation

The ligation of the linker cassette to the dsDNA fragments was performed using the Fast-Link™ Ligation Kit. The restriction digest mix was filled to 100µl with water,

exposed to a magnetic field and once with another 100µl of water. Samples were resuspended in the following reaction mix:

Reagent	Volume
H_2Odd	5µl
10x Fast-Link Ligation buffer	1µl
ATP (10mM)	1µl
Linker cassette	2µl
Fast Link Ligase (2U/µl)	1µl
∑	10µl

Incubation was for 5min at RT. After that, 90µl water was added and the samples were chilled on ice.

2.2.8.7 Denaturation

Samples were washed with 100µl water, with the beads stabilized on a magnet. After discarding of the supernatant samples were resuspended in 5µl of a 0.1M NaOH solution in order to remove the DNA from the beads. After 10min of incubation at RT on a shaking rotator at 300rpm, beads were removed by exposure to a magnetic field. The supernatant containing the DNA was transferred to a new reaction tube.

2.2.8.8 Exponential PCRs

The DNA harvested by denaturation was amplified in two independent exponential PCR reactions.

For the first exponential PCR the following mix was used:

Reagent	Volume
H_2Odd	40.5µl
10x PCR-buffer	5µl
dNTPs (10mM)	1µl
Taq DNA polymerase (5U/µl)	0.5µl
Primer SK LTR 3/4 bio (16.7pmol/µl)	0.5µl
Primer LCI (16.7pmol/µl)	0.5µl
DNA	2µl
∑	50µl

When TSP509I was used for restriction digest the primer SK LTR 3 bio was required. After MSEI-driven digestion, the primer SK LTR 4 bio was needed for the first exponential PCR. The DNA was amplified according to the following PCR program:

Denaturation	95°C	2min	
Denaturation	95°C	45s	35 cycles
Annealing	58°C	45s	
Elongation	72°C	1min	
Termination	72°C	5min	

The PCR products were subsequently captured on magnetic beads as described above. 20µl of the PCR product solution were mixed with 20µl of the beads and incubated for 1h at RT on a shaking rotator at 300rpm. After 60µl of water were added, the beads were stabilized on a magnet and the supernatant was discarded. The beads were washed twice with 100µl water, employing exposure to a magnetic field. Next, DNA was uncoupled from the beads by incubation in 10µl 0.1M NaOH solution for 10min at RT on a shaking rotator. After stabilization of the beads on a magnet, the DNA containing supernatant was transferred into a new reaction tube.

2µl of the harvested DNA were introduced into the second exponential PCR. The same protocol was used as for the first exponential PCR, except for the use of the

primer pair SK LTR 4/5 bio instead of the primer pair SK LTR 3/4 bio. TSP509I-digested products required the use of SK LTR 4 bio primer, whereas MSEI-digested DNA was amplified using SK LTR 5 bio primer.

Next, LAM-PCR products were purified as described in the Amplicon Library Preparation Method Manual by Roche (Rev. June 2010) using AMPure beads. 40ng of the purified DNA were applied into a third exponential PCR. For this PCR a Titanium primer was used which binds in the LTR region of the LAM-PCR products and contains a multiplex identifier sequence for the assignment of each amplicon to its according sample in sequencing. As the second primer, a biotinylated titanium linker was employed binding in the linker cassette of the DNA amplicons. The biotinylated part provides binding to the solid phase during sequencing.

The following PCR mix was used for the third exponential PCR:

Reagent	**Volume**
10x PCR-buffer	5µl
dNTPs (10mM)	1µl
Taq DNA polymerase (5U/µl)	0.5µl
454-Titanium primer (0.1pmol/µl)	0.25µl
454-Titanium linker (0.1pmol/µl)	0.25µl
DNA	Xµl
H_2Odd	Ad 50µl

The DNA was amplified running the following PCR program:

Denaturation	95°C	2min	
Denaturation	95°C	45s	12 cycles
Annealing	60°C	45s	
Elongation	72°C	1min	
Termination	72°C	5min	

The tagged LAM-PCR products were subsequently used for 454-sequncing as described below.

2.2.8.9 Gel Electrophoresis

In order to separate LAM-PCR products, 1-2% agarose gels were used or commercial high resolution Spreadex EL 1200 gels.

The agarose gel was composed of agarose and TBE buffer heated in a microwave to induce gel formation. After cooling of the liquid gel below 60°C 10µl ethidium bromide were added and mixed well with the gel. For gel loading samples were mixed 5:1 with 5x loading buffer and run for 1.5h at 140V.

For Spreadex gels, samples were mixed at a 5:1 ratio with a 5x Elchrom loading buffer. Gels were run in a SEA 2000 apparatus containing a 1:40 water-diluted Elchrom buffer for 90min at 130V. Subsequently, Spreadex gels were stained with a 0.5µg/ml ethidium bromide water solution for 15min at RT. DNA fragment size was examined under UV light in comparison to a DNA ladder.

2.2.8.10 454-Pyrosequencing

454-pyrosequencing involves the PCR-based introduction of a DNA adapter for the attachment to DNA-capture beads, a multiplex identifier, and a quality check key sequence to the LAM-PCR product. The bead/DNA proportion is adjusted in a way that each bead bears only a single DNA fragment (one clone per bead) with a total enrichment of 5-20%.

For that purpose, the DNA is quantified and the DNA molecules per volume are calculated using the following formula:

$$\text{Molecules}/\mu\text{l} = \frac{\text{sample concentration}\left(\frac{\text{ng}}{\mu\text{l}}\right) * 6.022 * 10^{23}}{656.6 * 10^{9} * \text{amplicon length (bp)}}$$

These beads are distributed in a water-oil emulsion, where DNA fragments are amplified by emulsion-based clonal amplification PCR (emPCR) to exponentially

increase the DNA copy number on each individual bead. After that, each bead is deposited into a single well of a picotiter plate. Sequencing following the Sanger method is based on the detection of a pyrophosphate signal generated by complementary nucleotide incorporation during DNA synthesis. For this process A, T, G and C dNTPs are flushed over the picotiter plate in a known order, so that in case of an incorporation event, pyrophosphate (PPi) is released from the incorporated dNTP. Beads are simultaneously deposited in the picotiter plate wells that bear sulfurylase and luciferase on their surface. Sulfurylase creates ATP from PPi and AMP, so that luciferase can hydrolase ATP and use luciferin to create a light signal. The light indicates the next added base and therefore also the next base of the sequenced molecule.

The tagged LAM-PCR products were purified according to the Amplicon Library Preparation Method Manual by Roche (Rev. June 2010) using AMPure beads. The DNA concentration was measured employing the PicoGreen dsDNA Assay Kit. All samples were pooled in equimolar fashion and used for emPCR at proper dilution. Amplification by emPCR was performed using the GS Junior Titanium emPCR Kit for uni-directional sequencing strategy (Lib-L) (manual Rev. April 2011). Sequencing was performed employing the GS Junior Titanium PicoTiterPlate Kit and the GS Junior Titanium Sequencing Kit (manual Rev. June 2010) on a GS Junior sequencer. Light signals were detected by the GS Junior Sequencer software and processed by GS Run Processor software to sequence read data files.

2.2.9 Statistical analysis

Statistical comparison of tumor sizes was performed using a paired two-sampled student´s T-Test in Microsoft Excel.

Statistical analysis of the data obtained by LAM-PCR and 454-sequencing was performed by Prof. Dr. Dr. Ulrich Abel (National Center for Tumor Diseases, Heidelberg). In addition to standard methods, such as Fisher’s exact test for equality of proportions, techniques were employed that were tailored to the special situation encountered here. This situation was characterized by complex serial sampling, the

absence of longitudinal observations on clone growth, an unknown number of clones present in the tumors, and the need to simultaneously account for observations gathered from different mouse generations. In particular, confidence interval p-values (a tool suited for “worst-case” analyses), confidence intervals for the parameter N of a binomial distribution with given success probability, stochastic modeling of the cell proliferation within clones using linear birth processes, and extreme-value distributions were employed. The details of these procedures are described in appendix C.

2.2.10 Flow Cytometry

Flow cytometry was used to phenotypically characterize cell cultures or purified tumor cells for the expression of cell surface markers or to sort antibody-marked populations. In order to exclude dead cells, propidium iodide (PI) was used intercalating into the DNA of dead cells, but leaving viable cells unstained. Thus, living cells appeared in the PI negative population.

2.2.10.1 Staining Procedure

Cells for flow cytometry were resuspended in HF and distributed into BD™ Falcon™ FACS tubes at a number less than $1x10^6$ cells per tube. All centrifugations were performed at 1200rpm for 5min. Fluorochrome conjugated antibodies for staining were diluted in HF. After centrifugation, cells were resuspended in 100µl antibody solution and incubated on ice for 30min. Next, 1ml of HF was added, followed by centrifugation. Samples were washed once with HFPI and subjected to further centrifugation. The supernatant was discarded and the cells were resuspended for measurement in 200-500µl HF. Measurement was performed using a BD™ LSRII flow cytometer or a FACS Aria™ cell sorter. Data were analyzed employing FACS Diva software.

2.2.10.2 Flow Cytometry Analysis and Cell Sorting

For cell sorting, $1x10^6$ and $2x10^7$ cells were stained for CD133 or CD44 as described above. For analysis of CD133 expression by flow cytometry, antibodies of clones AC133 and 293C3 were mixed 1:1 to cover all $CD133^+$ cells and used 1:20 each (1:10 in total). For cell sorting, the CD133 antibody concentration was increased to 1:10 for both antibodies (1:5 in total) to exclude that positive cells remain in the negative population. Based on CD133 expression, a negative, an intermediate and a positive fraction were sorted. The sorting purity was determined by reanalysis of the collection tube. To achieve a 100% purity of the negative fraction, a second sort was performed with the collected cells in case further $CD133^+$ events were detected upon reanalysis.

2.2.11 Indirect Immunofluorescence

Indirect immunofluorescence staining was performed to analyze the expression of intracellular markers in cultured cells and paraffin-embedded tissue or tumor spheres. Through the use of non-conjugated primary antibodies and fluorochrome-labeled secondary antibodies, a signal enhancement was achieved which provided sufficient signal intensity for confocal microscopy imaging.

2.2.11.1 Fixation of Cultured Cells for Staining

Cells were grown on Ø 20mm cover slips until desired confluence. Then cells were washed twice with ice-cold PBS and fixed for 20min in ice-cold fixation solution. Cells were then washed twice with PBS and stored in blocking buffer for at least 24h, or until later use for staining procedure.

2.2.11.2 Staining of Fixed Cells

The cultured cells were stained as described previously [177, 178]. All steps were performed by removing buffers after incubation with a glass Pasteur pipet connected

to a vacuum pump. All washing steps were done in blocking buffer, except where mentioned otherwise.

The blocking buffer covering fixed samples was discarded and cells were incubated for 10min in ice-cold permeabilization buffer. After that samples were washed three times. Next, cells were incubated for 10min in blocking buffer containing 2µg/ml Hoechst 33342 for staining of the nuclear DNA. After three washes, a total actin staining using phalloidin-PF647 diluted 1:50 in blocking buffer was performed where necessary for 30min in a dark wet-chamber. Next, after three washing steps in blocking buffer, samples were incubated with 100µl primary antibody solution diluted in blocking buffer for 1-16h in a dark wet-chamber. Before phalloidin or antibody staining the well-surface surrounding the cover slip was completely dried by vacuum aspiration without drying the cells on the cover slip. The antibody solution was applied directly on the cover slip so that it only covered the cells without spreading through the well. After primary antibody incubation, the samples were washed three times and secondary antibody staining was performed for 1h in a dark, wet chamber. The samples were then wash once in blocking buffer, once in PBS and finally washed in water to remove buffer salts. The cover slips were mounted in a 20µl drop of mounting medium on glass slides and kept in the dark until imaging.

2.2.11.3 Staining of Paraffin Embedded Tumor Tissue Slices or Spheroids

For histological and immunohistochemical analysis tumor tissue or tumor spheres were fixed with 10% formalin solution and embedded in paraffin or 30% albumin (Serva). 10 µm sections were deparaffinized by serial incubation in xylol for 2x 10min and rehydrated 5min in 100% EtOH, 5min in 96% EtOH, 5min in 70% EtOH and 2x 5min in H_2Odd. To unmask epitopes, tissue slides were cooked sequentially 2x 5min and 3x 2min in unmasking buffer using a microwave at 750W. After each cooking step the samples were incubated for 5min in the hot unmasking buffer. Next, the tissue was surrounded with a palp pen and incubated for 15min in 100µl permeabilization buffer in a wet chamber. After that, slides were blocked for 15min in blocking buffer. Subsequently, nuclear DNA was stained for 10min in blocking buffer containing 2µg/ml Hoechst 33342 in a dark wet-chamber. After 5min of washing in

blocking buffer, samples were incubated with 100µl primary antibody solution diluted in blocking buffer for 1-16h in a dark wet-chamber. Next, the samples were washed for 10min in blocking buffer and secondary antibody staining was performed for 1h in a dark, wet chamber. After washing 5min in blocking buffer and 5min in H_2Odd, samples were mounted in 30µl of mounting medium covered by a cover slip. Slides were kept in the dark until imaging.

2.2.12 Tumor Histopathology

The analysis of patient-derived and xenograft tumor material was performed in cooperation with Dr. Frank Bergmann and Prof. Dr. Wilko Weichert (Institute for Pathology, University Hospital Heidelberg).

2.2.12.1 Sampling and tissue fixation

Patient-derived tumor material was visually examined for tissue composition. Pathology samples were taken in a way that every differently colored area of the sample was contained. For histopathology of xenograft tumors, triangular pieces were cut. Murine organs were embedded entirely. The tissue was fixed in 10% formalin solution for 1-7 days. Finally, the tissue was dehydrated using an ascending EtOH series and embedded in paraffin wax. For further experimental procedures, 10µm tissue slices were manufactured using a microtome.

2.2.12.2 Hematoxylin/Eosin Staining

10µm tissue slides were re-hydrated as described above (2.2.11.3) and stained for 5min in hematoxylin, washed for 1 min with water, and stained another 1min with eosin. After subsequent washing for 1min in water, slides were mounted with 30µl mounting medium and a cover slip.

2.2.12.3 Histopathological Examination

Pathological analysis was performed by Dr. Frank Bergmann (Institute for Pathology, University Hospital Heidelberg). Hematoxylin/eosin-stained tissue slices of primary patient material were analyzed for tissue composition and estimated proportional tumor content. The xenograft tumors derived from different experimental arms were compared for tumor differentiation status and patient-specific characteristics of tissue appearance. For a better comparison, xenograft tumors of an individual patient from all experiments of this thesis project were analyzed altogether in one session.

2.2.13 Microbiology

2.2.13.1 Transformation of E. coli

For plasmid amplification, chemically competent E. coli were used. Frozen 100µl vials were thawed slowly on ice. Subsequently, 1µl of plasmid DNA was added to the bacteria. Transformation was supported by a head shock for 30s at 42°C. The mix was then cooled on ice for 2min. Bacteria were mixed with 900µl SOC-medium and incubated for 1h at 37° to enhance transformation efficiency. Finally, 5µl of bacteria suspension was distributed on a LB agar plate containing ampicillin, allowing the growth of only successfully transformed bacteria due to the plasmid-derived ampicillin resistance gene (AmpR).

2.2.13.2 Liquid cultures

Colonies from successfully transformed bacterial were picked and grown in 250ml LB medium containing 100µg/ml ampicillin for 12h at 37°C in a shacking incubator. The plasmids were purified using the EndoFree Plasmid Maxi Kit.

2.2.13.3 Restriction Digest

The integrity of used plasmids was analyzed by restriction digests to see whether the correct band pattern could be observed in a gel electrophoresis. The agarose gel electrophoresis was performed as described above (see 2.2.8.9). The following restriction digest mix was used:

Reagent	Volume
10x Restriction digest buffer (NEB)	2µl
Restriction enzyme (5U/µl)	1µl
Plasmid DNA	Xµl
H_2Odd	Ad 20µl

2.2.14 Microscopy Imaging

2.2.14.1 Light Microscopy

The morphology of cultured cells was assessed in a light microscope using Axiovision software to take pictures and generate scale bars.

2.2.14.2 Confocal Microscopy

A Leica SP5 confocal microscope was used to image samples stained by indirect immunofluorescence. Up to 4 channels were imaged simultaneously. For analysis of 3-dimentional samples, z-stacks were created imaging individual planes of the sample in a 0.5µm distance. Obtained data were processed using the LAS AF Lite software.

3 Results

The data presented in this part were submitted for publication on May 28, 2013 [179]. The experiments on pancreatic tumor-initiating cells (TIC) and stroma cells were performed in close collaboration with Dr. Claudia R. Ball from the National Center for Tumor Diseases (NCT), Heidelberg. This section only contains data obtained by myself, unless indicated otherwise. Analysis of tumor histology was performed by senior pancreatic pathologist Dr. Frank Bergmann (Institute for Pathology, University Hospital Heidelberg). The statistical analysis of data presented in chapter 3.4 was performed by Prof. Dr. Dr. Ulrich Abel from the NCT, Heidelberg.

3.1 Enrichment of Pancreatic Tumor Cells

Primary tumor cell cultures were established from patient-derived tumor tissue in order to investigate pancreatic TIC biology regarding their clonal composition, phenotypic diversity and their potential to generate stroma cells. The following sections describe the enrichment of TIC by *in vivo* and *in vitro* methods.

3.1.1 Surgically Resected Tumor Tissue Samples Vary in Tissue Composition

Primary patient-derived pancreatic tumor tissue was received from the Department for Surgery of the University Hospital Heidelberg. In total, 76 different samples were received. Examined tumor pieces had a weight between <0.1g and 4.2g (mean 0.61g, +/- 0.69g) and were dissociated using collagenase IV. The efficiency of tumor dissociation varied strongly between $2.5x10^3$ and $1.43x10^7$ living cells per 1g tumor tissue (mean $3.4x10^6$/g).

The tumor pieces were heterogeneous in color and often contained several areas of different color ranging from white to yellow, red or brown. When tumors were examined for tumor histology, different kinds of tissues were found in primary patient samples. In 20 of 45 examined samples PDAC tissue was detected (44%). Within the tumor bearing pieces, carcinoma content varied between 1% and 100% (mean 56%, +/-37.1%). Besides PDAC tissue, normal pancreas, inflamed pancreas (pancreatitis),

connective tissue, fat tissue, PDAC precursor lesions called pancreatic intraepithelial neoplasms (PanINs), benign neoplasms, and neuroendocrine tumors were also found (figure 8, table 2).

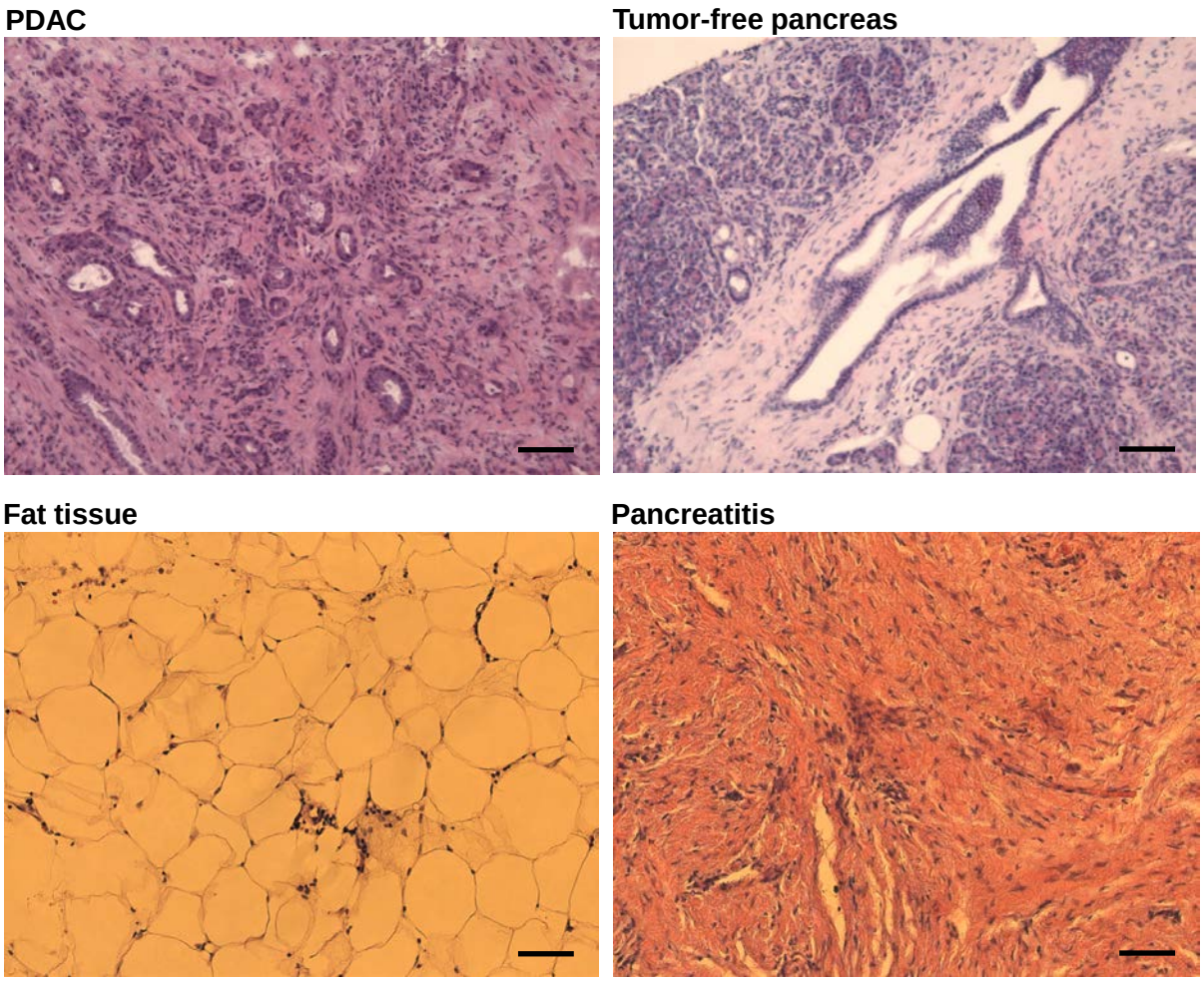

Figure 8: Histopathology analysis revealed varying tumor content in primary patient samples. Besides PDAC tissue patient-derived tumor material received from the surgery department contained various benign tissue types like normal pancreas, fat or pancreatitis tissue; scale bars: 100µm.

Table 2: Histopathology analysis of patient-derived tumor samples for tumor content and tissue composition.

Sample no.	Tissues contained	Tumor content (%)
1	Chronic pancreatitis	
2	Anaplastic PDAC	90
3	PDAC	80
4	Fat tissue	
5	PDAC + chronic pancreatitis	5
6	Muscle + connective tissue + chronic pancreatitis	
7	Normal pancreas	
8	Chronic pancreatitis	
9	Chronic pancreatitis	
10	PDAC	80
11	PDAC	1
12	Normal pancreas + connective tissue	
13	Normal pancreas	
14	Chronic pancreatitis	
15	Connective tissue	
16	Connective tissue	
17	Chronic pancreatitis	
18	Chronic pancreatitis	
19	Chronic pancreatitis	
20	Chronic pancreatitis + PanIN3	
21	Connective tissue	
22	Chronic pancreatitis	
23	PDAC	60
24	Adenosquamous PDAC	100
25	Chronic pancreatitis	
26	PDAC	50
27	Neuroendocrine tumor	
28	Chronic pancreatitis + PanIN1	
29	Chronic pancreatitis	
30	PDAC	70
31	Neuroendocrine tumor	
32	Chronic pancreatitis	
33	PDAC + chronic pancreatitis	1
34	PDAC	100
35	PDAC + chronic pancreatitis	20
36	PDAC	70
37	PDAC	100
38	Mucinous PDAC	60
39	Mucinous PDAC	2
40	PDAC	80
41	Chronic pancreatitis + PanIN3	
42	PDAC + chronic pancreatitis	50
43	PDAC	2
44	Microcystic serous cystadenoma	
45	PDAC	90

PDAC: pancreatic ductal adenocarcinoma; PanIN1-3: pancreatic intraepithelial neoplasm, stage 1-3.

3.1.2 Xenografting Facilitates Expansion of Primary Tumor Tissue

In order to enrich primary patient tissue derived tumor cells, suspension spheroids or adherent cultures were established in serum-free culture medium supplemented with growth supporting cytokines (FGF-basic, FGF10 and Nodal).

Purified single cell suspensions were cultured in ultra-low attachment plates to allow tumor-spheroid formation, a standard method to enrich for normal and malignant stem cells [44, 113, 135, 144]. However, from 49 attempts, no stable spheroid cultures were obtained. Alternatively, purified tumor cells or 2mm tumor pieces were plated in normal cell culture flasks under serum-free conditions to allow for the establishment of adherent cultures by the “outgrowth-method” (adapted from reference [175]). Through this outgrowth from tumor pieces, three tumor cell cultures were established from 20 tissue samples. These cells proliferated *in vitro* and displayed an epithelial morphology characterized by tight cell-to-cell contacts. Cells grew in a 3-dimensional colony-like fashion, so that these structures were named pancreatic tumor colonies (PTCs) (figure 9A). The colonies were surrounded by elongated cells with looser cell-to-cell contacts with a mesenchymal fibroblast-like appearance. Within 1 to 3 culture passages under serum-free conditions, fibroblast-like cells (FLCs) expanded and overgrew the epithelial colonies (figure 9B). Indeed, indirect immunofluorescence analysis of the freshly established cultures showed a heterogeneous population of tumor cells expressing the pancreatic duct epithelial marker cytokeratin 7 (Krt7), and cells that stained positive for the mesenchymal stroma markers vimentin, Thy1, and α-smooth-muscle actin (αSMA) (figure 9C-E). Thus, epithelial tumor cultures were not stable in adherent serum-free cultures established directly from patient material.

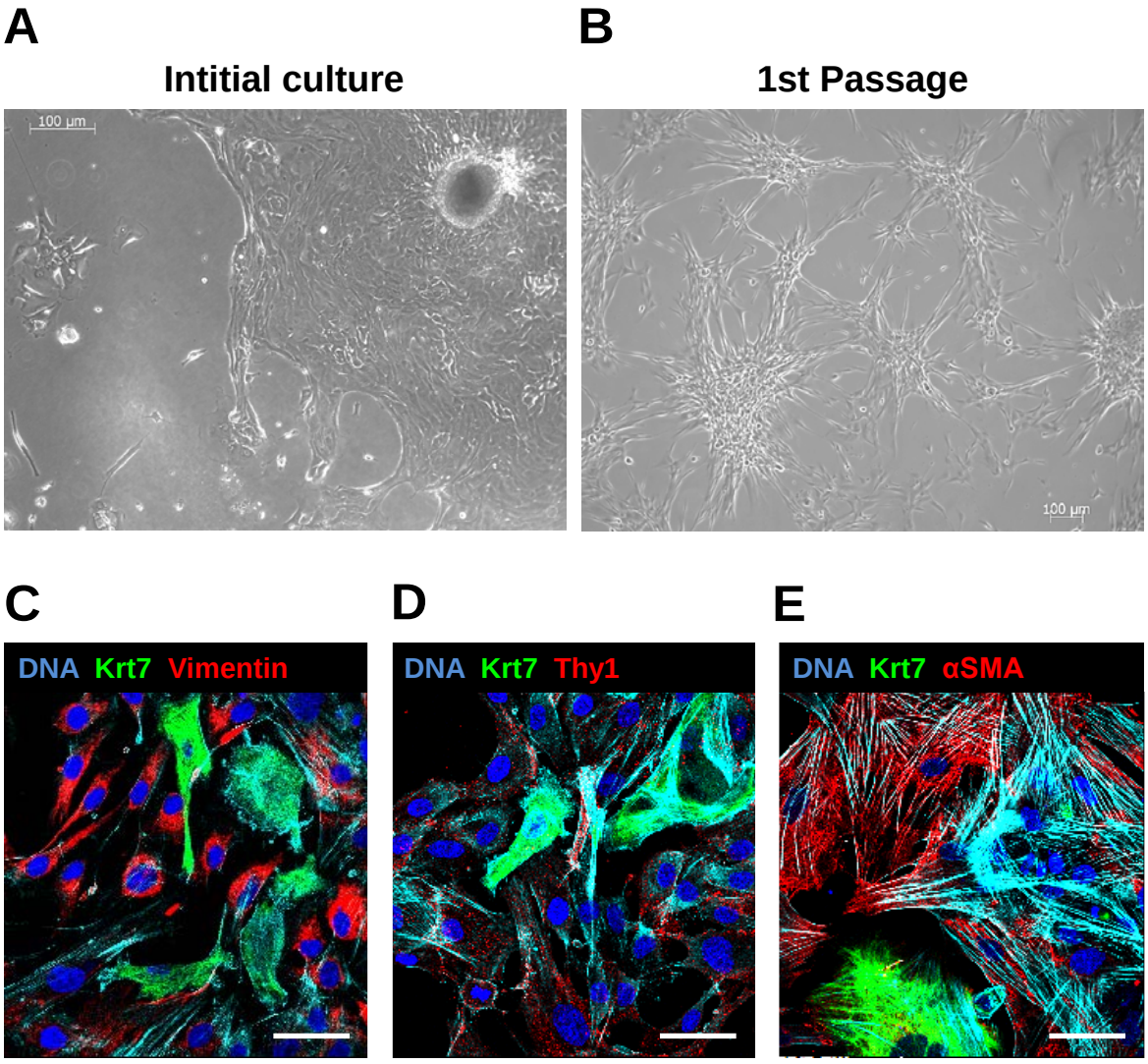

Figure 9: Establishment of primary pancreatic tumor cell cultures directly from surgically resected patient material. (A) After plating of 2mm tumor pieces in cell culture dishes tumor cells grew out of adherent tumor pieces and formed epithelial colonies. **(B)** After initial passaging of the cell culture shown in **(A)** no more cells of epithelial morphology were visible and instead fibroblast-like cells were seen; scale bars: 100µm. **(C-E)** Outgrowth cultures from tumor pieces of patient material showed cells of fibroblast morphology expressing mesenchymal stroma markers vimentin **(C)**, Thy1 **(D)** and α-smooth-muscle actin (αSMA) **(E)**. Pancreatic duct marker Krt7 was only expressed in tumor cells lacking mesenchymal markers; scale bars: 50µm.

To overcome the overgrowth of epithelial tumor cells by mesenchymal fibroblast-like cell types in cell culture, small tumor pieces (2-10mm size) or purified tumor cells were transplanted directly under the skin or under the kidney capsule of NOD.Cg-Prkdc^{scid}Il2rg^{tm1Wjl}/SzJ (NSG) mice to initiate xenograft tumors. When 2mm tumor

pieces were transplanted under the kidney capsule, one sample out of 16 formed a tumor (6.25%). To enhance the efficiency of xenograft tumor formation, larger tumor pieces (up to 0.5cm^3) were transplanted under the skin of NSG mice. With that methodology, patient tissue was cut in a way that every differently colored area of the tumor piece was transplanted. This strategy increased the probability of transplanting a tumor containing part. After this change in tissue processing, 9 samples initiated tumors from 29 transplanted (31%). When primary adherent serum-free cultured epithelial colonies were transplanted, 2 out of 2 xenografting attempts were successful. In total, 12 patient samples engrafted in NSG mice out of 47 tried (25.5%). Initial xenograft tumors formed within 8 weeks to 9 months after transplantation. Engrafted tumor samples were serially transplantable for up to 14 passages in mice that were evaluated. Resulting xenograft tumors closely resembled the original patient`s tissue in histology (figure 10).

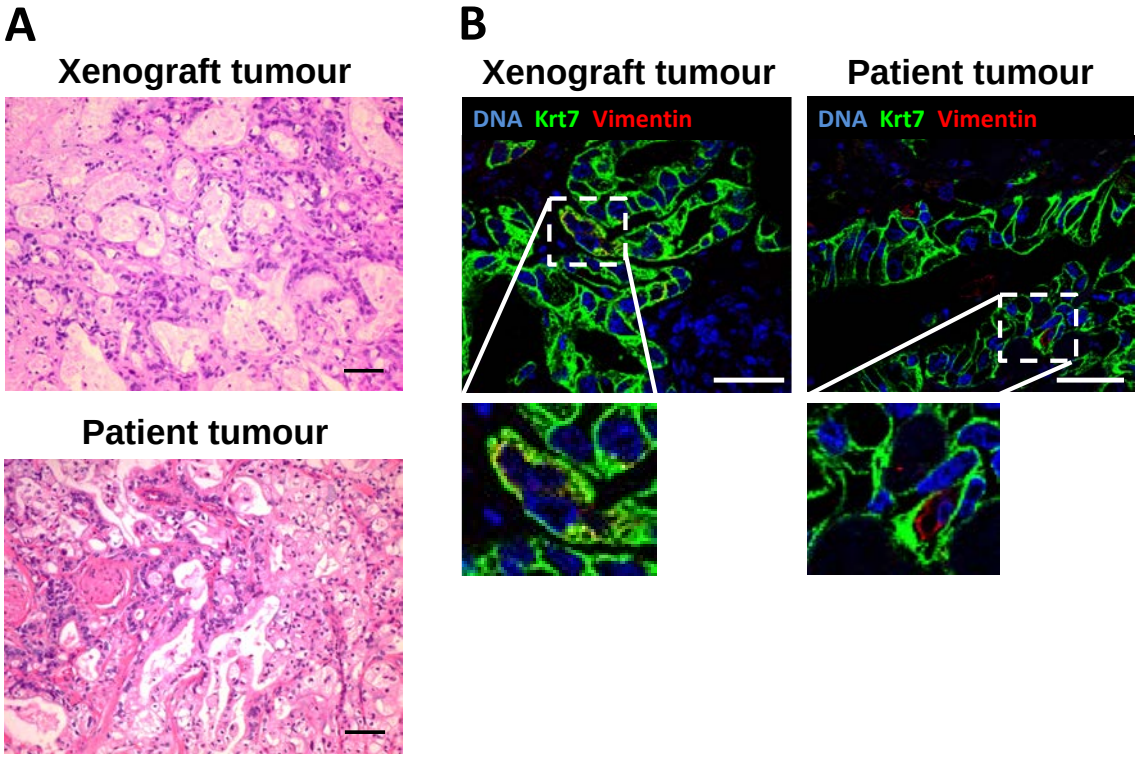

Figure 10: Histology of a pancreatic xenograft tumor tissue compared to the original patient sample. (A) The xenograft tumor closely resembled the patient`s tumor tissue in histology; scale bars: 100µm. **(B)** Adherent cultures initiated xenograft tumors in NSG mice that contained Krt7$^+$ irregular duct structures and a subpopulation of rare vimentin$^+$ cells, alike the respective patient tumor; scale bars: 50µm. Figure modified from [179].

3.1.3 Establishment of Primary Cell Cultures from Xenograft Tumor Material

After expansion of patient-derived tumor material in NSG mice, the establishment of spheroid and adherent colony cultures was repeated using the xenograft tumor tissue instead of direct patient tissue.

3.1.3.1 Pancreatic Tumor Spheroids are not Expandable in Suspension Culture

In contrast to direct patient tissue, xenograft tumor derived cells from three PDAC patients (P1-P3) formed large spheroid structures within 1-7 days of culture in ultra-low attachment plates using serum-free medium plus cytokines FGF-basic, FGF10 and Nodal (figure 11A). In these structures, cells survived in culture for up to 12 months until termination of the experiment, and initiated tumors in NSG mice. However, spheroid cells proliferated poorly *in vitro*, as was indicated by a constant decrease of cell numbers counted at each passaging step (figure 11B). In 4 out of 6 cases cells died within 2 culture passages.

3.1.3.2 Adherent Epithelial Tumor Colonies Stably Growth from Xenograft Tumor Tissue

As an alternative system to non-expandable spheroids, pancreatic tumor colony (PTC) cultures were established from xenograft tumor material of four patients (P1-P4) by the outgrowth-method [175] (figure 11A). For this purpose, tumor pieces of 1-2mm size were plated in normal cell culture flasks to allow adhesion. Derived 3-dimensional PTCs grew exponentially (figure 11B) for up to 16 passages examined without any signs of senescence. As was observed for colony cultures grown directly from patient material, PTCs derived from xenograft tumors were again surrounded by fibroblast-like cells after outgrowth from tumor pieces. However, in contrast to the cultures grown from fresh patient tissue, these cells were lost by passaging. PTC cells of P1-P4 formed tumors in NSG mice to 97.9% efficiency when at least $5x10^3$ cells were transplanted. Moreover, even 100 transplanted cells formed tumors, as observed for P1 and P4.

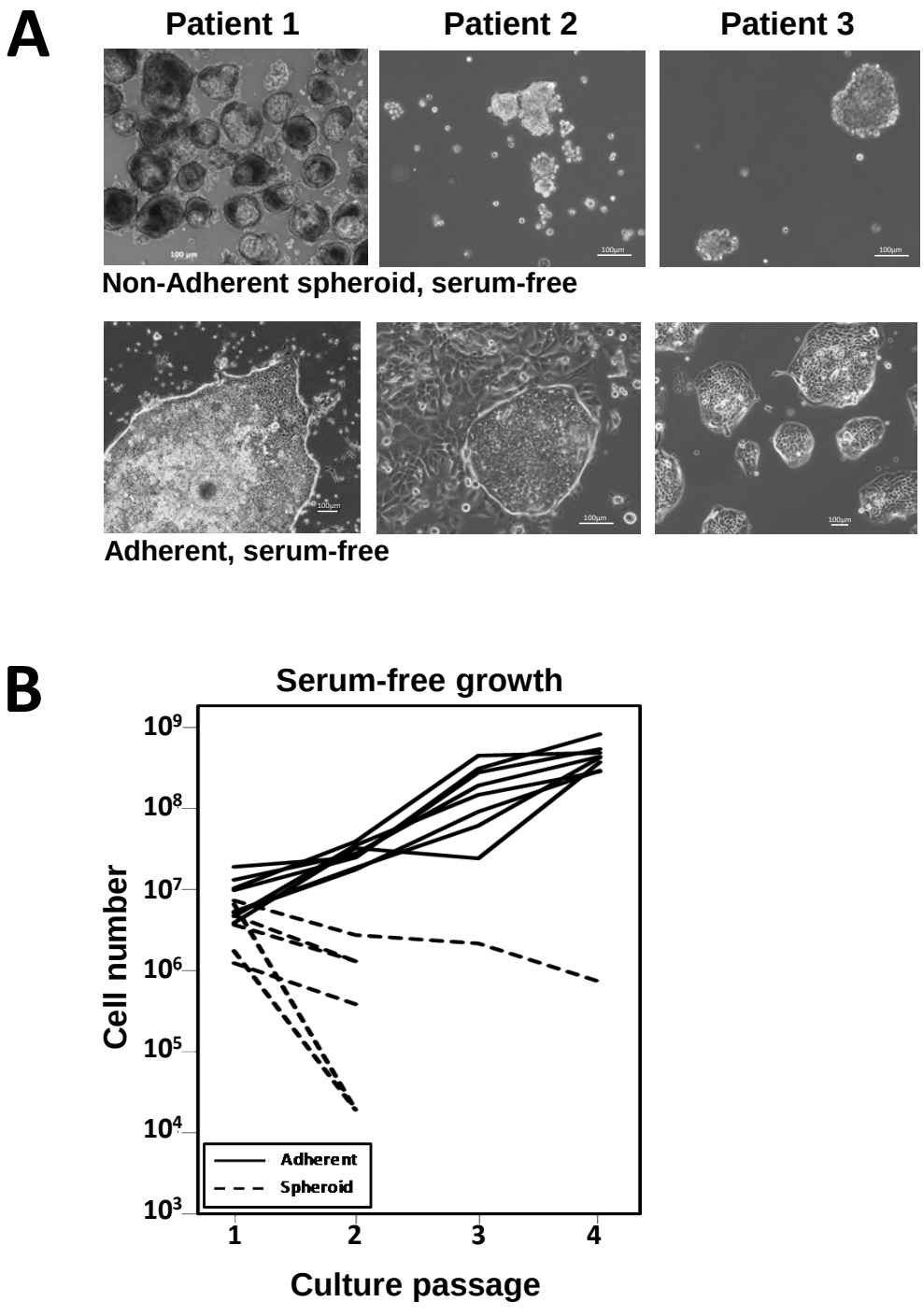

Figure 11: Cell culture of primary pancreatic tumor cells under serum-free conditions. (A) TIC can be kept in serum-free culture as suspension spheroids or adherent three-dimensional colonies; scale bars: 100µm. **(B)** The number of cells in spheroid cultures decreases after each passaging step, whereas adherent cultures grow exponentially. Figure modified from [179].

Phenotypic characterization of spheroid and colony cells revealed an undifferentiated phenotype indicated by the high expression of surface markers that have been associated with pancreatic TIC function including CD133, CD44, CD24 and the epithelial marker EpCam [143, 144] (figure 12). Moreover, spheroid and colony cultures derived from P1 were examined for Krt7 and vimentin expression by indirect immunofluorescence analysis. In both culture models, cells displayed an epithelial phenotype characterized by tight cell-to-cell contacts, high expression of the pancreatic duct marker Krt7 and absence of mesenchymal marker vimentin (figure 13A). However, besides the ductal differentiation marker Krt7 cells from three of four patients (P1, P2 and P3) co-expressed the acinar-specific transcription factor Ptf1a (only examined in adherent colonies, figure 13).

Summary chapter 3.1

Primary patient-derived tumor tissue varies strongly in tissue composition and tumor content. Thus, xenografting in NSG mice was employed to expand tumor material and obtain tissue that was free of benign human cell types. From these xenograft tumors, spheroid and adherent colony cultures could then be established *in vitro* under serum-free conditions. Primary pancreatic tumor cell cultures displayed a mixed cellular phenotype characterized by high TIC surface marker expression and the co-expression of ductal and acinar differentiation markers. Because spheroid cultures did not expand *in vitro*, exponentially growing tumor colony cultures were used for analyzing the differentiation potential and the clonal composition of pancreatic TIC, as described below.

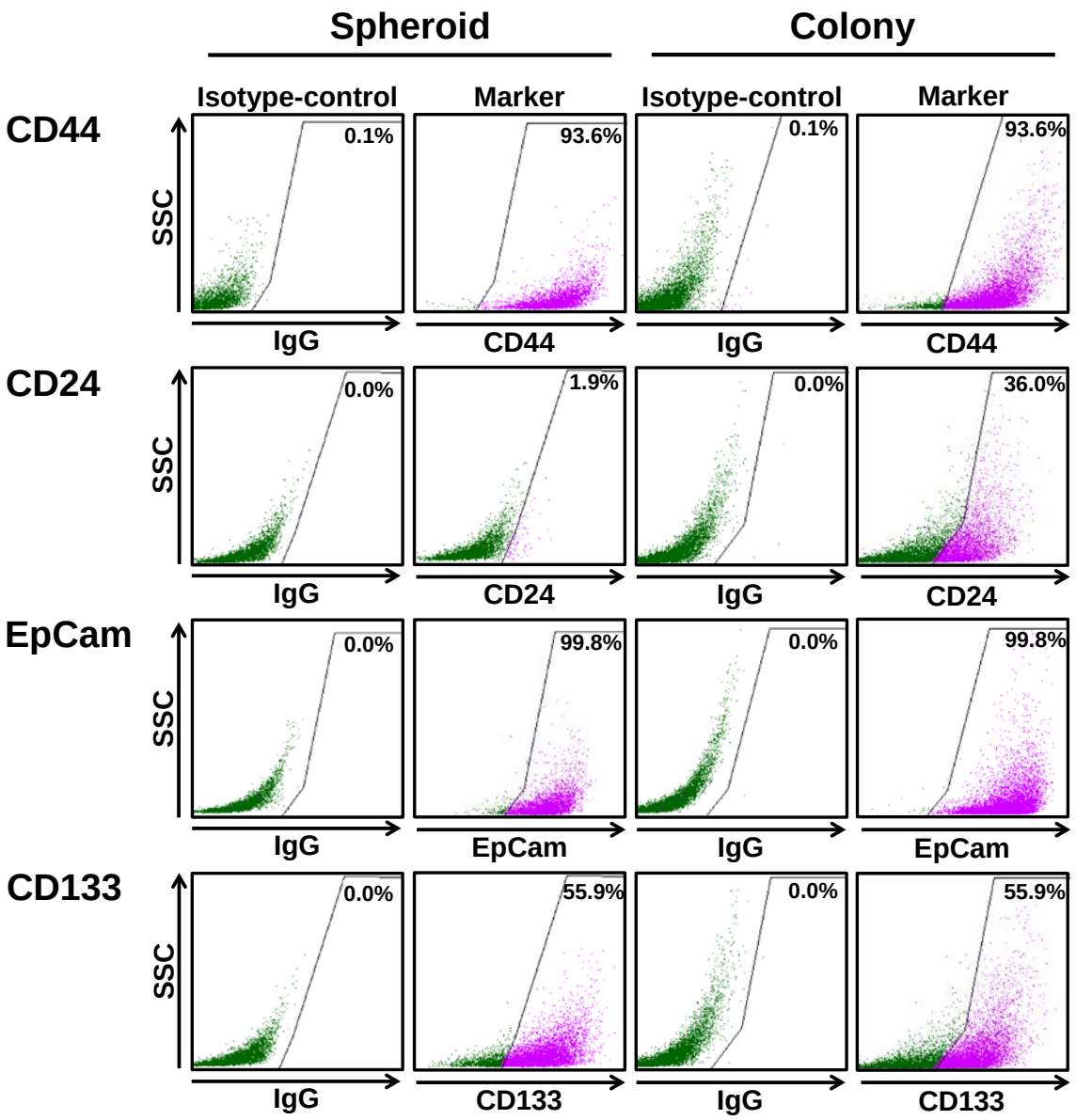

Figure 12: Characterization of serum-free grown primary pancreatic tumor cell cultures for TIC associated surface marker expression. Representative 3rd passage suspension spheroid and adherent colony cultures showed expression of pancreatic TIC function associated markers CD44, CD24, and CD133 and the epithelial marker EpCam. Appropriate isotype controls revealed that unspecific antibody binding was not higher than 0.1%. Antibody staining was plotted against sideward scatter (SSC). Percentage numbers in gates indicate proportion of positively stained cells.

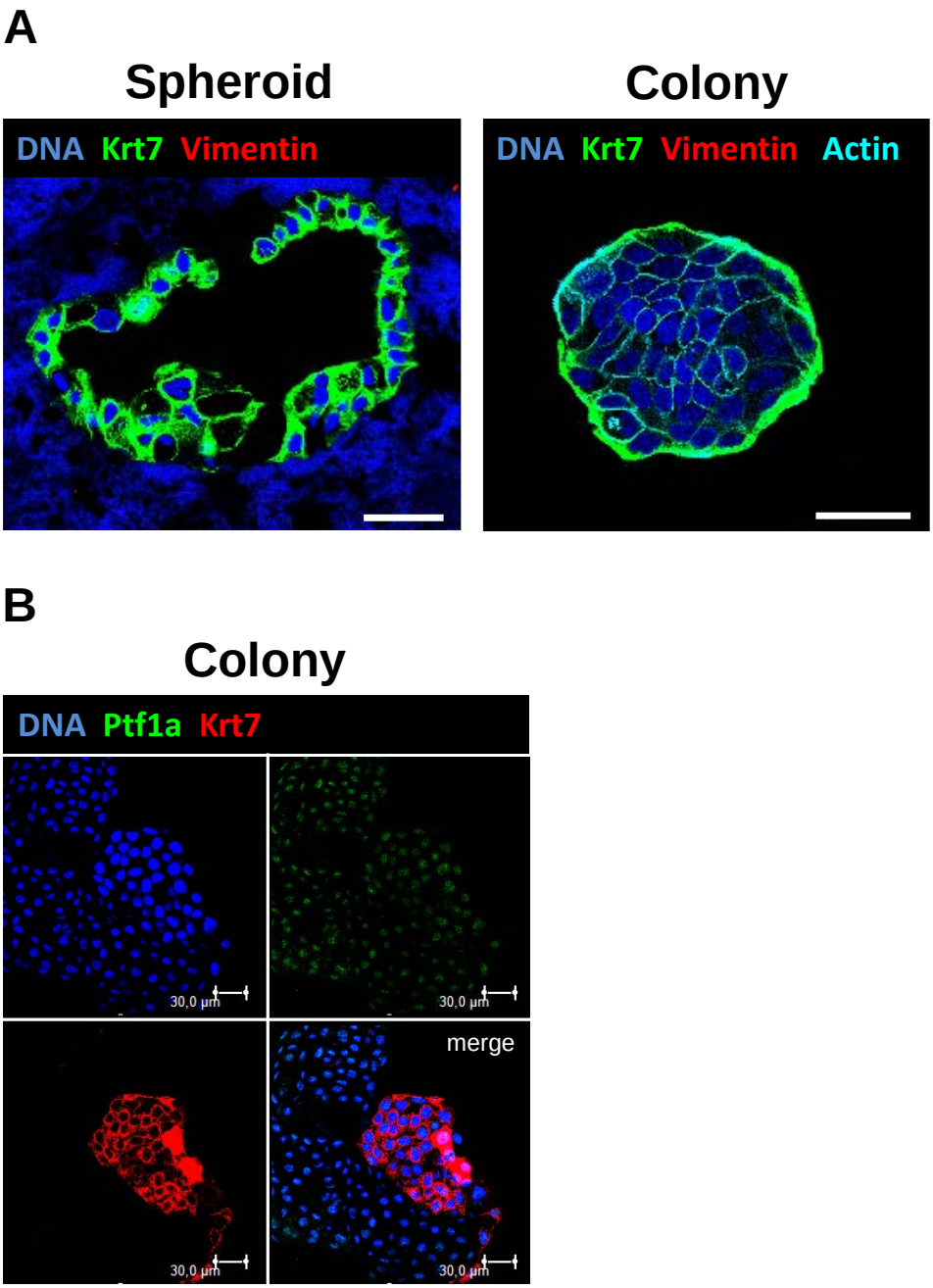

Figure 13: Characterization of serum-free primary pancreatic tumor cell cultures for pancreatic differentiation markers. (A) Adherent colonies and suspension spheroids displayed epithelial morphology and expression of the pancreatic duct marker Krt7, but stained negative for mesenchymal Vimentin; scale bars: 50µm. **(B)** Colony cells frequently co-expressed Krt7 and the acinar marker Ptf1a; scale bars: 30µm. Figure modified from [179].

3.2 Phenotypic Diversity of Pancreatic TIC

Tumor-initiating cells (TIC) and stem cells were previously hypothesized to share functional and phenotypic characteristics. For example, surface markers of benign stem cell population were frequently postulated to associate with tumor-initiating function (see section 3.1.3). This section describes experiments performed to attempt functional differentiation of pancreatic TIC to investigate, whether functional differentiation of pancreatic TIC is possible and, on the other hand, whether TIC function is stably associated to a certain phenotype.

3.2.1 Serum Treatment and Withdrawal of Growth Factors Alter Colony Cell Morphology

As described in section 3.1.3, pancreatic tumor colony (PTC) cells growing in serum-free medium stimulated by the growth factors FGF-basic, FGF10 and nodal displayed an undifferentiated phenotype characterized by the expression of markers previously shown to be associated with functional TIC populations in PDAC and other solid tumor entities (see section 1.3). In order to differentiate PTC cells, “serum treatment” was applied. In this thesis, this was defined as cultivation in RPMI1640 medium supplemented with 10% fetal bovine serum (FBS) and withdrawal of growth factors. Such cultures will be referred below as “serum-treated culture” and the original colony cultures as “serum-free controls”. Culture conditions similar or identical to serum treatment were described previously to induce partial differentiation of PDAC and glioma TIC [144, 180, 181]. Subsequently, the morphology of the adherent cells changed strongly. Under these conditions, cells derived from 4 individual patients (P1- P4) did no longer grow as 3-dimensional epithelial colonies, but instead formed monolayers of much larger and irregular shaped cells with increased cell diameter (figure 14). Serum-treated cells displayed loosened cell-to-cell contacts and polymorphous cell shapes. The resulting cell monolayer appeared disorganized and highly heterogeneous. Serum-treated and serum-free control cultures were equally able to grow in culture until the experiment was terminated after 12 months representing 11 passages.

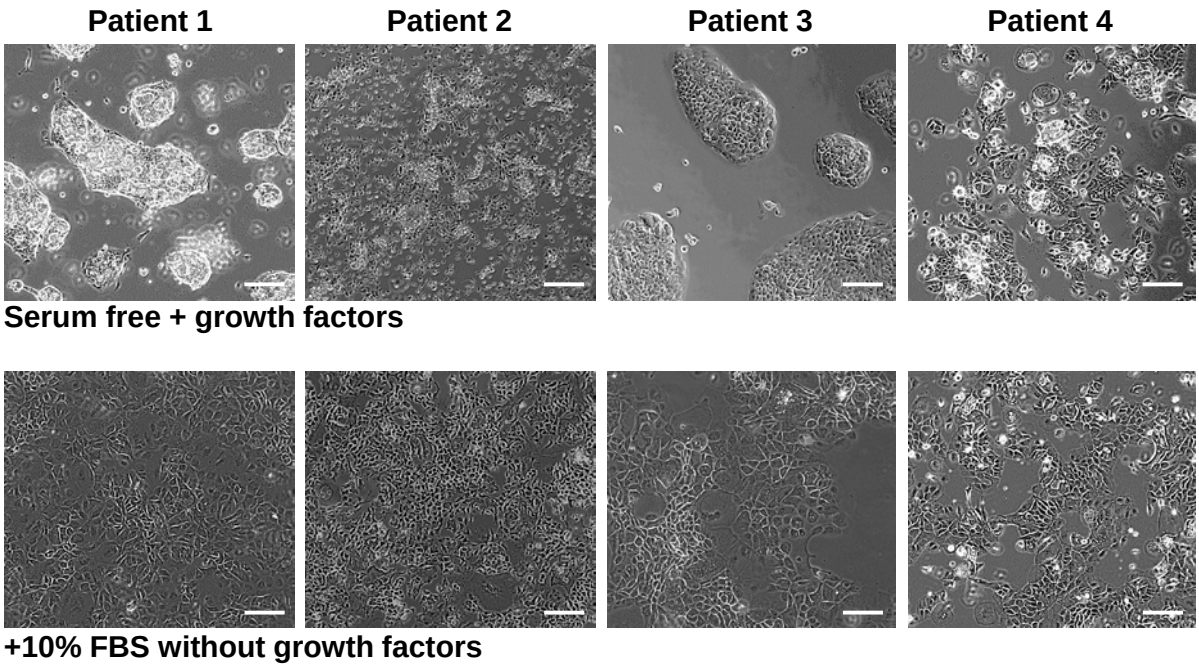

Figure 14: Serum treatment changed PDAC colony cell morphology. Cells derived from four PDAC patients treated with 10% FBS containing medium without growth factors lost 3-dimensional growth and formed monolayers. Serum-treated cells showed loosened cell-to-cell contacts and irregular shapes compared to serum-free controls; scale bars: 100µm.

3.2.2 Serum Treatment Alters the Phenotype of Adherent Colonies

Alterations in cell biology induced by the change in culture conditions were monitored for 5 to 10 passages, with direct comparison of serum-free controls and serum-treated cells derived from the same serum-free established initial culture (figure 15). Possible changes of the cellular differentiation status were monitored via comparative gene expression profiling. The up- or down-regulation of a certain gene in serum-treated cultures was defined as a change in the absolute expression (fold-change) of at least 1 (up) or -1 (down) respectively, representing double or half expression compared to the controls. To distinguish between short and long-term effects, expression profiling was performed at culture passage 3 and 8. Here, 3 passages in 10% FBS containing medium without growth factors represented a time of 25-118 days (P1: 25-26 days; P2: 27-69 days; P3: 47-118 days; P4: 85-105 days), and 8 passages represented a time period of 75-190 days (P1: 75-76 days; P2: 64-129 days; P3: 174-190 days; P4: 85-105 days).

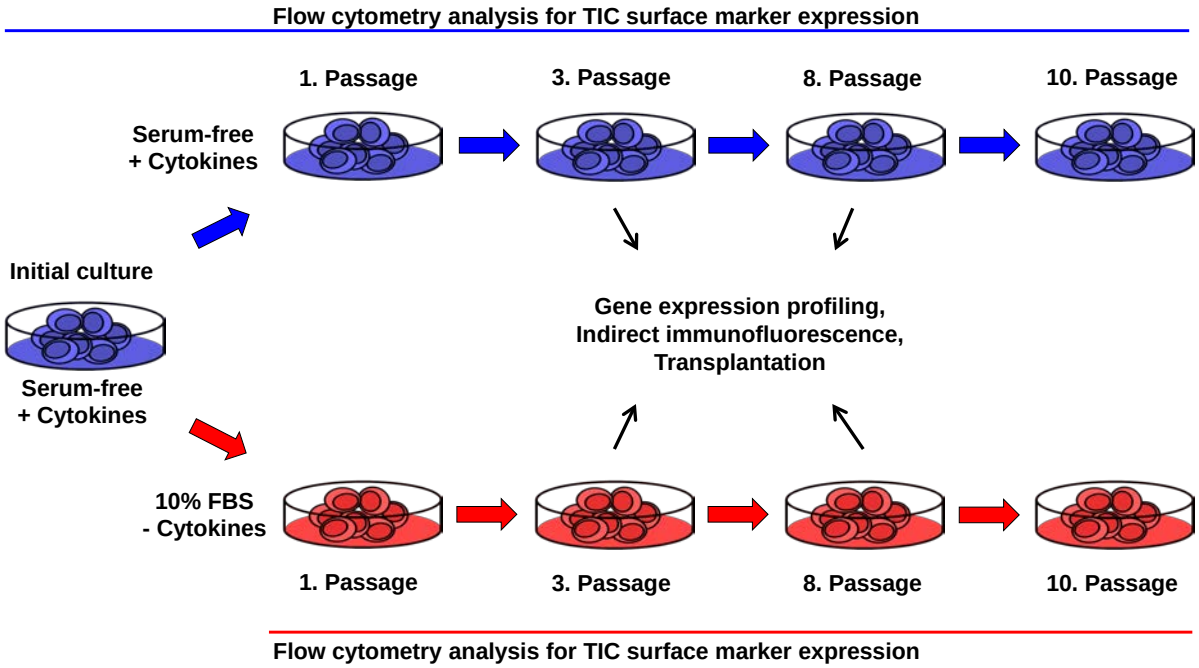

Figure 15: Serum treatment of adherent colony cultures. An initial serum-free culture was split and cultured to equal parts in parallel for up to 10 passages either in serum-free medium containing growth factors or in 10% FBS supplemented medium without growth factors. Initial culture and every subsequent passage were analyzed for pancreatic TIC associated surface marker expression by flow cytometry. In addition, at culture passage 3 and 8 comparative gene expression profiling and simultaneous transplantation into NSG mice were performed to monitor phenotypic and functional differentiation of pancreatic TIC. Besides flow cytometry also indirect immunofluorescence staining was used at passages 3 and 8 to verify gene expression profiling results on protein level.

Gene expression profiling revealed that serum treatment strongly altered the gene expression of cultured primary PDAC cells (figure 16A). The changes in gene expression, however, were specific for each individual patient, such that serum-free and serum cultured cells of each patient clustered together in a dendrogram (figure 16B). Within the cultures of a specific patient, serum-treated cultures clearly differed from the controls. The global gene expression profile was examined for changes involving previously described markers, which would indicate a shift in the phenotypic differentiation of PDAC cells. The analysis focused on genes that indicate a differentiation into the acinar [31, 182-185], ductal [1, 4] and islet cell lineage [186, 187] (appendix A).

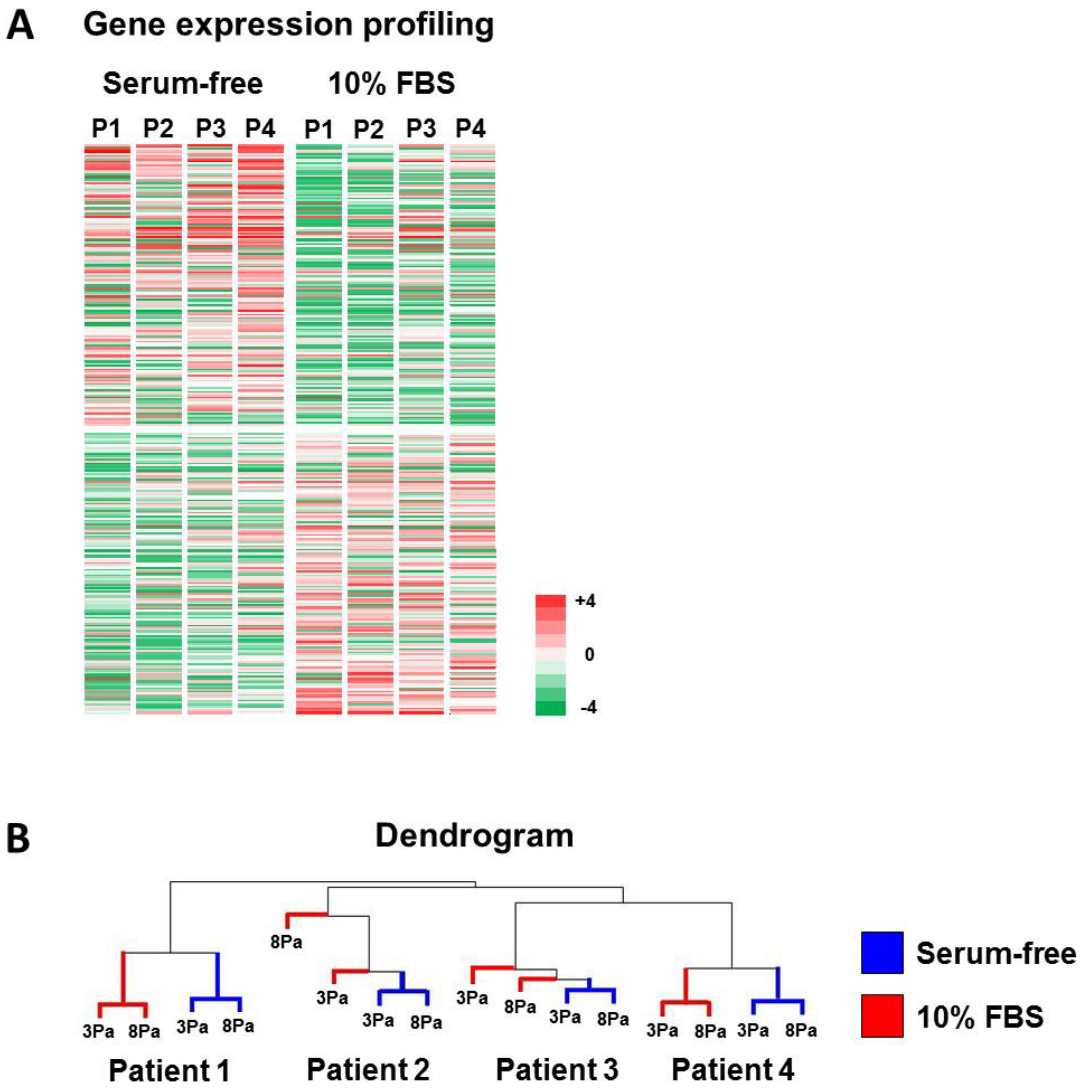

Figure 16: Serum treatment changed gene expression in a patient specific manner. (A) Global gene expression prolife changed upon serum treatment of adherent tumor colony cells; P1-P4: patients 1-4. **(B)** The gene expression profiles of PDAC cell cultures passaged for three or eight passages (3Pa, 8Pa) either in serum-free or 10% FBS supplemented medium without growth factors clustered together for each of four patients. Within the expression profiles of one individual patient serum-treated cultures clustered distinct from serum-free controls.

Under serum-free conditions, cells expressed pancreatic duct and acinar markers as described above (figure 13). Upon serum treatment expression of the duct marker cytokeratin 7 (KRT7) was found to be increased in 3 out of 4 patients (P2, P3, P4) at passage 3 and in 2 patients (P2, P3) at passage 8 (table 3, appendix A). Duct markers like mucin 1 (MUC1), cabonic anhydrase II (CA2) and hepatocyte nuclear factor 6β (HNF6β) were also up-regulated rather than less expressed by serum-

treated cells of P2 and P3. However, examination of acinar markers after serum treatment revealed an up-regulation of genes encoding acinar specific trypsin enzymes (PRSS1, PRSS2 and PRSS3) in P2 and P3. By contrast with all other patients, cells of P1 rather down-regulated ductal and acinar differentiation markers. Differentiation into the pancreatic islet lineage was not observed (appendix A).

Different from pancreatic lineage specific genes, upon serum treatment the expression of markers previously described for pancreatic TIC (CD24, CD133 and ALDH1) [143, 144, 148], reprogramming factors that have also previously been associated with pancreatic TIC function (SOX2 and KLF4) [161, 162, 188] and normal progenitors of the developing pancreas that also modulate pancreatic regeneration in adults (SOX9, NOTCH1 and HES1) [19-23, 36-38] were frequently lower expressed. This indicated a differentiation-like phenotype. These changes appeared in a patient and culture passage specific manner (table 3, appendix A). Substantial changes in the expression of other relevant markers, like CD44, CXCR4, OCT4 and PDX1 were not observed (appendix A).

The results obtained by gene expression profiling were confirmed on the protein level (table 3). CD133, CD44, CD24 and EpCam expression was assessed through flow cytometry for every passage from initial culture establishment until passage 5 to 10. These experiments were performed in duplicates (Ex1 and Ex2, figure 17). Cells from P2 in particular down-regulated the TIC surface marker CD133 to 0% within 5 culture passages as measured by flow cytometry in both Ex1 and Ex2. In, contrast, under-serum free conditions this marker stayed highly expressed by P2 cells at a proportion >10%. For P1, a similar down-regulation of CD133 was observed, but less strongly than had been observed for P2. In contrast, P3-derived cells that showed a low CD133 expression under serum-free control conditions up-regulated CD133 upon serum treatment and reached values comparable to those of the other three patients. CD24 was mildly down-regulated for P1 and P2, whereas for P3 and P4 no substantial differences were measured. For both serum-treated and serum-free control cells of all patients, CD44 and EpCam were equally strong expressed.

Table 3: Differential expression of markers associated with undifferentiated cell populations or mature pancreas cells after serum treatment and withdrawal of growth factors.

Patient	Down-regulated markers in 3Pa	Up-regulated Markers in 3Pa	Down-regulated markers in 8Pa	Up-regulated markers in 8Pa
P1	NOTCH1 ALDH1A1 CA2 MUC1 HNF6β PRSS3	ALDH1A3	KLF4 ALDH1A1 CD133 EpCam KRT19 MUC1 HNF6β PRSS3	NOTCH1 ALDH1A3 CD24 PRSS1
P2	SOX2 MYC KLF4 NOTCH1 ALDH1A1 CD133 HES1	KRT7 MUC1 PRSS2 PRSS3	ALDH1A1 ALDH1A2 CD133 SOX9	ALDH1A3 HES1 CA2 KRT7 MUC1 PRSS3
P3	SOX2 SOX9 MUC1	ALDH1A3 KRT7 PRSS1 PRSS2 PRSS3	SOX2 KLF4 HES1	ALDH1A3 CD133 KRT7 CA2 PRSS1 PRSS3
P4	KLF4 CD133	ALDH1A3 KRT7	CA2 MUC1	-

Serum-treated cultures showed differential expression of markers characteristic for undifferentiated cells (blue color) or acinar and ductal differentiation markers (red color) compared to serum-free cultured controls. Markers of undifferentiated cells were more frequently down-regulated upon serum treatment and differentiation markers were more frequently up-regulated. Gene expression profiling was performed after three culture passages (3Pa, green background) or eight culture passages (8Pa, orange background) for four patients (P1-P4).

For both cultures under comparison, indirect immunofluorescence (IF) analysis for intracellular markers was performed at culture passages 3 and 8. Staining for Sox2 and Krt7 confirmed patient specific expression changes. The cells of all patients expressed Krt7 at high levels under any cell culture condition. However, up-regulation of this marker by serum treatment was also apparent on the protein level, especially for cells of P2, which also showed the strongest down-regulation of Sox2 (figure 18, table 4).

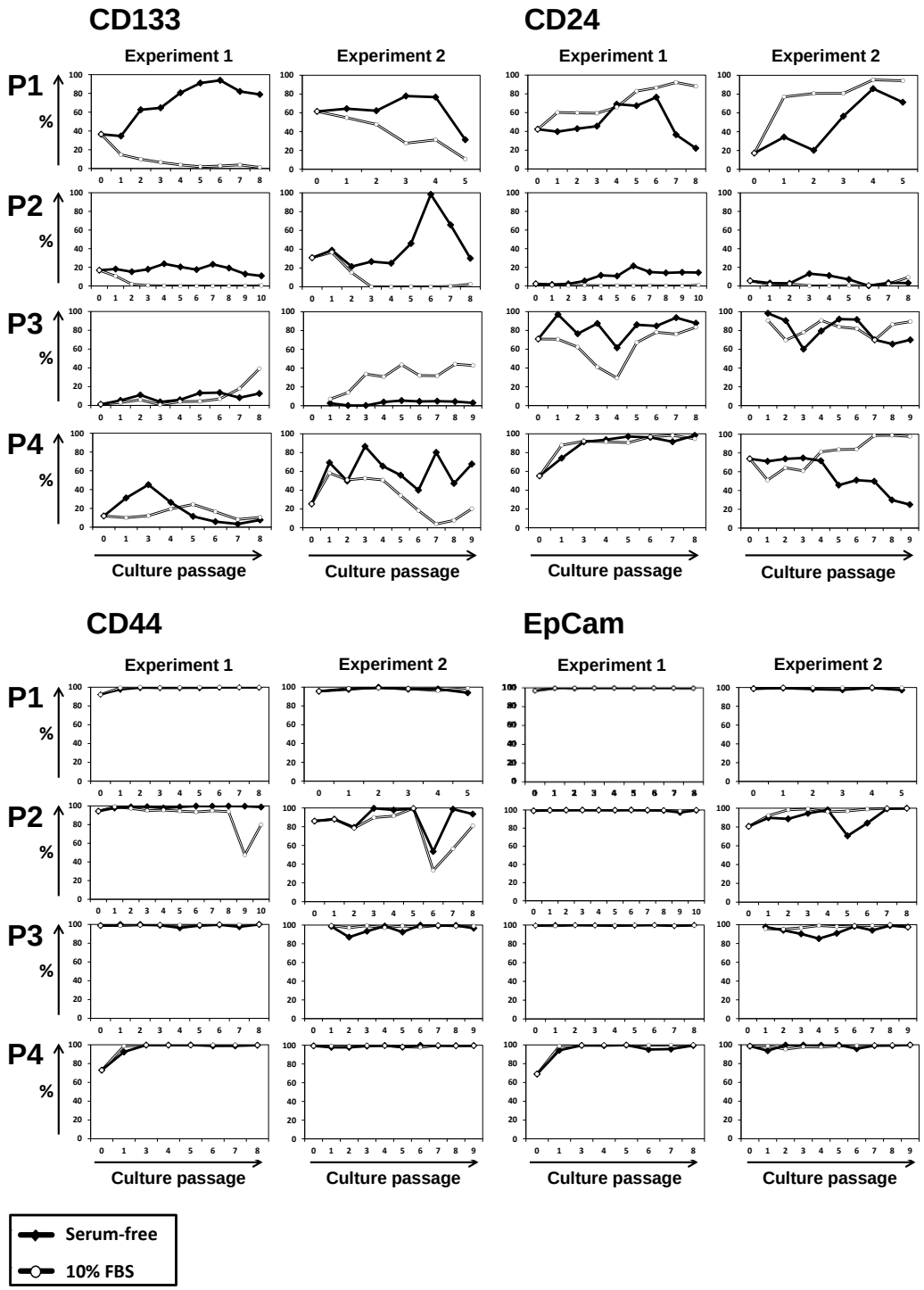

Figure 17: Expression of TIC associated surface markers and EpCam in PDAC cultures under serum-free conditions and after serum treatment. PDAC cultures of four patients (P1-P4) passaged five to ten times showed patient specific expression of CD133. P1 and P2 derived cells down-regulated CD133 after change from serum-free to 10% FBS containing medium without growth factors. In contrast, P3 cells showed higher CD133 values under serum conditions. CD24 was slightly down-regulated by serum treatment for P1 and P2. CD44 and EpCam expression did not differ between both culture conditions. Analysis was performed in two independent experiments (1 and 2).

Table 4: Phenotypic characterization of primary adherent PDAC cell cultures under serum-free conditions and after serum treatment.

	Patient 1		Patient 2		Patient 3		Patient 4	
Marker	Serum-free	10% FBS	Serum-free	10% FBS	Serum-free	10% FBS	Serum-free	10% FBS
Flow Cytometry								
CD133	10 - 94%	1 - 55%	11 - 98%	0 - 37%	0.3 - 14%	1 - 45%	12 - 87%	3 - 60%
CD44	75 - 100%	96 - 100%	86 - 100%	45 - 100%	87 - 100%	97 - 100%	73 - 100%	70 - 100%
CD24	2 - 85%	59 - 96%	0.2 - 22%	0.1 - 10%	60 - 98%	25 - 91%	55 - 94%	55 - 99%
EpCam	87 - 100%	96 - 100%	81 - 100%	92 - 100%	90 - 100%	95 - 100%	69 - 100%	95 - 100%
Indirect Immunofluorescence								
Krt7	+	+	+	+	+	+	+	+
Ptf1a	+	+	+	+	+	+	-	-
Amylase	+	+	n.d.	n.d.	+	+	n.d.	n.d.
Vimentin	+/-	+	-	-	-	-	+	+
Sox2	+/-	+	+	+/-	+	+	-	-
Oct4	+	+	+	+	+	+	+	+
Klf4	+	+	n.d.	n.d.	n.d.	n.d.	n.d.	n.d.

Surface markers previously described to associate with pancreatic TIC function were measured by flow cytometry. Intracellular markers were investigated via indirect immunofluorescence staining. Cultures were assigned + when marker positive cells were noticed in more than one independent visual field of the same sample, +/- was indicated when only single positive cells were visible and – if no positive cells were found; n.d = not determined. Table modified from [179].

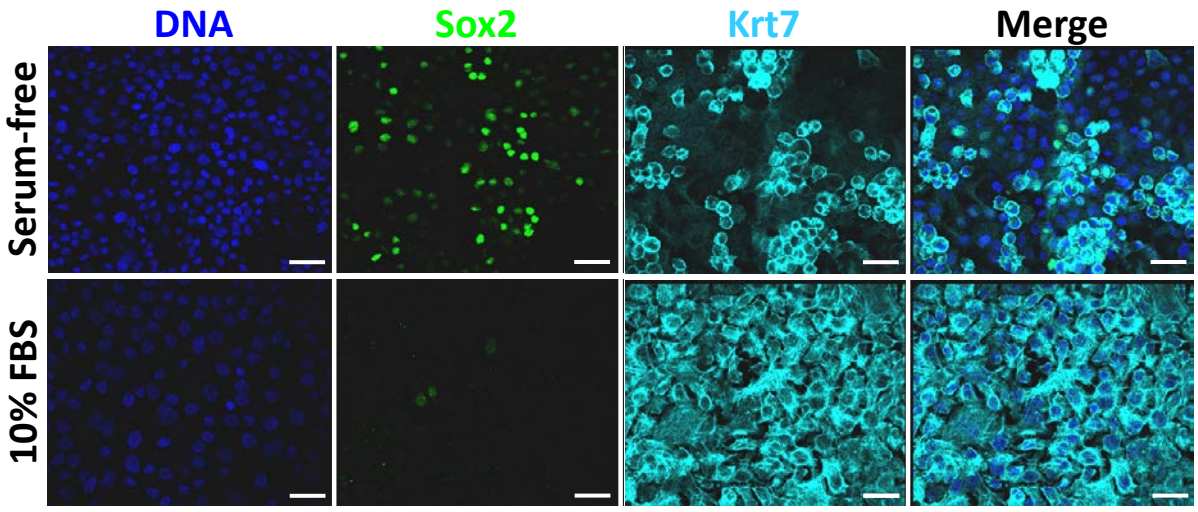

Figure 18: Differentiation-like phenotype of serum-treated PDAC cells. Tumor colony cells of patient 2 (P2) down-regulated Sox2 and up-regulated the pancreatic duct epithelium marker Krt7 after change of culture conditions from serum-free to 10% FBS supplemented medium and withdrawal of growth factors; scale bar: 30µm. Figure modified from [179].

3.2.3 PDAC Cells Retain TIC Potential after Serum Treatment

The results described in the previous section indicate a partial phenotypic differentiation of colony cells by serum treatment. To examine whether the cells were functionally differentiated, we tested their ability to form subcutaneous tumors after 3 and 7 or 8 passages in 10% FBS containing medium without cytokines. Cells from all 4 patients gave rise to xenograft tumors, indicating sustained tumor-initiating potential (figure 19 and 20) without any changes in the patient-specific histology (figure 20). The sizes of tumors initiated by serum-treated cells were not significantly different from tumors formed by serum-free control cells upon transplantation of 3rd passage cells (figure 19). After 7 to 8 passages of serum treatment, the tumor weights were significantly lower ($p<0.001$), but tumors grew in 20 of 24 animals compared to 23 of 24 observed for controls. The tumors induced by serum-treated and control cells were equally transplantable into secondary and tertiary recipient mice (2°/3°), again without differences in histology (figure 20). However, tumors from serum-treated cells passaged 7 to 8 times were again significantly smaller in secondary mice ($p<0.005$), but cells engrafted in 12 out of 12 animals compared to 10 out of 12 observed for serum-free control cells. In third generation mice no substantial differences in tumor weights were measured. However, it is worth mentioning that for individual patients, serum treatment specifically induced a higher or lower tumor weight compared to serum-free control tumors (figure 19).

3.2.4 CD133$^-$ PDAC Cells Initiate Tumors and Reconstitute the CD133$^+$ Population

CD133 has previously been described to predict for TIC function in heterogeneous cell populations derived from primary PDAC samples [144]. Similar findings have been made in other solid tumor entities [135-138]. By contrast with what was observed in the literature, *in vitro* expression of CD133 did not seem to correlate well with the *in vivo* data described above. Thus, the potential of CD133 as TIC marker was assessed by cell sorting. Between $1x10^6$ and $2x10^7$ serum-free cultured control or serum-treated cell populations were sorted according to their CD133 (P2, P3) or combined CD133/CD44 (P1) expression.

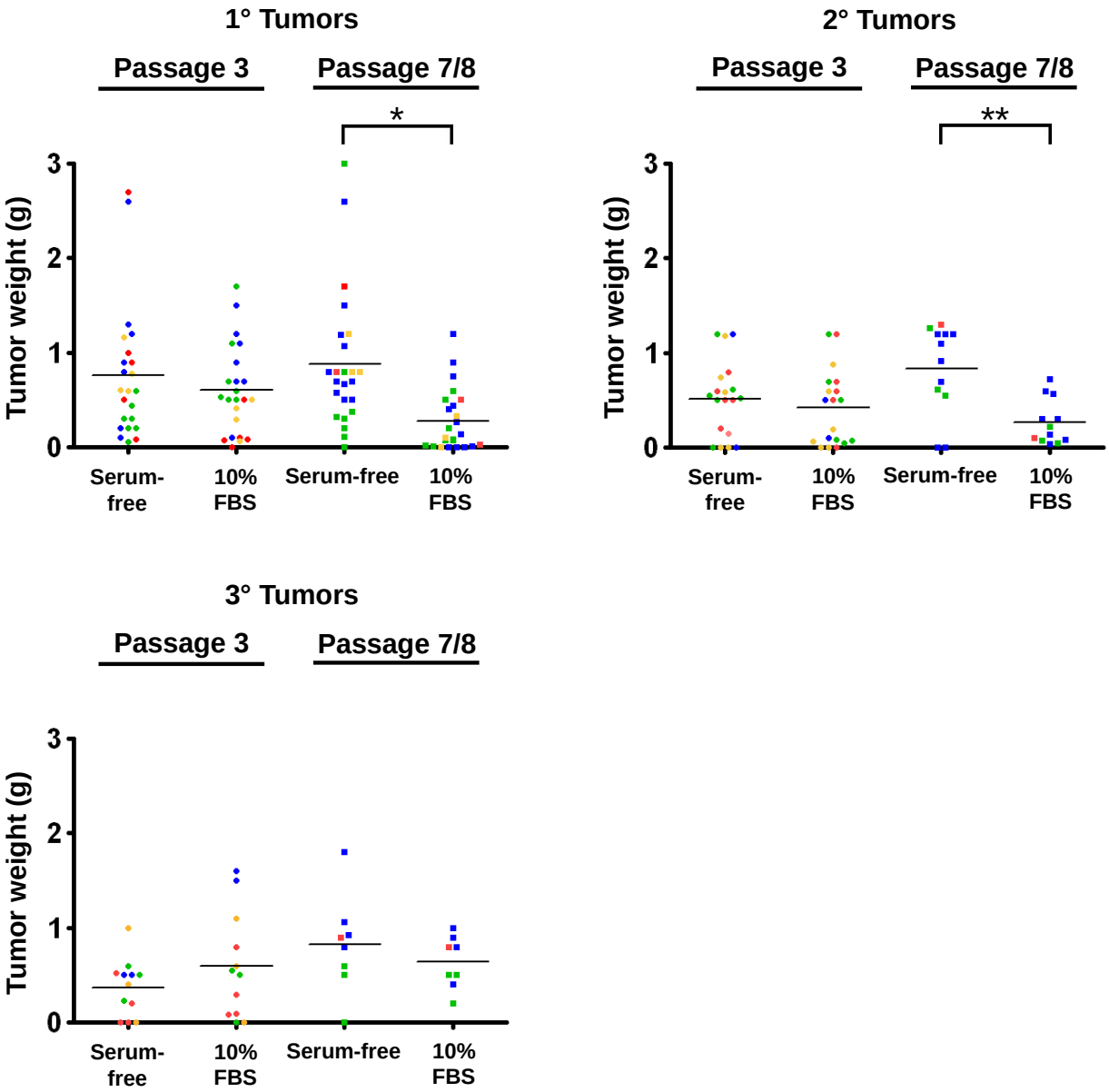

Figure 19: Serum-treated colony cells retained TIC potential in serial transplantation. First generation tumors (1°) in NSG mice initiated by cells cultured for 3 passages in serum containing medium without growth factors had equal weights compared to control tumors initiated by serum-free grown colony cells (n=23). In secondary (2°) (n=19) and tertiary (3°) (n=12) animals no significant differences were observed. After 7 or 8 passages under serum conditions 1° tumors were significantly smaller (*p<0.001), but still 20 of 24 transplantations derived tumors (23 of 24 observed in controls). In 2° animals transplanted derived from 7 or 8 passage serum-treated cells again significantly smaller tumor weights were measured (**p<0.005), but also a higher engraftment in 10 of 12 mice compared to 12 of 12 observed for control cells. For 3° tumors no differences were observed. Tumor weight indicated in grams (g). Graphs show results of four patients (P1-P4), indicated by differently colored dots representing one tumor each; P1: red; P2: green; P3: blue; P4: yellow.

The purity of CD133-negative sorted fractions ranged to 100% (table 5). Upon subcutaneous transplantation into NSG mice, however, all fractions formed tumors equally (table 5, figure 21A). Tumors derived from sorted CD133 negative cells expressed CD133 to an equal proportion as tumors originating from the respective $CD133^+$ fraction (table 5, figure 21B). No differences were detectable in histology (figure 22), and all fractions showed equal tumor-initiating capacity in serial transplantation. Moreover, when P1 cells were sorted for combined CD44 and CD133 expression all fractions showed equal tumor-initiating capacity and serial transplantability (table 5). As observed for CD133, the proportion of $CD44^+$ cells in the transplanted fraction was not predictive for CD44 expression in the resulting xenograft tumors.

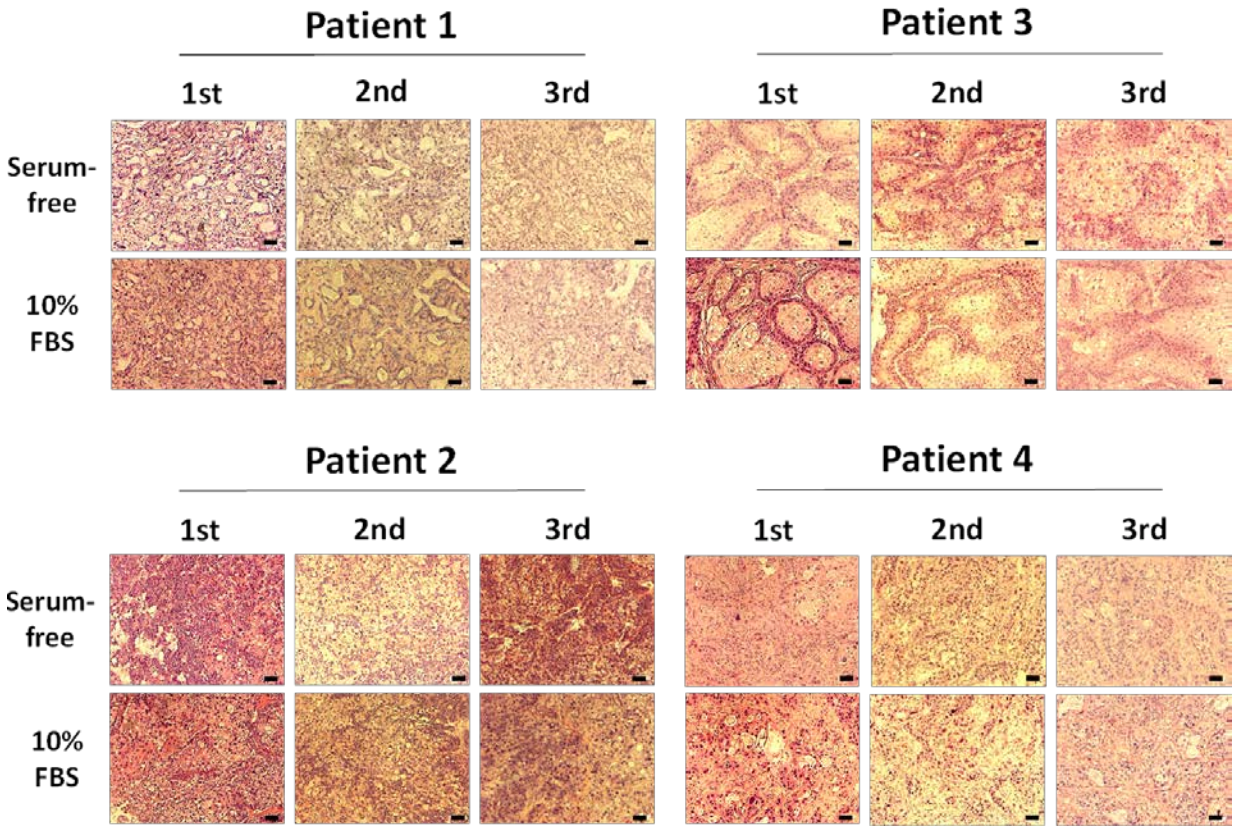

Figure 20: The histology of xenograft tumors remains unchanged in serial transplantation. No difference in the histology of xenografted tumors was observed after serial transplantation of serum-treated or serum-free control TIC; scale bars: 100µm. Figure modified from [179].

Table 5: CD133(/CD44) expression did not predict for tumor-initiating potential.

Patient 1

Fraction	Sorted from	% CD44-/ CD133- in sort re-analysis	% CD44+/ CD133- in sort re-analysis	% CD44-/ CD133+ in sort re-analysis	% CD44+/ CD133+ in sort re-analysis	Tumor (g)	CD44 in vivo (%)	CD133 in vivo (%)
$CD44^-/CD133^-$	Serum-free	93.2	3.6	2.8	0.4	1.9	6.2	42.4
$CD44^+/CD133^-$	Serum-free	49.1	45.5	4.7	0.7	0.9	6.5	36.1
$CD44^-/CD133^+$	Serum-free	33.1	4.8	61.0	1.1	1.2	5.7	39.4
$CD44^+/CD133^+$	Serum-free	51.5	12.3	32.9	3.3	1.6	4.2	35.1

Patient 2

Fraction	Sorted from	% CD133 in sort re-analysis	Tumour 1 (g)	CD133 in vivo (%)	Tumour 2 (g)	CD133 in vivo (%)
$CD133^-$	Serum-free	0.6	0.8	31.9	0.6	n.d.
$CD133^{+/-}$	Serum-free	56.7	0.45	20.8	0	
$CD133^+$	Serum-free	99	0.15	21.7	0	

Fraction	Sorted from	% CD133 in sort re-analysis	Tumour 1 (g)	CD133 in vivo (%)	Tumour 2 (g)	CD133 in vivo (%)	Tumour 3 (g)	CD133 in vivo (%)
$CD133^-$	10% FBS	0.0	0.4	22.8	0.6	21.9	0.1	n.d.

Patient 3

Fraction	Sorted from	% CD133 in sort re-analysis	Tumour 1 (g)	CD133 in vivo (%)	Tumour 2 (g)	CD133 in vivo (%)
$CD133^-$	10% FBS	1.8	1.1	0.2	0.7	0.7
$CD133^{+/-}$	10% FBS	22.9	0.35	0.2	0.3	0.4
$CD133^+$	10% FBS	51.8	0.4	0.2	0.6	0.5
$CD133^{--}$	10% FBS	0.1	0.5	0.2	n.d.	

Sorted $CD133^+$ and $CD133^-$ cell fractions from three patients were equally capable to form tumors in NSG mice. Tumors formed from highly purified $CD133^-$ and $CD133^+$ cell fractions contained an equal proportion of cells expressing CD133 (CD133 *in vivo*). Cells of patients 2 and 3 were transplanted in duplicates or triplicates (Tumor 1, 2 or 3). Tumor weights are specified in grams (g). Besides CD133 positive enriched fractions ($CD133^+$) intermediate fractions ($CD133^{+/-}$) were sorted. For enrichment, $CD133^-$ cells were sorted once ($CD133^-$) or twice ($CD133^{--}$). Cells derived from patient 1 were sorted for CD133 and CD44 simultaneously. Also CD44 expression in transplanted fractions did not correlate with tumor growth and with the $CD44^+$ proportion in initiated tumors (CD44 *in vivo*). Purity of transplanted sort fractions is indicated by the % proportion of marker positive cells measured in reanalysis. Table modified from [179].

When 100% CD133 negative cells of P2 were taken into culture, cells reconstituted CD133 expression within 8-35 days (table 6). In contrast, under serum conditions this effect was not observed and CD133 values stayed at 0.0-0.1% at days 1, 8 and 35.

These data show that there is a subpopulation of $CD133^-$ TIC capable of giving rise to $CD133^+$ PDAC cells *in vivo* and *in vitro*.

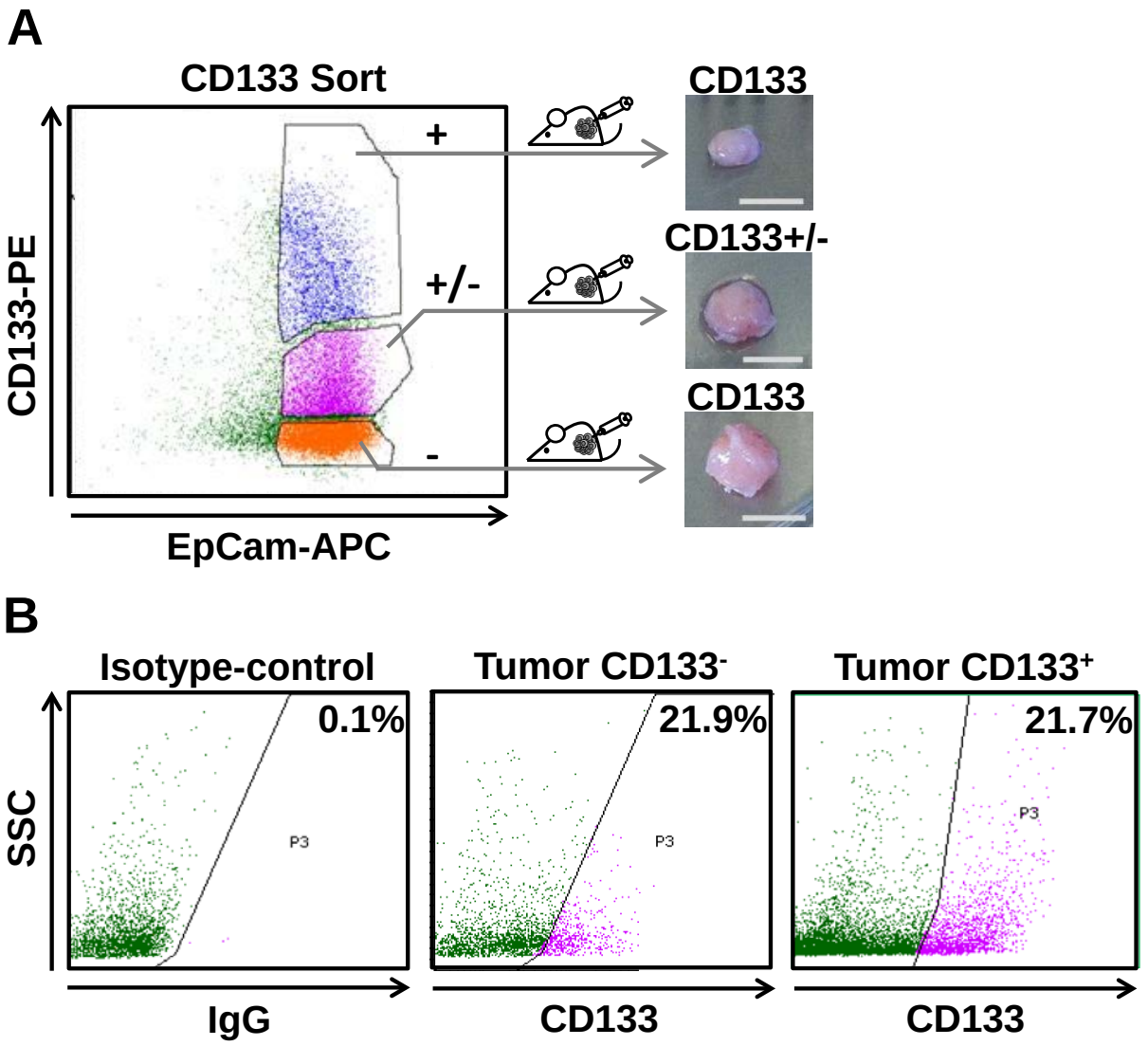

Figure 21: Phenotypic plasticity of pancreatic TIC. (A) After transplantation of sorted $CD133^+$, intermediate and $CD133^-$ cell populations, all fractions equally initiated tumors (scale bars: 1cm). **(B)** Tumors initiated by CD133 enriched or CD133 depleted fractions showed equal proportions of $CD133^+$ cells. Figure modified from [179].

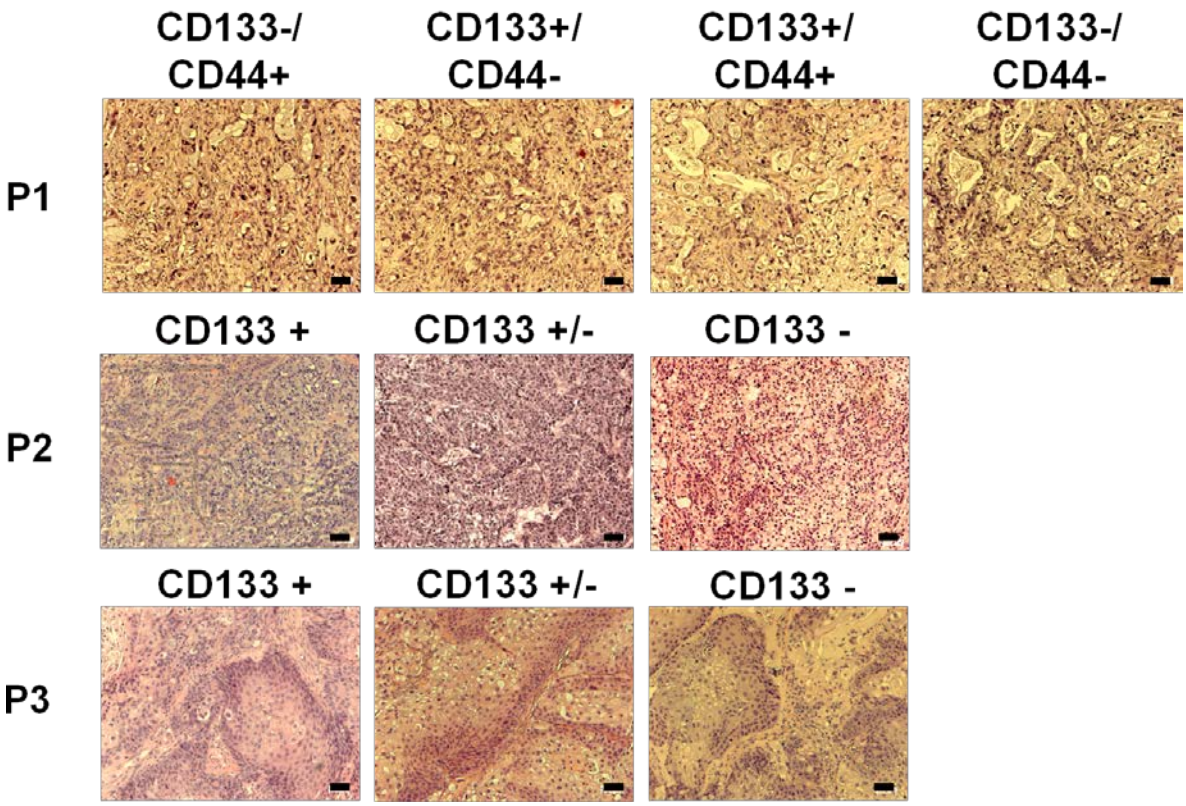

Figure 22: Depletion or enrichment for CD133 and CD44 by cell sorting had no influence on xenograft tumor histology. All sorted fractions formed tumors with similar patient specific histology. The figure shows results for three patients (P1-P3); scale bars = 100µm. Figure modified from [179].

Table 6: CD133-negative PDAC cells restored CD133 expression *in vitro*.

Culture	Stain	Day 1	Day 8	Day 35
P2 serum-free	CD133	0.0%	1.9%	38.5%
P2 serum-free	IgG	0.0%	0.1%	0.1%
P2 10% FBS	CD133	0.0%	0.1%	0.0%
P2 10% FBS	IgG	0.0%	0.0%	0.0%

Serum-treated cells derived from P2 were sorted for CD133 negative cells to 100% purity and cultured in growth factor supplemented serum-free medium or 10% FBS containing medium without growth factors. Compared to isotype controls (IgG) serum-free cultured cells up-regulated CD133 to values regularly measured for P2. In 10% FBS containing medium no such CD133 expression was observed. Table shows flow cytometry data indicating the percentage proportion of $CD133^+$ cells in culture measured 1, 8 and 35 days after sort.

Summary chapter 3.2

Tumor colony cultures were treated with 10% FBS-containing medium without growth factors and subsequently lost three-dimensional growth and tight cell-to-cell contacts. Cells commonly down-regulated markers characteristic for undifferentiated cell populations and up-regulated pancreatic differentiation markers. Despite this differentiation-like phenotype, cells retained their tumorigenicity and self-renewal in NSG mice. Sorting for pancreatic TIC markers CD133 and CD44 revealed no correlation between these cell surface molecules and tumor growth. Moreover, pure negatively sorted fractions restored CD133 expression *in vitro* and *in vivo*.

3.3 Clonal Composition of the Pancreatic TIC Compartment

Despite recent evidence for tumor-initiating cells (TIC) or so-called cancer stem cells (CSC) in pancreatic cancer (see section 1.3.2) the clonal dynamics within the pancreatic TIC compartment remain unknown. To visualize the contribution of individual TIC clones to long-term tumor growth tumor colony cells of 3 patients (P1-P3) were lentivirally marked and serially transplanted into highly immunodeficient NOD.Cg-Prkdc^{scid}Il2rg^{tm1Wjl}/SzJ (NSG) mice over three generations (figure 23). The tumors which formed were harvested and dissociated to receive a single cell suspension. A representative proportion of dissociated tumor cells was analyzed by LAM-PCR (see section 1.4) and subsequent high-throughput 454-sequencing for lentiviral integration sites (IS) as described previously [113, 163, 168, 169, 189]. An equal proportion of the single cell suspension as analyzed by LAM-PCR was further transplanted into next generation recipient mice.

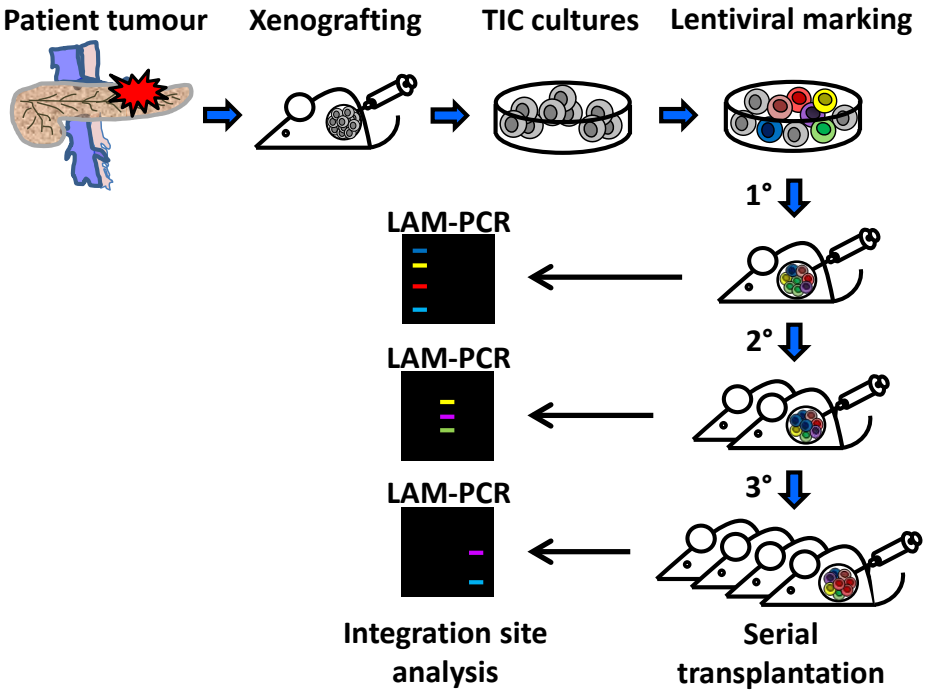

Figure 23: Clonal composition of the pancreatic TIC compartment. Primary human pancreatic tumor-initiating cells (TIC) were expanded in xenograft tumors and adherent cultures. TIC were genetically marked by transduction with lentiviral vectors and transplanted under the skin, the kidney capsule or into the pancreas of NSG mice. Cells dissociated from first generation tumors (1°) were serially transplanted into second (2°) and third (3°) generation mice. Lentiviral insertion sites (IS) in the genome of TIC clones were analyzed by LAM-PCR and high-throughput sequencing using large aliquots of DNA isolated from dissociated cells derived from all tumors. Figure was taken from [179].

3.3.1 Efficient Lentiviral Marking Does not Change Xenograft-Tumor Biology

To analyze the clonal composition of the pancreatic TIC compartment, tumor colony cells derived from three patients (P1-P3) were lentivirally marked using a self-inactivating (SIN) lentiviral vector (LV106). Prior to transduction, tumor colony cells were passaged 1 to 5 times in serum-free medium to remove murine cells from the colony cultures. At a multiplicity of infection (MOI) between 1 and 40, the cells were transduced to an efficiency of 35.5% to 97.5% (P1: 50%; P2: 97.5%; P3: 35.5% and 83%) measured 3 days after transduction. Upon transplantation of between $1x10^4$ to $5x10^5$ cells under the skin, the kidney capsule or orthotopically into NSG mice, tumor formation time was not altered by lentiviral marking (transduced: 6-13 weeks; non-transduced: 6-12 weeks). No differences of tumor histology were observed between lentivirally marked and unmarked tumors (figure 24).

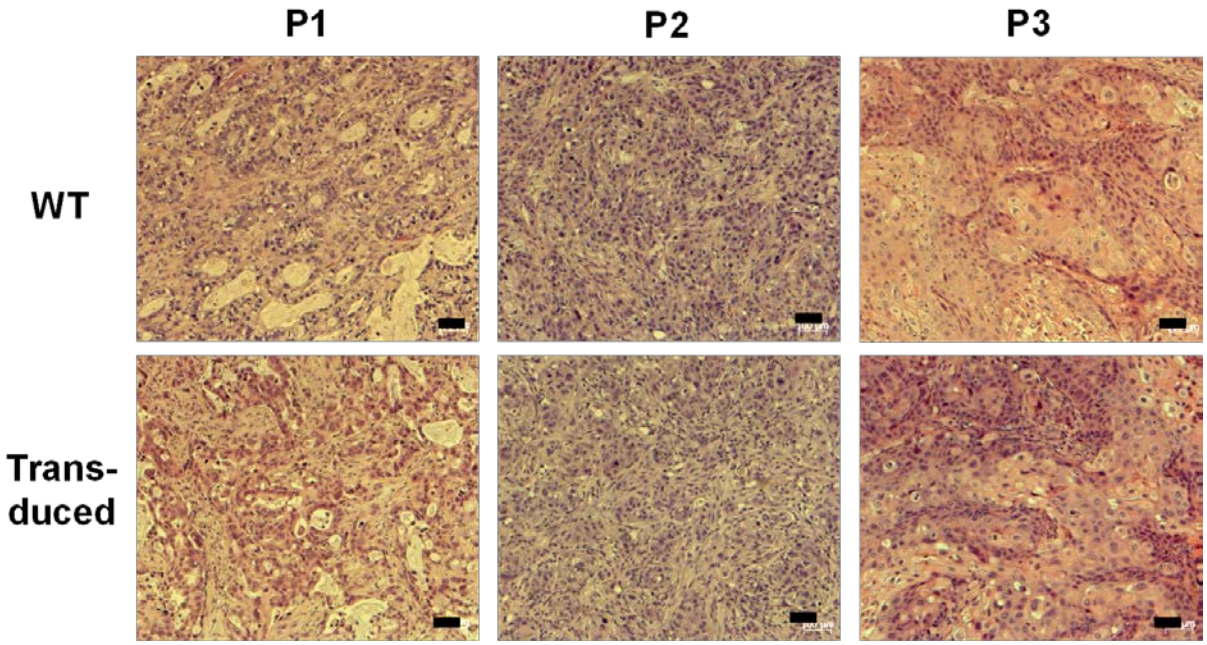

Figure 24: Lentivirally marked tumors retain their patient specific histology. Histopathology analysis of transduced and wild type (WT) xenograft tumors revealed no differences for 3 examined patients (P1-P3). Figure modified from [179].

3.3.2 Pancreatic Xenograft Tumors Show Little Clonal Overlap in Serial Transplantation

Using lentivirally marked cells of patients P1-P3, five different experiments were performed, one for P1 (P1-1), one for P2 (P2-1) and three for P3 (P3-1, P3-2 and P3-3). During serial transplantation the tumor tissue was expanded in each experiment from one primary mouse (1°) to two or three secondary mice (2°), and then to between two and six tertiary (3°) mice. Each tumor generated within the serial transplantation line was dissociated to obtain a homogenous single cell suspension. In generations 1° and 2°, 1/3 to 1/2 of all purified cells were further transplanted into next generation recipient mice in equal proportions. Genomic DNA was isolated from 2% to 10% of all purified tumor cells in all three generations and analyzed by LAM-PCR. The experimental procedure of LAM-PCR creates a single DNA fragment of a specific size for each TIC clone (see section 1.4). In gel electrophoresis of these LAM-PCR products, the 1°, 2° and 3° tumors were observed to be highly polyclonal (figure 25A). However, the DNA band pattern in the gels seemed to be unique for each individual tumor. To identify and track individual TIC in long-term tumor growth, LAM-PCR products were subjected to 454-high-throughput-sequencing to find the exact site of the vector-genome junction that is unique for every individual clone. Through subsequent data analysis using BLAT [190], clones were visualized in a heat-map for each experiment and sorted by their relative contribution to individual tumors (figure 25B and figure 26).

Analysis of detected integration sites (IS) representing individual TIC clones revealed a homogeneous distribution throughout all human chromosomes. Thus, no bias due to vector-driven expansion of certain clones was noted (appendix B). In 1st generation tumors, between 4 and 16 IS were detected representing between 0.003% and 0.113% of the transplanted lentivirally marked tumor cell clones (figures 31 and 32). The total number of IS detected per tumor remained constant in the subsequent generations (2° tumors: 2-18; 3° tumors: 3-21). Strikingly, the majority of IS in 2° and 3° tumors were different from those detected in 1° samples. From a total of 203 distinct IS found in all five experiments, 53 (26.1%) were contained in 1° tumors, whereas 150 (73.9%) were found in 2° and 3° tumors. The IS detected in primary mice accounted for 13%-40% of all IS in the respective experiment, so that

60%-87% were found in 2° and 3° animals. Thus, the majority of 2° and 3° tumor mass was formed by clones not detected in 1° tumors. Moreover, between 20% and 95% of all IS in individual tumors were unique, indicating that they were not found in any other tumor of the analysis (table 7). Taking together all experiments, 141 of 203 distinct IS were unique (69.5%).

Table 7: Integration site analysis of lentivirally marked tumors in serial transplantation.

Tumor	P1-1 total	P1-1 novel	P1-1 unique	P2-1 total	P2-1 novel	P2-1 unique	P3-1 total	P3-1 novel	P3-1 unique	P3-2 total	P3-2 novel	P3-2 unique	P3-3 total	P3-3 novel	P3-3 unique
1°	7	7 (100)	5 (71.4)	15	15 (100)	3 (20)	11	11 (100)	10 (90.9)	16	16 (100)	8 (50)	4	4 (100)	2 (50)
2°	5	4 (80)	1 (20)	13	8 (61.5)	5 (38.5)	6	6 (100)	4 (66.7)	9	6 (66.7)	4 (44.4)	7	7 (100)	4 (57.1)
2°	8	8 (100)	5 (62.5)	8	3 (37.5)	2 (25)	6	6 (100)	4 (66.7)	18	14 (77.8)	11 (61.1)	11	9 (81.8)	6 (54.5)
2°	2	1 (50)	0 (0)												
3°	6	3 (50)	2 (33.3)	21	8 (38.1)	5 (23.8)	7	5 (71.4)	4 (57.1)	12	7 (58.3)	5 (41.7)	3	3 (100)	2 (66.7)
3°	11	6 (54.5)	4 (36.4)				7	5 (71.4)	4 (57.1)	14	9 (64.3)	5 (35.7)	4	1 (25)	0 (0)
3°													4	2 (50)	1 (25)
3°	10	4 (40)	2 (20)	21	8 (38.1)	5 (23.8)	4	3 (75)	3 (75)	9	3 (33.3)	1 (11.1)	9	8 (88.9)	7 (77.8)
3°	4	1 (25)	1 (25)				5	5 (100)	5 (100)	13	9 (69.2)	7 (53.8)			
3°	3	2 (20)	0 (0)												
3°	10	6 (60)	4 (40)												

Individual serially transplanted xenograft tumors of three generations (1°/2°/3°) are depicted as rows. Colors indicate which 3° tumors descend from which 2° tumor. Table shows results of five experiments from three different patients; P1-x: patient number 1–experiment number x. The number of total insertion sites (IS) represents all IS in a respective tumor, independent if that IS was also found elsewhere in the same experiment. Novel IS are those which appear at first time and were not detected in generation(s) before, but may be detected again in subsequent tumors of that experiment. Unique IS were found only in one individual tumor and never before or again. Proportion in % of total IS is indicated in brackets for novel and unique IS.

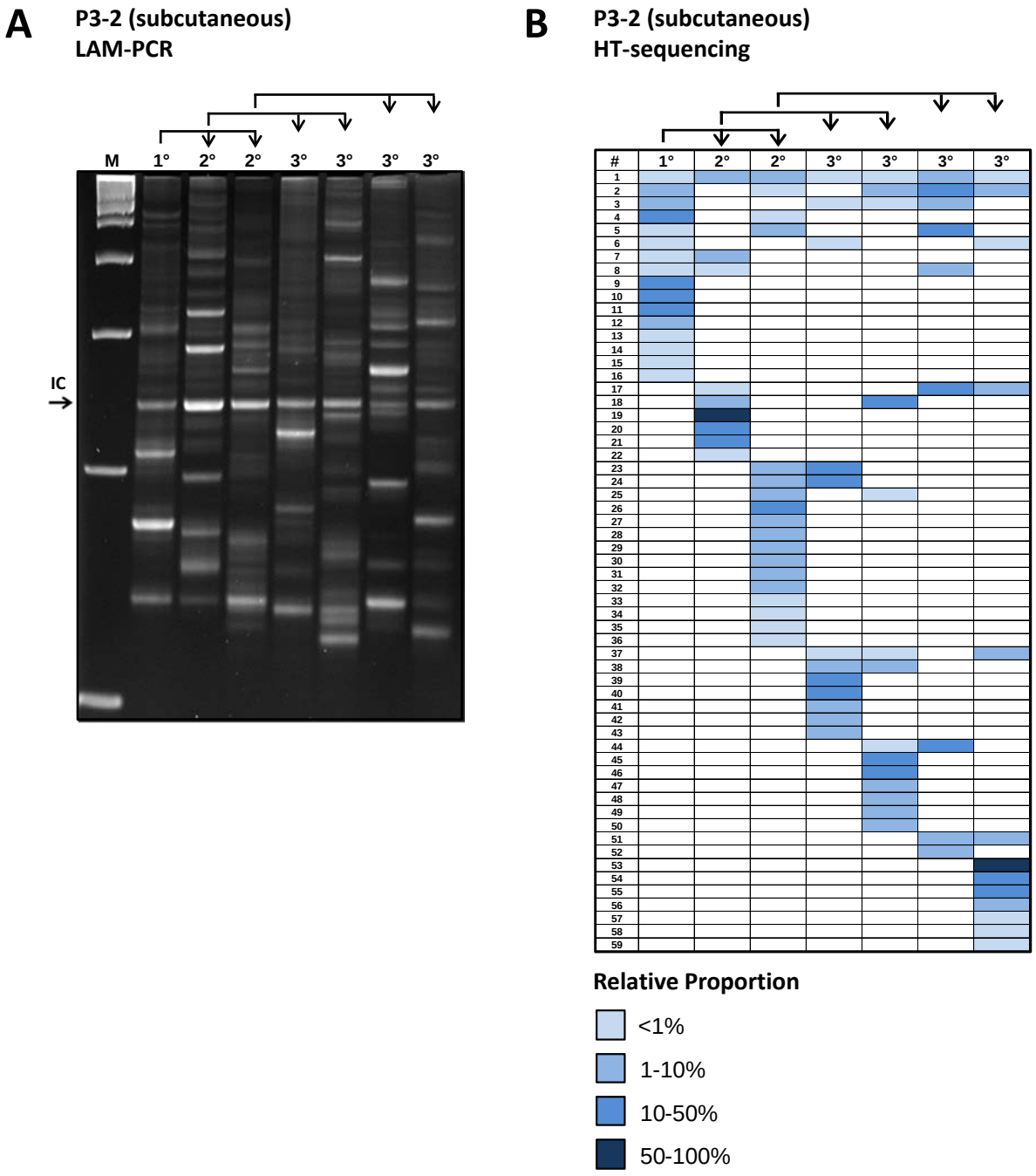

Figure 25: Serially transplanted xenograft tumors shared low clonal overlap. (A) Gel electrophoresis of LAM-PCR products depicts individual TIC clones as DNA bands of a clone specific size; tumors of serial transplantation line over 3 generations (1°/2°/3°) in NSG mice were highly polyclonal. Band pattern appeared unique for each individual tumor reminiscent of a low clonal overlap between distinct tumors. **(B)** High-throughput-sequencing (HT-sequencing) of LAM-products followed by identification of the TIC clone specific genomic integration site confirmed low clonal overlap between distinct tumors, so that the majority of tissue mass in 2° and 3° tumors was formed by clones that were not detected before. This figure shows data of experiment 2 using lentivirally marked cells of patient 3 (experiment P3-2). Blue colored fields indicate relative contribution of individual clones to their respective tumor (see color legend); rows of the heat-map indicate individual lentiviral insertion sites; columns represent individual xenograft tumors; arrows specify serial transplantation steps; IC: internal control. Figure modified from [179].

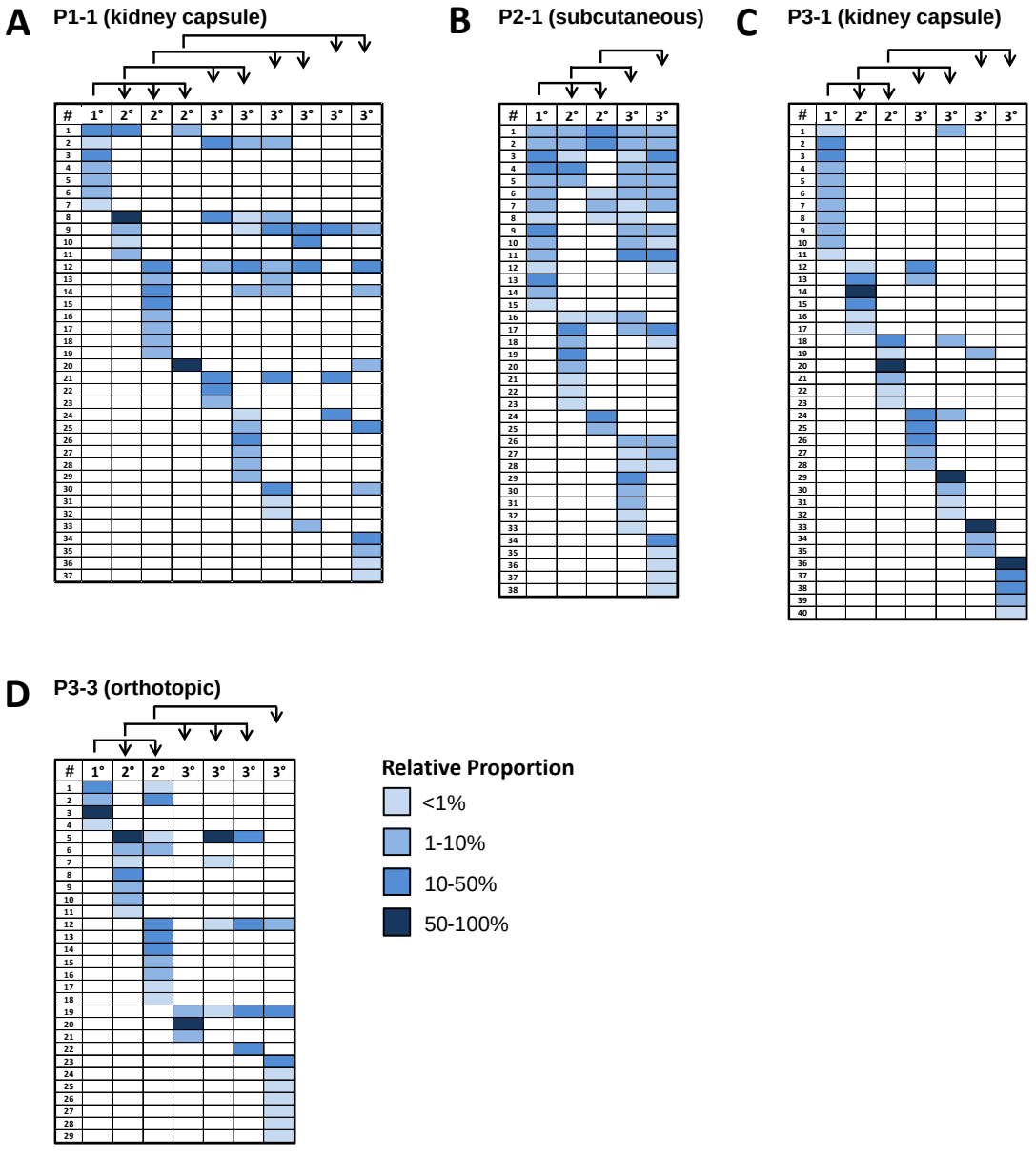

Figure 26: Clonal succession drives long-term tumor growth in pancreatic cancer. (A-D) LAM-PCR and high-throughput-sequencing visualize TIC clones by their specific lentiviral insertion sites (IS), indicated as rows in the heat-map. Individual xenograft tumors of the serial transplantation line over 3 generations (1°/2°/3°) are depicted as columns. Tumors were grown subcutaneously **(B)**, under the kidney capsule **(A, C)** or in the pancreas (orthotopic) **(D)** of NSG mice. Serially transplanted tumors are mainly formed by distinct successive clones. Lentivirally marked tumor cells derived from 3 patients were transplanted; P1-x: patient number 1–experiment number x; Blue colored fields indicate relative contribution of individual clones to their respective tumor (see color legend); arrows specify serial transplantation steps. Figure modified from [179].

454-sequencing confirmed the observation made in gel electrophoresis, namely, that each tumor of an individual experiment bears a largely distinct set of TIC clones. To quantify this observation, the clonal overlap between one tumor and its next generation progeny was calculated. For that evaluation, the clonal overlap was calculated by dividing the IS shared between a parental tumor and its successive next generation progeny by the number of IS contained in the parental tumor. In 31 of such parental tumor pairs, the clonal overlap was calculated to be between 0% and 50% (mean 19.4%, +/-16.4%). When pairs of tumors were transplanted from one parental tumor, the clonal overlap between both next generation tumors was calculated by the division of the number of total IS shared by both tumors through the number of total distinct IS found in sum of both tumors. Thereby, for 17 of such fraternal tumor pairs, a clonal overlap between 0% and 60% (mean 14.2%, +/-14.2%) was observed. Moreover, most often the strongest clones contributing to tumor formation disappeared after re-transplantation and were replaced by clones that were not detected before (figure 25 and 26). This analysis therefore demonstrated that the tumorigenic activity of pancreatic TIC clones was transient, and long-term tumor growth was mainly driven by the succession of such clones.

3.3.3 Statistical analysis

The statistical analysis of the data described in this chapter was performed by Prof. Dr. Dr. Ulrich Abel from the NCT, Heidelberg. The findings described below were formulated in close collaboration.

3.3.3.1 Clone numbers and sizes

The results shown in 3.3.2 show that after re-transplantation from primary mice into next-generation recipients large TIC clones were frequently replaced by clones that had not been previously observed. However, these later-detected clones must already have been present in the primary mice, because those 2° and 3° tumors, where these clones initially appeared in LAM-PCR analysis, were initiated by dissociated tumor cells of the 1° tumors. To retrieve a measurement for the clone

sizes of these later-detected clones we calculated an upper 99% confidence bound for the number of cells in clones present but not detected in 1° generation xenograft tumors. The number of cells contained in undetected clones was limited from 50 to 262 in 1° (table 8). Assuming the worst case, that each undetected clone consists of a single cell, this is also an upper bound for the number of undetected clones.

Thus, taking into account the 29 to 59 distinct clones that were detected by LAM-PCR for individual experiments, one can safely assume that at most 96 to 302 clones were contained in 1° generation tumors resulting in a seeding efficiency of between 0.026% and 2.7% (table 8). Moreover, from these results it is possible to derive upper bounds for the mean size of TIC clones that were initially detected in 2° and 3° tumors, but not in 1° samples. According to this analysis, the mean size of later-detected clones in 1° was between 1 to 9 cells at an upper 99% confidence bound (appendix C, table 8). However, considering an upper 99.999% confidence bound this number did not exceed 2-20 cells (appendix C).

Table 8: Statistical analysis of clone sizes, clone numbers and seeding efficiencies.

Experiment	Total detected clones	Later detected clones (in 2° and 3°)	Max. cell number in clones not detected in 1°	Later detected clone max. mean size in 1° (cells)	Lentivirally marked cells transplanted	Max. number of engrafted clones	Max. seeding efficiency in 1° (%)
P1-1	37	30	149	5	250000	186	0.074
P2-1	38	23	205	9	48750	243	0.498
P3-1	40	29	262	9	415000	302	0.073
P3-2	59	43	50	1	415000	109	0.026
P3-3	29	25	67	3	3550	96	2.704

Xenograft tumors initiated by lentivirally marked PDAC cells were serially transplanted of three generations (1°/2°/3°). The majority of total clones is detected in 2° and 3° tumor generation. The maximal (max.) number of cells in undetected clones in 1° tumors was calculated assuming the worst case that each undetected clone consists of a single cell. Since the number of later-detected clones represents the minimal number of clones not detected in 1°, an upper bound for the mean number of cells in undetected clones is obtained by dividing the maximal number of cells in undetected clones by the minimal number of undetected clones in 1°. Adding the detected clones and the maximal number of undetected clones gives the maximal number of engrafted clones. Division of the maximal number of engrafted clones by the number of transplanted lentivirally marked cells yields the maximal seeding efficiency. Table shows results of five experiments from three different patients; P1-x: patient number 1–experiment number x. Maximum numbers are understood to represent upper 99% confidence bounds.

3.3.3.2 Analysis of proliferation rates and seeding efficiency

The data were further analyzed to elucidate the following null hypotheses:

a) Proliferation rates of all clones in a tumor are identical.

b) Proliferation rates of clones in the primary or secondary mice do not change from the parental to the next generation (“constant growth rates”).

c) Seeding efficiencies of clones in a tumor are identical.

Since the analysis had to account for a “natural variation” of clone sizes, a stochastic process (see appendix C) was used to derive clone size distributions and p-values.

a) To refute the null hypothesis, it was determined that there existed no proliferation rate low enough to be statistically compatible with the observed number of clones undetected in 1° (thus having zero cells in the sample analyzed), and high enough to accommodate the size of the largest clone in 1°, after adjustment for this particular choice ($p<0.0001$ for each experiment). Thus, the null hypothesis of identical proliferation rates can be rejected.

b) Changes of proliferation rates were established based on a single clone, namely, the one that was undetected in 1° and of maximum size after formation of 2° tumors. It was shown that one of these sizes of this clone (in 1° or 2°) was too extreme to be statistically compatible with an identical proliferation rate, taking into account that more than one cell of this clone was potentially transplanted into 2°. This analysis was only performed for experiments P1-1, P2-1, P3-1 and P3-2, where the tumor formation time in 2° was at least as long as in 1°. After adjusting for the multiplicity of testing, the results were statistically significant ($p<0.05$) for all experiments except P1-1. So, the null hypothesis that proliferation rates remain unchanged after re-transplantation can be rejected.

c) Two bounds for the seeding efficiency were compared: First, a lower bound s_l was derived from the fact that from each clone undetected in 1°, but detected in 2° or its corresponding 3°, at least one cell was successfully transplanted into 2°. Second, an upper bound s_u was derived from the clone which had maximum size among all clones in 1° that were undetected in 2°. The upper bound was obtained from a 99.9%

confidence bound for the maximum cell number of this clone in 2°. This comparison was done for P1-1, P2-1, P3-1and P3-2. Using an exact test, it was shown that $s_l < s_u$ in all experiments ($p<0.01$ after adjustment for multiplicity), allowing for the rejection of the null hypothesis that seeding efficiency was identical across the clones.

Summary chapter 3.3

Primary pancreatic TIC can efficiently be marked by transduction with lentiviral vectors in order to study the clonal composition of the pancreatic TIC compartment in serial transplantation in NSG mice. The majority of clones detected by LAM-PCR and subsequent high-throughput sequencing appeared in later generations, and not in primary tumors. Especially large clones contributing strongly to tumor formation in one generation were frequently replaced after transplantation into next generation mice by such clones that were quiescent before. The proliferation rate of individual TIC clones changed dramatically between distinct tumor generations, indicating a switch between an active and a quiescent state. Thus, serially transplanted tumors displayed low clonal overlap between distinct tumor generations, demonstrating a long-term tumor growth maintained by the succession of transiently active TIC.

3.4 The Clonal Origin of the Pancreatic Cancer Associated Stroma

The desmoplastic reaction in pancreatic ductal adenocarcinoma (PDAC) represents a substantial proportion of a patient`s tumor tissue. Tumor and stroma cell populations interact via direct cell-to-cell contacts and paracrine signaling that promotes tumor growth and metastases formation (see section 1.2.3). However, the clonal origin of the stromal fibroblast-like cell types (FLCs) in PDAC remains unknown. Either FLCs derive from a tumor-independent source or from neoplastic cells as has been described for breast cancer [104].

3.4.1 Human Stroma Cells Can Be Cultured and Propagated from Primary Patient Tumor Tissue

Primary FLCs were cultivated from primary tumor tissue derived from five patients (P5-P9) to characterize the *in vitro* phenotype of PDAC-associated stroma cells. Stroma cultures were established by the outgrowth method [175] in RPMI1640 medium containing 10% FBS. Patient-derived tumor tissue pieces of <2mm size were placed in cell culture flasks allowing the outgrowth of adherent cells. Within 1 to 8 weeks, cells adhered and grew as monolayers. These cells were slim and elongated, reminiscent of fibroblasts, or they displayed characteristics of frazzled myofibroblast morphology, containing visible actin stress fibers in the cytoplasm (figure 27). The doubling time of these cultures was between 7 and 28 days. Cells could be passaged up to 11 times (P5: 11; P6: 10; P3: 5; P4: 3), representing a culture period of up to 11 months. After that, cells stopped proliferation or perished, detaching from the ground of the culture dish. Upon transplantation into NSG mice, P5-P9 derived stroma cells never induced tumors in any of the 21 transplanted animals, irrespective of the cell number or culture passage transplanted (table 9).

Table 9: Primary patient-derived stroma cell cultures were non-tumorigenic.

Patient	Culture Passage	Cell number transplanted	Tumor formation frequncy
P5	1	$1x10^6$	0/1
P5	4	$2x10^5$	0/2
P5	5	$2x10^5$	0/3
P5	7	$5x10^5$	0/2
P5	7	$1.4x10^6$	0/1
P6	1	$1x10^5$	0/2
P7	0	$2.5x10^5$	0/2
P7	7	$5x10^5$	0/3
P8	1	$2x10^5$	0/2
P9	0	$1x10^6$	0/3
			∑ 0/21

Cultured stroma cells of five patients (P5-P9) did not induce tumors when transplanted into NSG mice at different culture passages using varying cell numbers. Culture passage 0 indicates freshly established unpassaged cell cultures.

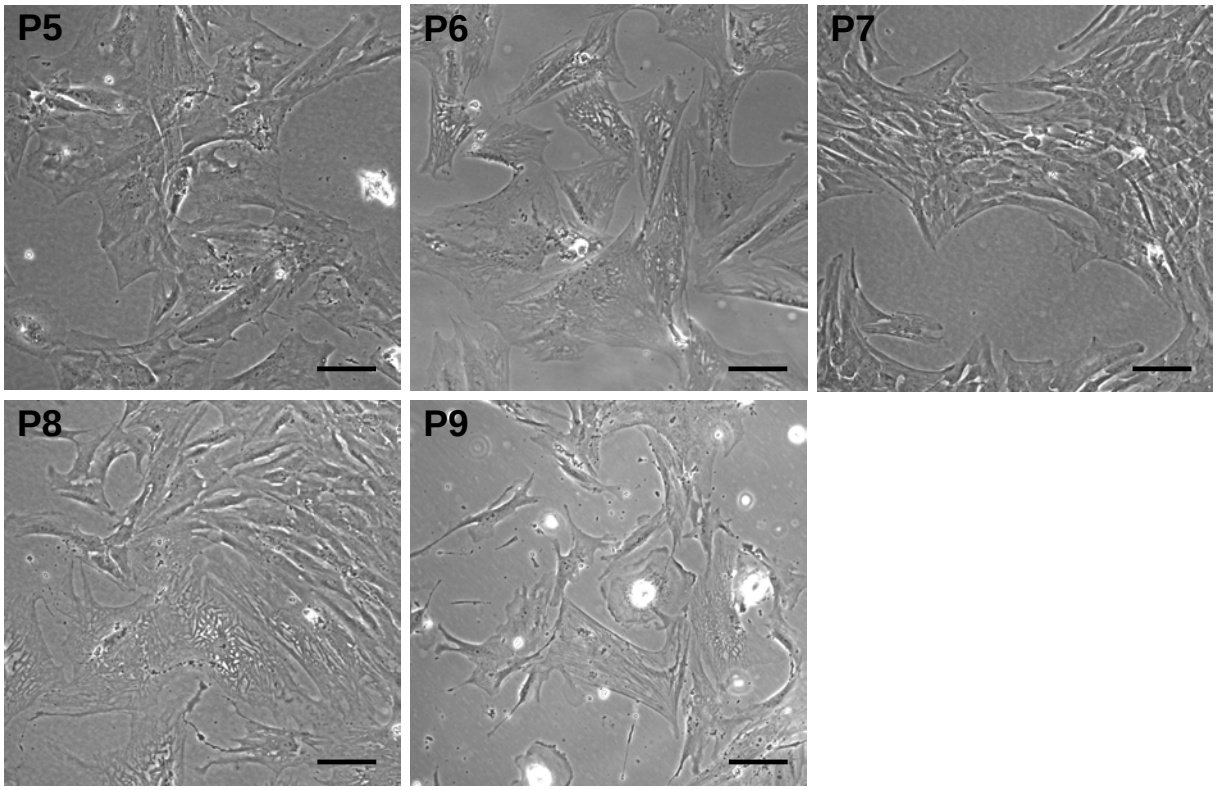

Figure 27: Stroma cells derived from primary PDAC patient tissue grew in cell culture. Cells of five different patients (P5-P9) were cultured adherently showing fibroblast or myofibroblast morphology; scale bars = 100µm.

A phenotypic characterization of stroma cultures by flow cytometry revealed high expression of CD44 at 97% to 100% (table 10). CD133 was never expressed, whereas small subpopulations (0.1% to 1.1% of all cells) were positive for EpCam or CD24. Stroma cultures strongly expressed the mesenchymal markers vimentin and α-smooth-muscle-actin (αSMA), but also the fibroblast marker Thy1 (CD90) (table 10). The epithelial marker cytokeratin 7 (Krt7) was detected by indirect immunofluorescence staining in cultures extracted from 3 out of 5 examined patients (P5, P7 and P8). Here, Krt7 was co-expressed together with mesenchymal markers by the stroma cells (P5 and P8), and/or by a subpopulation of very small cells residing on top of the stromal myofibroblasts (P5 and P7) (table 10, figure 28).

Table 10: Phenotypic characterization of primary stroma cultures of human origin.

Marker	Patient 5	Patient 6	Patient 7	Patient 8	Patient 9
Flow Cytometry					
CD133	**0.0%**	**0.0%**	**0.0%**	**0.0%**	**0.0%**
CD44	**99.9%**	**97.7%**	**99.8%**	**99.9%**	**99.6%**
EpCam	**0.6%**	**0.1%**	**0.5%**	**0.0%**	**0.3%**
CD24	**1.1%**	**0.0%**	**0.1%**	**n.d.**	**0.0%**
Indirect Immunofluorescence					
Krt7	**+**	**n.d.**	**+/-**	**+/-**	**-**
Vimentin	**+**	**+**	**+**	**+**	**+**
αSMA	**+**	**+**	**+**	**+**	**+**
Thy1	**+**	**+**	**+**	**+**	**+**
Nestin	**+/-**	**+/-**	**+/-**	**n.d.**	**n.d.**
Desmin	**-**	**-**	**+/-**	**n.d.**	**n.d.**
Klf4	**+**	**+**	**+**	**n.d.**	**+**

Representative flow cytometry analysis of stroma cultures from 5 different patients revealed high CD44, low EpCam or CD24 and no detectable CD133 expression. Cells stained positive for mesenchymal stroma markers vimentin, α-smooth-muscle-actin (α-SMA) and Thy1. Some cultures co-expressed the pancreatic duct marker Krt7. Cultures contained single nestin^{+} cells but were mainly negative for desmin. KLF4 was expressed throughout examined cultures. Cultures were assigned + when marker positive cells were detected minimum two independent visual fields of the sample, +/- when only single positive cells were observed and – if all cells were negative; n.d = not determined.

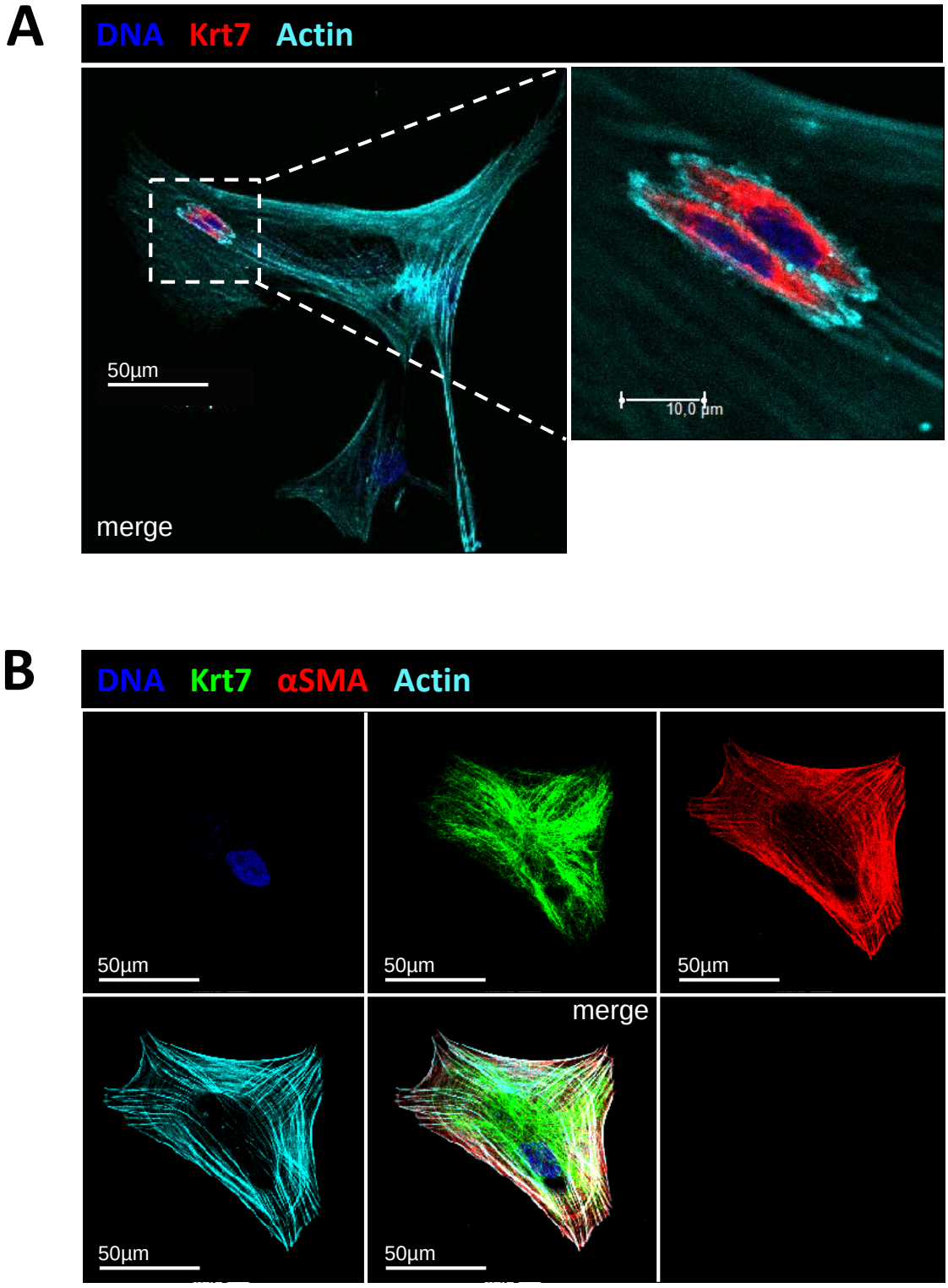

Figure 28: Cytokeratin 7 (Krt7) was expressed in primary human PDAC derived stroma cultures. (A) A subpopluation of small cells residing on stromal fibroblasts expressed the pancreatic duct epithelium marker Krt7, whereas the stroma cells were Krt7 negative. **(B)** Individual stroma cells co-expressed Krt7 and mesenchymal stroma markers like α –smooth-muscle-actin (αSMA).

3.4.2 Xenograft-Tumor Derived Stroma Cells Express Murine and Lack Human Markers

In order to investigate a possible clonal relation between stromal FLCs and pancreatic tumor cells, the stroma compartment of xenograft tumors was characterized. In cases where neoplastic cells had given rise to their own stroma, these tumors should contain human FLCs. Tumors initiated by serum-free cultured tumor colony cells of four different patients (P1-P4) were analyzed. Upon histological examination, areas of tumor-associated stroma were apparent in xenograft tumors for all four patients (figure 29).

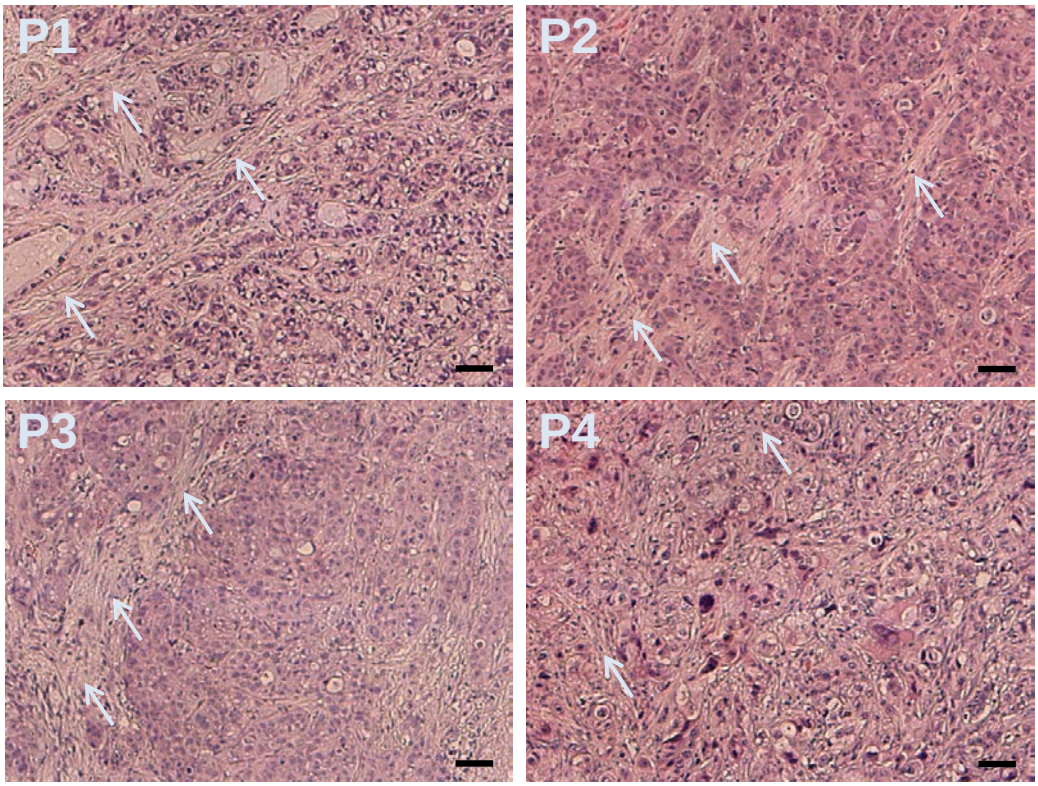

Figure 29: Human xenograft tumors contained regions of desmoplatic stroma. Stromal areas of (arrows) surrounded epithelial tumor cell clusters as observed for all four examined patients (P1-P4).

However, flow cytometry analysis of purified cells revealed that human fibroblast marker Thy1 was not expressed in xenograft tumors. Instead, a substantial population of cells (4-20%) stained positive for that cell surface protein`s murine specific epitope Thy1.2 (table 11). To detect potential Thy1-negative human FLCs in

xenograft tumors, outgrowth cultures were stained for human and murine stroma markers via indirect immunofluorescence. Here, FLCs were detected which exhibited characteristic myofibroblast morphology with parallel actin stress-fibers (figure 30, arrows). These cells stained negative for human vimentin and Krt7, but expressed murine Thy1.2.

Table 11: Expression of human and murine epitopes of the stromal cell surface marker Thy1 in xenograft tumors.

Patient	Isotype control (%)	Thy1 (%)	Thy1.2 (%)
P1	0.1	0.1	8.6
P2	0.1	0.1	14.6
P3	0.1	0.0	4.9
P4	0.1	0.1	19.7

Representative xenograft tumors of 4 patients (P1-P4) contained a substantial proportion of Thy1.2$^+$ murine stroma cells. Values obtained for human stroma marker Thy1 were indistinguishable from the appropriate isotype controls.

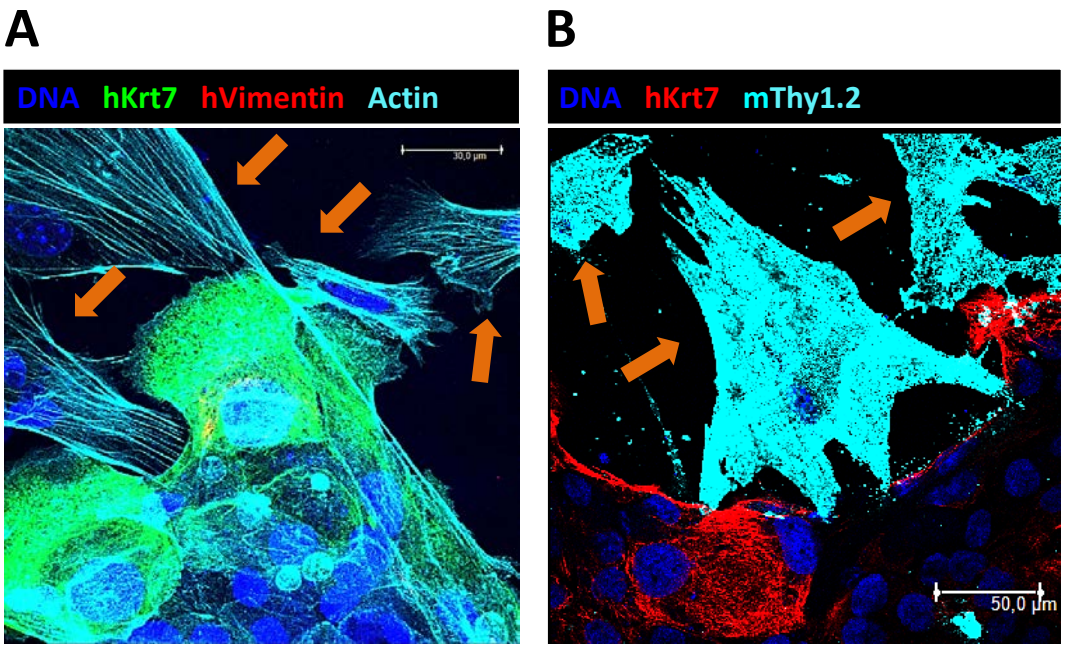

Figure 30: Xenograft tumors contain stroma cells expressing murine markers. Outgrowth cultures from xenograft tumors show cells of stroma morphology (arrows) that are negative for human vimentin (hVimentin) and human Krt7 (hKrt7), but express murine Thy1.2 (mThy1.2); hKrt7 and hVimentin are exclusively expressed in cells of the neoplastic epithelial compartment; scale bars: 50µm. Figure modified from [179].

Interestingly, single cells that showed human Krt7 expression also were positive for murine Thy1.2, reminiscent of fusion cells between human tumor cells and murine FLCs. These cells were multinuclear in every case, and always displayed at least one dotted (figure 31, green arrow) and at least one homogeneously Hoechst stained nucleus (figure 31, orange arrow).

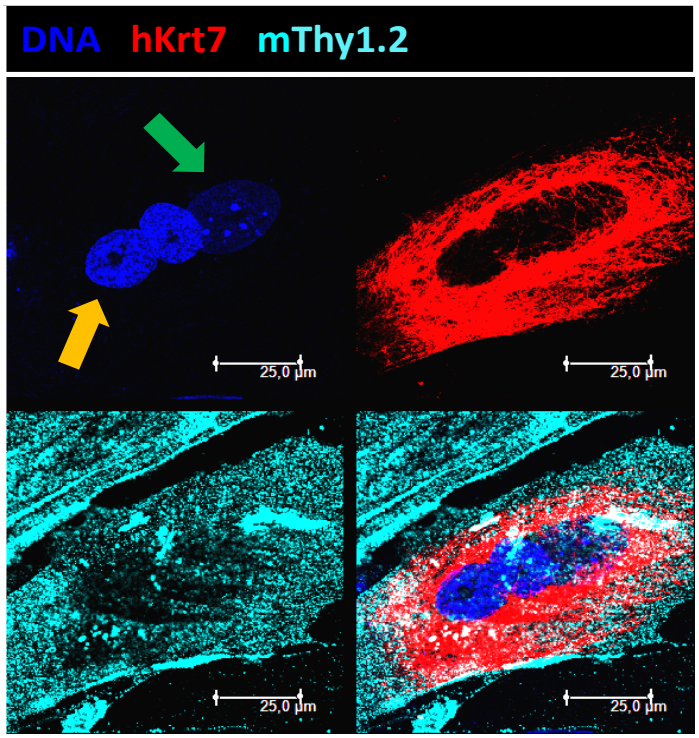

Figure 31: Human xenograft tumors in mice contained cells having combined expression of human tumor and murine stroma markers. Polynuclear cells of stromal morphology from human xenograft tumors co-expressed human cytokeratin 7 (hKrt7) and murine Thy1.2 (mThy1.2). Cells contained at least one nucleus homogeneously stained by Hoechst (orange arrow) and one displaying a dotted staining (green arrow); scale bars: 25µm.

3.4.3 Primary Human Stromal Fibroblasts Poorly Contribute to Xenograft Tumor Formation when Co-Transplanted

In order to investigate whether human stromal cells can engraft into xenograft tumors, cultured FLCs from P7 were co-transplanted into three NSG mice together with P1 derived tumor colony cells. Co-transplantation was performed in 1:1 ratio with $5x10^5$ cells of each compartment. Prior to transplantation P7 derived stroma cells

displayed a proportion of 81.1% $Thy1^+$ cells (compared to 0.0% for the appropriate isotype control). To easier distinguish between tumor and stroma cells, 2 of 3 transplanted mice received $EGFP^+$ FLCs that were transduced with lentiviral vectors (LV106) using a multiplicity of infection of 20 (MOI 20) or 40 (MOI 40). The transduction efficiency was 80.5% for MOI 20 and 84.1% for MOI 40. As a control, a 4^{th} mouse received $5x10^5$ tumor cells without stroma.

Six weeks after transplantation, mice were sacrificed to examine tumors for engrafted stroma cells. Histology and weights of the tumors were similar between all animals, regardless of whether stroma cells were co-transplanted (0.6g, 0.7g, 1g) or not (0.7g) (figure 32 A, B).

The stroma content of the tumors was examined using flow cytometry. Again, high proportions of murine $Thy1.2^+$ stromal FLCs (>10%) were observed. Human $Thy1^+$ cells were detected only in the stroma co-transplanted animals with untransduced stroma (0.1%) or MOI 40 transduced stroma (0.2%). The proportion of EGFP expressing cells was 0.1% for MOI 20 and 0.2% for MOI 40. Moreover, the proportion of $EpCam^+$ and $CD133^+$ tumor cells remained unaffected by stroma co-transplantation at 40-55% for EpCam and 10-50% for CD133 (table 12).

Outgrowth cultures were established from the control tumor without co-transplanted stroma and from the tumor with co-transplanted MOI40 transduced stroma. In addition to EGFP expression, the cells were stained by indirect immunofluorescence for human vimentin and human Krt7 to distinguish between tumor and stroma cells. Cultures derived from the tumor without co-transplanted stroma contained no cells with EGFP or human vimentin expression (figure 32C). By contrast, the stroma co-transplanted tumor contained clusters of EGFP and human vimentin double-positive cells. However, these were infrequent and only found in isolated spots of the outgrowth culture. Krt7 was exclusively expressed by cells of epithelial morphology, and not by $EGFP^+$ stroma cells.

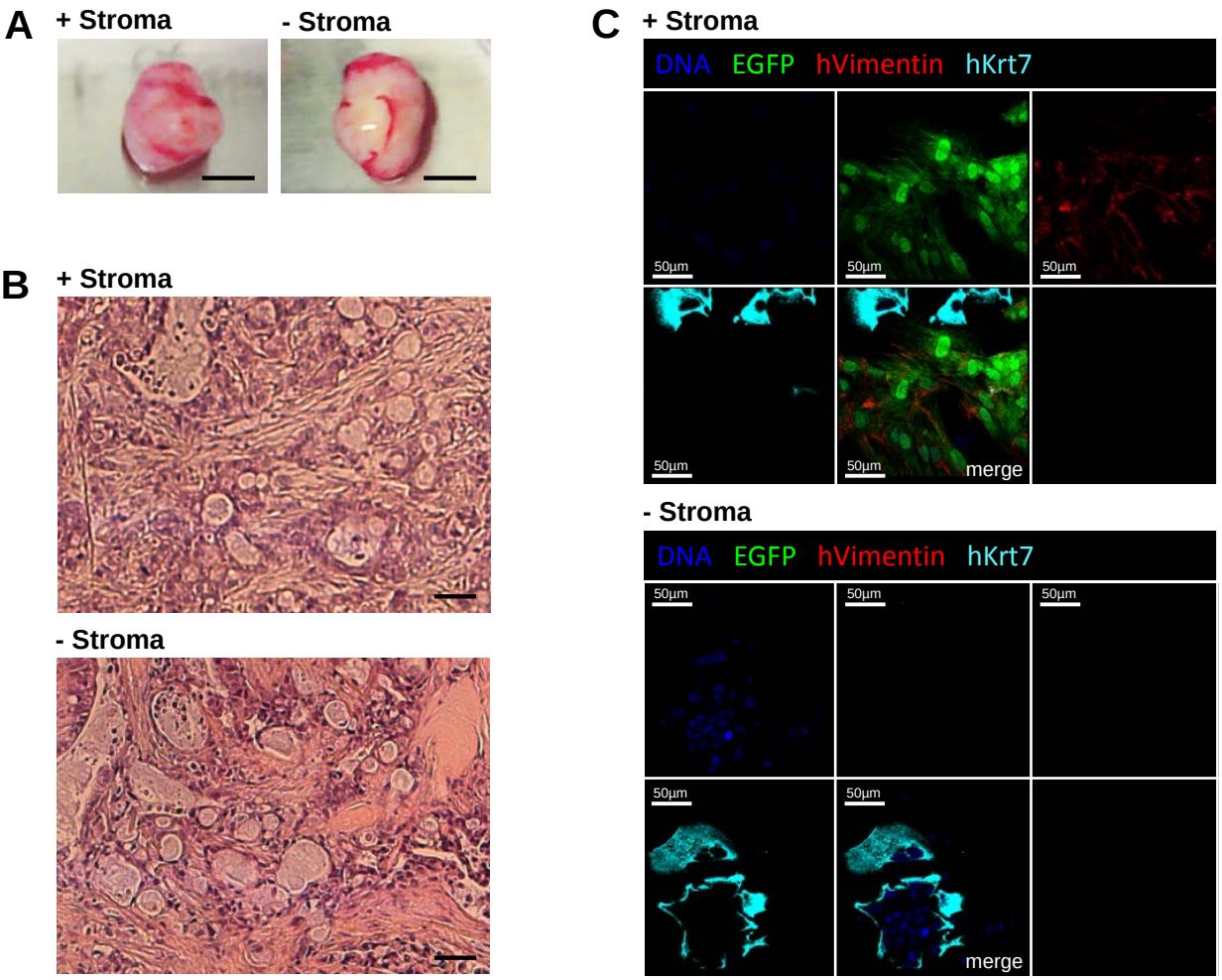

Figure 32: Co-transplanted stroma cells engrafted poorly into xenograft tumors and did not change tumor biology. (A) Tumor weights were unaffected by stroma co-transplantation; scale bars = 1cm. **(B)** Tumor histology appeared equal between both tumor entities; scale bars = 100µm. **(C)** Outgrowth cultures from xenograft tumors contained human vimentin (hVimentin) and EGFP co-expressing stroma cell clusters only when stroma cells were co-transplanted; scale bars = 50µm**.**

Table 12: Co-transplanted human stroma cells showed poor contribution to xenograft tumor formation.

Marker	TIC - stroma (%)	TIC + untransduced stroma (%)	TIC + stroma MOI 20 (%)	TIC + stroma MOI 40 (%)
EpCam	41.2	44.4	45.0	52.4
CD133	23.9	10.8	20.2	47.7
Thy1	0.0	0.1	0.0	0.2
Thy1.2	11.3	16.1	20.3	17.3
EGFP	0.0	0.0	0.1	0.2

A low proportion of $EGFP^+$ and human $Thy1^+$ cells was detected in xenograft tumors after 1:1 co-transplantation of untransduced or transduced stroma (MOI 20 or 40) cells with pancreatic TIC. Stroma co-transplantation did not affect the expression of tumor markers EpCam and CD133 in resulting xenograft tumors. Mouse stroma marker Thy1.2 was strongly expressed compared to human Thy1.

Summary chapter 3.4

Primary pancreatic tumor-associated stroma cells could be cultured from primary patient-derived tumor tissue, and grew under serum conditions for a limited time. These cells displayed morphology and marker expression reminiscent of fibroblasts or myofibroblasts. Xenograft tumors initiated by pancreatic TIC in NSG mice contained no human stroma cells. Instead, tumor cells recruited murine fibroblast-like stroma cells, which constituted a significant proportion of the xenograft tumor mass. Human stroma cells co-transplanted with TIC into NSG mice engrafted during tumor formation, but accounted for a very low proportion of all tumor cells compared to the respective murine stroma cell population.

4. Discussion

4.1 Primary PDAC Cells can be Enriched and Expanded via Xenografting

In recent years an increasing number of research studies on tumor-initiating cells (TIC) used primary patient derived tissue instead of permanent cell lines. Primary material has a closer connection to the original patient, because permanent cell lines may acquire additional mutations and change in their biology by years of cell culture [191-193]. Experiments using primary cell cultures instead of cell lines might therefore lead to results that better translate into clinics.

Thus, the experiments in this thesis project addressed phenotypic and functional characteristics of pancreatic TIC and were performed by using surgically resected pieces of PDAC tumors. However, the carcinoma content of the patient derived tissue varied substantially as observed in histopathology. Benign contaminations might bias experiments investigating distinct tumor cell populations, so that dissociated cells from primary tumors could not be used for clonal marking. Moreover, the contained benign cell types expanded in primary cell cultures and prevented stable tumor cell culture establishment. In contrast to that, stable primary cell cultures in other solid tumor entities were established directly from primary material without prior xenografting [113, 135, 137, 180]. The amount and the quality of the tumor material provided could be an explanation for these differences. Unlike patients suffering from tumors of the brain or colon epithelium, most PDAC patients do not undergo surgery in advanced stages of the disease (www.cancer.org), so that mainly small tumors are available for research. Potentially curative surgery of small PDAC tumors requires resection of adjacent benign tissue that might explain the low tumor content in primary tissue samples.

However, these limitations could be overcome by transplanting patient derived tumor pieces into NSG mice. A sub-fraction of patient samples formed serially transplantable xenograft tumors that resembled the original patient’s tumor. By that procedure benign human cell types were lost and spheroid or adherent cultures could be established efficiently from resulting xenograft tumors. FLC contaminations which were purely of murine origin after xenografting (see section 4.4) were rapidly lost by passaging. Obviously, murine FLCs are less competitive under serum-free culture

conditions than human FLCs. The use of xenografting as a method to outcompete benign human cell types has not been described in literature so far. Previously, xenografting was though applied as a method to expand pancreatic primary tissue for therapeutic compound screens *in vivo* [194, 195].

The results of this thesis show that xenografting can diminish the high variability in carcinoma content, keep primary tumor material accessible for research without prior *in vitro* cultivation, and purify it from benign human cell types. This kind of processing of tumor tissue was needed, because stable cell culture establishment was not possible otherwise and benign contaminations might potentially bias the results of performed experiments in an unpredictable way, especially clonal marking experiments as depicted in chapter 3.3. Thus, xenografting enabled biological comparison of distinct cell populations within the heterogeneity of an individual patient`s tumor and between different patient samples.

4.2 Adherent Colony Cultures Expand Primary PDAC Cells *in Vitro*

As described in the above section, xenografting was a requirement for the establishment of stable primary cell cultures. From dissociated xenograft tumor cells suspension spheroids were cultured under serum-free conditions and stimulated with cytokines FGF2, FGF10 and Nodal. FGF2 and FGF10 support the growth of the developing pancreas epithelium [11-13] and the activin/nodal pathway is described to drive the self-renewal and tumorigenicity of pancreatic TIC [145]. Under these culture conditions spheroid cells displayed an epithelial morphology and highly expressed markers as previously depicted for pancreatic TIC [143, 144].

The concept of spheroids for the cultivation of undifferentiated cell populations was initially established by Reynolds and Weiss [44] who cultured normal neural stem cells (NSCs) from central nervous system tissue of adult mice as suspension neurospheres in a serum-free medium supplemented with the growth factors FGF-basic and EGF. These authors showed that nearly all spheroid cells were nestin^{+} reminiscent of NSCs and that a non-adhesive substrate and the stimulation with EGF were required for proliferation of these cells. Later, Singh et al. [135] initially

cultivated spheroids of malignant cells from primary brain tumor tissue in an analogous approach. Other groups adapted spheroid cultures for research on other solid tumors like colorectal cancer [113, 137], Ewing´s sarcoma [138] or pancreatic cancer [144]. In analogy to such previous studies on solid tumors, in this thesis spheroid cultures could be established and induced tumors in NSG mice. Contrary to these studies, however, spheroid cells did not show sufficient *in vitro* growth, so that an expansion of a TIC containing tumor cell population was not achieved by this method. Biological differences between the primary PDAC cells used in this project and the primary cell of other solid tumor entities might be the reasons for this discrepancy. Compared to previous studies of pancreatic TIC [144, 145], where spheroids were cultured not longer than five weeks, this thesis had a much higher need for passaging and *in vitro* expansion of TIC containing cell cultures.

Thus, using equal culture conditions as for spheroids, adherent colonies were established from tumor pieces by the outgrowth-method [177] as an alternative[175][175][175]. Similar to spheroids, adherent colonies showed epithelial morphology, high TIC marker expression and induced tumors in NSG mice. Comparable adherent cultures were previously used for glioma cells [180]. In particular, researchers described much better characteristics for adherent primary glioma cell cultures compared to spheroids when using serum-free medium supplemented with FGF-basic and EGF. Adherent cells were easier to handle, displayed less apoptosis and expressed lower levels of differentiation markers. The need for a non-adherent culture that was described by Reynolds and Weiss for NSCs, was constituted by a proliferation stop and not by the enhanced differentiation observed upon adhesion [44]. Thus, if cells do proliferate well under adherent conditions, the establishment of non-adherent spheroid cultures by the use of ultra-low attachment or other techniques to enforce suspension growth might not necessarily lead to better culture characteristics or enrichment of a more undifferentiated cell population. In line with this, the results depicted in chapters 3.1 and 3.2 clearly demonstrate that adherent primary PDAC colonies provide a culture system suitable to expand and investigate the biology of pancreatic TIC. Consequently, suspension spheroids, which did not grow exponentially, were not required in this study.

4.3 Phenotypic and Functional Plasticity of Pancreatic TIC

4.3.1 Pancreatic TIC Switch Their Phenotype without Loss of Tumor-Initiating Potential

In order to investigate whether TIC potential is associated to a certain phenotype of pancreatic tumor cells, adherent colony cultures were stimulated with serum-containing medium and the withdrawal of growth factors. This serum treatment frequently resulted in an up-regulation of pancreatic differentiation markers and a down-regulation of prominent markers that were described for various stem cell populations, pancreatic progenitor cells or pancreatic TIC. Thus, indeed phenotypic alterations were induced that reminded of a more differentiated cell population. Though, when the data of all patients was merged, serum treatment of minimum 25 days in early passages did not significantly affect tumor growth and serial transplantability in NSG mice. The differentiation potential of pancreatic TIC has so far only been addressed on a phenotypic, but not on a functional level. In literature, the down-regulation of TIC markers like CD133, the up-regulation of Krt7 and morphological changes including increased cell size and irregular cell shapes were already described upon comparable changes in culture conditions [144, 145]. Yet, the results of chapter 3.2 showed no correlation between such phenotypic changes and *in vivo* tumor growth, indicating no functional differentiation of PDAC cells.

Different to the results for early passages, the tumors induced by late passage serum-treated cultures were significantly smaller after the same period of time than the control tumors. Yet, after 75-190 days of cell culture in serum containing medium it cannot be excluded that the cells gained additional genetic/epigenetic alterations which might be responsible for the altered tumor growth. Due to the long culture time until a significant effect was observed, such clonal selection might rather explain the lower mean tumor weight than a partial functional differentiation stimulated by serum treatment.

Permanent glioma cell lines and primary cell cultures were described to acquire such additional mutations along long-term cell culture in serum containing medium [181, 191-193]. Lee et al. observed [181] that primary glioma cells cultured in serum containing medium without growth factors lost their tumorigenicity in mice already at

early passages, lacked the ability to differentiate and gained additional mutational hits, findings which were not observed for serum-free cultures. At late passages serum-treated glioma cells regained TIC potential, but the resulting xenograft tumors did not resemble the original patient tumor in histology and the xenograft tumors induced by serum-free grown control cells.

Contrary, to the observations for primary glioma cell cultures, in this thesis it was demonstrated that after similar changes in cell culture, pancreatic TIC neither to lost their tumorigenic capacity nor the ability to recapitulate the whole heterogeneity of the patient`s tumor. Irrespective of how long tumors were passaged *in vivo* or in cell culture, and in whichever medium, an effect on the patient specific histology was never observed. This indicates that different from their glioma counterparts and normal stem cell populations, pancreatic TIC are resistant to irreversible functional differentiation by serum treatment including the withdrawal of growth factors, even though they acquired a differentiation-like phenotype. A possible explanation for this observation would be that pancreatic TIC are able to dynamically switch their differentiation status and thereby reverse the effects of serum treatment upon transplantation. Strikingly, the cell sorting experiments described in chapter 3.2 clearly demonstrated that CD133 expression could be fully restored by CD133 negative TIC *in vitro* and *in vivo* in a context dependent manner. In NSG mice, the proportion of marker positive cells in the transplanted fraction did not influence tumor biology regarding weight, marker expression or histology. Thus, after transplanting phenotypically diverse TIC all fractions equally gave rise to their patient`s characteristic tissue that is clear evidence of phenotypic plasticity in the PDAC TIC population.

These data are furthermore opposing the role of CD133 in PDAC described in literature. Here, sorted CD133-negative cells did not initiate tumors in NSG mice at higher cell numbers ($1x10^6$), as transplanted in our setting ($5x10^3$-$5x10^5$) [144]. The finding that CD133 does not predict for pancreatic TIC function is encouraged by the fact that its level of expression in PDAC tumors does not correlate with patient survival [196]. However, PDAC is not the first kind of cancer, where CD133 was postulated as TIC marker, followed by the later detection of a $CD133^-$ tumorigenic population. Such contradicting studies exist for colorectal cancer [137, 141] and

gliomas [136, 140]. As described above, pancreatic cancer patients do not undergo surgery when tumors are in an advanced stage of the disease. So, mostly small, early stage tumors are resected and available for research. This explains the observed variation in carcinoma content described in chapter 3.1 for the tumor samples provided by surgery. It is tempting to speculate that other groups in the field of PDAC research might face the same obstacles of benign contaminations in their tumor samples. Thus, sorting for CD133 expression from a mixture of malignant and benign cell populations derived from dissociated patient tissue could lead to an enrichment for tumor cells in the positive collection tube, which would result in an enrichment for benign cells in the negative fraction. In theory, this might explain the previously published data for the role of CD133 as a TIC associated marker in PDAC [144].

This kind of bias might also have affected the initial study identifying CD44/CD24/EpCam triple-positive TIC in PDAC [143]. Also in this study patient material was used directly without previous xenografting. Chapters 3.1 and 3.2 demonstrate that after adherent culture establishment from xenograft tumors, nearly all cells were positive for CD44 and EpCam. The vast majority of cells that did not display the CD44/CD24/EpCam phenotype, were thus still double-positive for two of these markers. Based on the data of this thesis project, one cannot exclude that triple CD44/CD24/EpCam negative PDAC cells are indeed largely non-tumorigenic. However, these cells represent a small minority of all cells in primary cultures. Nonetheless, to associate TIC potential to cells expressing the common epithelial marker EpCam appears questionable in an epithelial cancer. The negative fraction in such sorting experiments would exclude the majority of epithelial cells and thus might substantially enclose, for example, stroma, blood or endothelial cells contained in fresh patient tissue, as previously stated [197].

In recent years, TIC markers have gained importance for the enrichment of tumorigenic cell populations. But it seems that the relevance of phenotypic markers originally described in benign adult stem cell compartments for TIC identification was frequently overestimated in the past. For example, Bonnet and Dick described in 1997 [109] that acute myeloid leukemia (AML) is maintained by a small subpopulation of TIC sharing the undifferentiated $CD34^{++}/CD38^{-}$ phenotype of their

healthy hematopoietic stem cell counterparts. However, later Bonnet and colleagues corrected that the CD38 antibody used in previous study, inhibited the *in vivo* engraftment, and that TIC also resided in the $CD38^+$ and the $CD34^-$ fraction [198, 199]. Considering the data presented in this thesis, the significance of CD133 in pancreatic cancer appears overstated in a similar way [144]. Due to the strong phenotypic plasticity of PDAC TIC indicated by the results of chapter 3.2 one has to note that the altered expression of certain markers cannot represent a surrogate for a functional TIC assay *in vivo*. TIC must be defined by their functional characteristics of tumorigenicity and their ability of recapitulating the patient`s tumor heterogeneity in an animal model independent of their phenotype.

Similar to the findings of this thesis, phenotypic plasticity was recently described for melanoma TIC by Quintana et al. [200]. The authors could not enrich for TIC via sorting for any melanoma TIC marker described, or for 20 other heterogeneously expressed proteins. Similar to the results presented above, melanoma cells also repeatedly up- and down-regulated established TIC markers without functional changes *in vivo*. The results of this thesis, however, do not exclude that factors associated with the self-renewal of embryonic stem cells, like SOX2 [188], or regulators of pancreatic regeneration, like Notch1 [38], are functionally implicated in pancreatic TIC biology. They might rather indicate that the expression of certain markers or transcription factors can be reversibly acquired and lost, so that a possible functional differentiation of PDAC cells could be reversible.

4.3.2 Long-Term Tumor Growth in PDAC is Maintained by the Successive Recruitment of Transiently Active TIC Clones

The hierarchical cancer stem cell concept postulates that only a subpopulation of long-term self-renewing, tumor-initiating cells (TIC) can maintain tumor growth (reviewed by [48, 114, 115]). This functional characteristic can be measured by serial transplantation into immunodeficient mice [109-113]. In this thesis, such serial transplantation of lentivirally marked primary TIC was used to analyze the clonal dynamics within the pancreatic TIC compartment. The results of chapter 3.4 revealed a surprisingly low clonal overlap between serially transplanted tumors and,

concomitantly, an unexpectedly dynamic clonal composition of the disease. Tissue formation was mainly driven by distinct TIC after each transplantation step into a subsequent mouse generation. This was a surprising discovery, since the established clones that contributed strongly to tumor formation in one generation represented a high proportion of the further transplanted cell fraction. In case that such large clones retained tumorigenic capacity after primary tumor formation one could expect that they would also engraft preferentially into the next tumor generation. In contrast, predominantly large clones were lost after re-transplantation, and replaced by clones that underwent only a few cell divisions or even by single cells that did not proliferate at all in the parental tumor. That these small clones were not detected in the earlier tumor generation(s) can be explained by the sampling size of 2-10% analyzed from each individual tumor. The statistically determined sizes of later-detected clones of up to 9 cells (99% confidence bound) represent upper limits. Therefore, small clones that were not contained in the fraction sampled for analysis after tumor dissociation could be present in the fraction of cells re-transplanted. Thus, cells contained in small clones had a higher tumorigenic capacity than the cells derived from already established large clones that seemed to give rise to mainly non-tumorigenic progeny.

The data clearly demonstrate that the activity of individual TIC is temporarily restricted. Therefore, long-term tumor growth in pancreatic cancer is not maintained by a stable long-term self-renewing TIC subpopulation, but rather by the successive recruitment of new clones acquiring TIC potential. The clonal dynamics observed here allowed no classification of TIC based on differences in their self-renewing potential and thus do not point to a hierarchical organization of the pancreatic TIC compartment. These results are in contrast to a hierarchical cancer stem cell model. Even though only a subpopulation of the cultured pancreatic TIC engrafted into NSG mice, the clonal dynamics in PDAC sharply differed from what has been described for acute myeloid leukemia (AML) [109, 111, 127], chronic myeloid leukemia (CML) [128-130, 201] and colon cancer [43, 113], where a hierarchical organization of the TIC compartment was observed. Extensive self-renewal of long-term TIC (LT-TIC) is the driving force within a hierarchically organized TIC compartment, as was previously demonstrated in colorectal cancer by Dieter et al. [113]. These authors used the

same strategy of LAM-PCR based tracking of lentivirally marked primary TIC, as applied in this thesis project. In contrast to the data of this thesis, the LAM-PCR-derived DNA fragments of certain clones were found only in the primary tumor generation, whereas a minority of fragments was there throughout all three tumor generations in NSG mice. Thereby Dieter et al. demonstrated that, indeed, certain clones had a limited self-renewing activity and contributed to tumor formation only initially, whereas other clones displayed long-term self-renewal and maintained tumor progression continuously.

Thus, the clonal succession of transiently active TIC in PDAC is a fully new model for long-term tumor growth in solid tumor entities (figure 31). Individual TIC only transiently contribute to tumor formation and produce mainly non-tumorigenic progeny with little or no self-renewal. Thus, besides the phenotypic plasticity described above, pancreatic TIC also hold a profound functional plasticity. The LAM-PCR based investigations of TIC clonality in pancreatic and colon cancer demonstrate that biological differences between malignancies arising from different organs can be strong. The fact that in this study only a small proportion of transplanted culture cells engrafted into primary mice could also be due to clonal selection by the artificial mouse system. The TIC frequency might be substantially higher in patient tumors.

Statistical analysis of the clonal data presented in chapter 3.4 has revealed that TIC clones recruited in later generations can exist in a quiescent status undergoing not more than five cell divisions before their activation. However, *in vivo* models for TIC function cannot distinguish between non-tumorigenic cells and TIC that are temporally in a quiescent status. Thus, later-detected clones in serial transplantation might either consist of bulk tumor cells that gain TIC potential after re-transplantation, or of non-proliferating TIC that become activated. In this work the term “quiescent TIC” for undetected small clones is meant to consider both possibilities. Whichever alternative is true, the conversion of quiescent pancreatic TIC into an active tissue-forming status even appears to be reversible, since certain clones found in the analysis even repeatedly appeared and disappeared.

Quiescent stem cells that persist without or with poor proliferation have previously been described in the normal hematopoietic system [202-204]. In quiescence, hematopoietic stem cells (HSCs) show only a few divisions per life time [205], have reduced energy metabolism and are thus more resistant against chemotherapeutics [202, 203, 206-208]. In neoplasms, dormant TIC have been described in leukemia [209-211] and colon cancer [113]. Quiescence of normal stem cells and TIC has also been linked to drug resistance (reviewed by [207, 212]). In leukemia, quiescent populations are shown to be more resistant to the action of chemotherapeutics than fast dividing tumor cells since the high metabolism of proliferating cells represents a weak points for drugs targeting cell cycle and signaling pathways [211, 213]. Hence, breaking the dormancy of TIC by cell-cycle activating agents combined with chemotherapy was recently proposed as a promising approach for future therapy [207, 214].

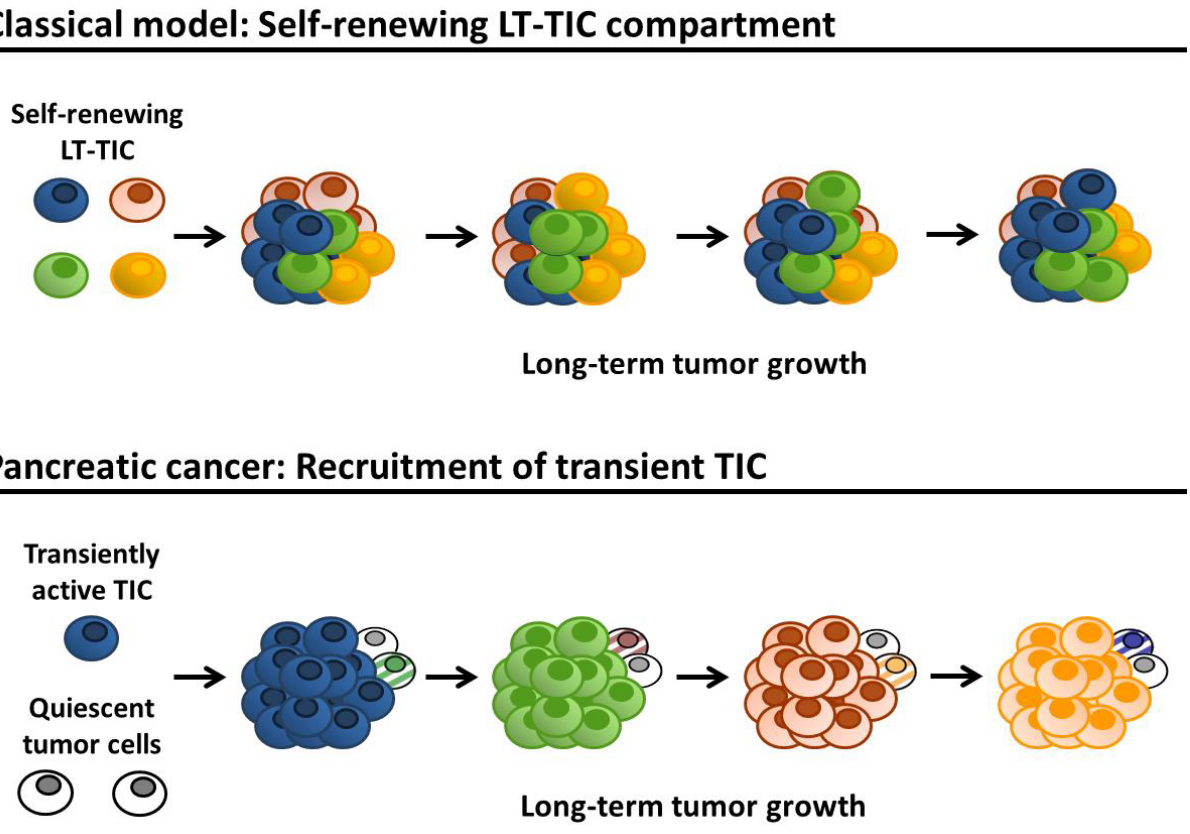

Figure 33: The clonal dynamics maintaining long-term tumor growth differ between distinct malignancies. The clonal dynamics within the pancreatic TIC compartment fundamentally differ from the classical cancer stem cell concept of a hierarchical organization and long-term tumor growth driven by an intensively self-renewing TIC subpopulation. In pancreatic cancer, transiently active TIC drive long-term tumor growth in a clonal succession. Figure taken from [179].

The capacity of TIC to cycle between a tumorigenic and a quiescent status has been recently discovered in melanoma as well [215, 216]. Here, epigenetic changes can act as regulators of this transition. Roesch et al. [215] discovered that the epigenetic demethylation of H3K4 by Jarid1B is defining a quiescent subpopulation of tumorigenic cells in melanomas. Upon loss of Jarid1B, these cells commenced strong proliferation and lost TIC potential while producing non-tumorigenic progeny. Jarid1B-dependent tumorigenicity was also shown to be repeatedly reversible. The findings described in melanoma are somehow similar to observations of this thesis. It is speculative, but possible, that epigenetic changes are involved in the regulation of the switch between a quiescent and an active mode of PDAC TIC. This has to be elucidated in further studies.

Studies on leukemia and colon cancer supported the idea that the clonal dynamics underlying malignant tissue formation caricature their benign counterparts, a theory initially formulated by Pierce and colleagues [122-126] (see section 1.3.1). Due to the clonal dynamics observed in this thesis, pancreatic cancer also fits into that scheme. The pancreas is an organ that is not under constant regeneration as is the colon epithelium or the blood system. Regeneration in the adult pancreas occurs due to the damage induced by the dedifferentiation of terminally differentiated acinar cells into a status in which these cells acquire for a short term the ability to give rise to new acinar tissue and re-differentiate back upon closure of the lesion [36-38]. Thus, the recruitment of transiently active stem cells and the cycling switch between an undifferentiated and differentiated status seem to apply for normal and malignant tissue formation in the adult pancreas. Regulatory factors in the process of acinar cell dedifferentiation might possibly also define the recruitment of TIC, such as factors that work in pancreatic development.

4.4 PDAC TIC Recruit Murine Stroma Cells into Xenograft Tumors

One aim of this thesis was to examine a possible clonal connection between pancreatic TIC and stromal fibroblast-like cell types (FLCs). The conversion of epithelial tumor cells to such non-tumorigenic stroma cells by EMT was recently described for breast cancer by Petersen et al. [104]. The data shown in chapters 3.1

and 3.3 demonstrate that both epithelial tumor cells and stroma cells could be cultivated from primary patient tumors. Surprisingly, stroma cells in culture partially displayed cytokeratin 7 (Krt7) expression, which is a marker of pancreatic duct cells and is commonly found in PDAC and other solid tumors [217]. Krt7 has thus been used as a tumor cell marker to distinguish between cancer-associated fibroblasts and tumor cells in cholangiocarcinoma [218]. Petersen and colleagues described a similar Krt7 expression and interpreted it as residual expression of epithelial markers after EMT [104]. However, after the transplantation of stroma-free pancreatic colony cultures, the resulting xenograft tumors did not contain cells staining positive for stroma markers when human-specific antibodies were used. Instead, a subpopulation of cells in outgrowth cultures established from these tumors expressed Thy1.2 epitopes, the murine version of the human stroma marker Thy1. The data clearly show that pancreatic tumor cells do not give rise to stromal FLCs in NSG mice, but rather recruited murine FLCs into the xenograft tumor to create their preferred microenvironment. Of course, these results only represent the situation in the murine xenograft model system and do not decisively exclude a different scenario in the patient`s body. Factors stimulating the conversion of epithelial tumor into stroma cells in humans might not be present in mice. Obviously, however, factors used by PDAC cells to attract stroma into tumors appear conserved between humans and mice. In particular, PDGF, a major modulator of desmoplastic stroma [84, 97-99, 175], is highly conserved throughout mammals [219]. Thus, human PDGF secreted by human PDAC cells might stimulate murine receptors, thereby contributing to murine stroma formation in human xenograft tumors.

Interestingly, outgrowth cultures from xenograft tumors contained cells that co-expressed of human Krt7 and murine Thy1.2. Since both antibodies were tested to be highly species-specific these cells reminded of fusions between human tumor and murine stroma cells. This finding was supported by the observation that all examined cell expressing human and murine markers were polynuclear and always contained a homogeneously stained and a dotted nucleus. Nuclei of murine cells in mixed human/mouse cell populations appear dotted in Hoechst or DAPI staining in comparison to human nuclei [220]. Fusion cells between cancer and stroma compartment are already described in human prostate cancer to influence tumor

progression [221]. If such fusion cells also exist in PDAC patient tumors might be revealed in future studies. Although the data of this thesis cannot exclude that the observed $Krt7^+$ primary stroma cells isolated from patient tissue might be derived from neoplastic cells, they could also be derived from possible fusion events.

5. Conclusions and Outlook

This thesis project clearly demonstrated that xenografting of primary patient-derived tumor tissue and adherent cell culture under serum-free conditions facilitate tumor cell enrichment and expansion. The tissue bank propagated in mice created in the course of this study will provide an ideal experimental platform for future investigations regarding PDAC TIC biology. Furthermore, this methodology might also work in other tumor entities.

The phenotypic plasticity of pancreatic TIC unraveled here showed that TIC function is not strictly associated to a certain phenotype. Even the role of established markers like CD133 has to be revised in PDAC. In future, the search for TIC associated markers should rather concentrate on proteins that are indeed directly implicated in TIC biology, and not simply a pure phenotypic marker reminiscent of benign stem cell populations like CD133. However, if previously non-tumor-initiating cells acquire TIC potential by the up- and down-regulation of these functional regulators, the future use of TIC markers in research and clinics might be questionable.

This work provides a new model of long term tumor growth in solid tumors that substantially differs from the hierarchical model that our group has recently described for colon cancer. In contrast to the hierarchical cancer stem cell model the data demonstrate that long term tumor growth in pancreatic cancer is maintained by the clonal succession of TIC that can reversibly switch between functionally active and quiescent states. The tumorigenicity of pancreatic TIC appears temporarily restricted and context-dependent. Future projects will need to investigate which mechanisms define the activity and quiescence of these cells. The development of a therapeutic approach that can specifically suppress the recruitment of TIC into a tumor tissue generating mode might also have great potential to increase PDAC patient survival.

Altogether, this work has provided new insights into the phenotypic diversity and the clonal dynamics of the pancreatic TIC compartment. This information might represent a basis for future projects further investigating the biology and vulnerability of pancreatic TIC.

6. References

1. Cleveland, M.H., et al., *Exocrine ontogenies: on the development of pancreatic acinar, ductal and centroacinar cells.* Semin Cell Dev Biol, 2012. **23**(6): p. 711-9.
2. Cockell, M., et al., *Identification of a cell-specific DNA-binding activity that interacts with a transcriptional activator of genes expressed in the acinar pancreas.* Mol Cell Biol, 1989. **9**(6): p. 2464-76.
3. Rose, S.D., et al., *The role of PTF1-P48 in pancreatic acinar gene expression.* J Biol Chem, 2001. **276**(47): p. 44018-26.
4. Reichert, M. and A.K. Rustgi, *Pancreatic ductal cells in development, regeneration, and neoplasia.* J Clin Invest, 2011. **121**(12): p. 4572-8.
5. Leeson, T.S. and R. Leeson, *Close association of centroacinar/ductular and insular cells in the rat pancreas.* Histol Histopathol, 1986. **1**(1): p. 33-42.
6. Parsons, M.J., et al., *Notch-responsive cells initiate the secondary transition in larval zebrafish pancreas.* Mech Dev, 2009. **126**(10): p. 898-912.
7. Logsdon, C.D. and B. Ji, *The role of protein synthesis and digestive enzymes in acinar cell injury.* Nat Rev Gastroenterol Hepatol, 2013.
8. Golosow, N. and C. Grobstein, *Epitheliomesenchymal interaction in pancreatic morphogenesis.* Dev Biol, 1962. **4**: p. 242-55.
9. Wessels, N. and J. Cohen, *Early pancreas organogenesis: morphogenesis, tissue interactions, and mass effects.* Developmental Biology, 1967. **15**: p. 237-70.
10. Gittes, G.K., et al., *Lineage-specific morphogenesis in the developing pancreas: role of mesenchymal factors.* Development, 1996. **122**(2): p. 439-47.
11. Le Bras, S., et al., *Fibroblast growth factor 2 promotes pancreatic epithelial cell proliferation via functional fibroblast growth factor receptors during embryonic life.* Diabetes, 1998. **47**(8): p. 1236-42.
12. Miralles, F., et al., *Signaling through fibroblast growth factor receptor 2b plays a key role in the development of the exocrine pancreas.* Proc Natl Acad Sci U S A, 1999. **96**(11): p. 6267-72.
13. Miralles, F., et al., *Interplay between FGF10 and Notch signalling is required for the self-renewal of pancreatic progenitors.* Int J Dev Biol, 2006. **50**(1): p. 17-26.
14. Hart, A., S. Papadopoulou, and H. Edlund, *Fgf10 maintains notch activation, stimulates proliferation, and blocks differentiation of pancreatic epithelial cells.* Dev Dyn, 2003. **228**(2): p. 185-93.
15. Norgaard, G.A., J.N. Jensen, and J. Jensen, *FGF10 signaling maintains the pancreatic progenitor cell state revealing a novel role of Notch in organ development.* Dev Biol, 2003. **264**(2): p. 323-38.
16. Kobayashi, H., et al., *Retinoid signaling controls mouse pancreatic exocrine lineage selection through epithelial-mesenchymal interactions.* Gastroenterology, 2002. **123**(4): p. 1331-40.
17. Crisera, C.A., et al., *Expression and role of laminin-1 in mouse pancreatic organogenesis.* Diabetes, 2000. **49**(6): p. 936-44.
18. Kadison, A., et al., *Retinoid signaling directs secondary lineage selection in pancreatic organogenesis.* J Pediatr Surg, 2001. **36**(8): p. 1150-6.
19. Gu, G., J. Dubauskaite, and D.A. Melton, *Direct evidence for the pancreatic lineage: NGN3+ cells are islet progenitors and are distinct from duct progenitors.* Development, 2002. **129**(10): p. 2447-57.
20. Kawaguchi, Y., et al., *The role of the transcriptional regulator Ptf1a in converting intestinal to pancreatic progenitors.* Nat Genet, 2002. **32**(1): p. 128-34.
21. Kopinke, D., et al., *Lineage tracing reveals the dynamic contribution of Hes1+ cells to the developing and adult pancreas.* Development, 2011. **138**(3): p. 431-41.

22. Kopp, J.L., et al., *Identification of Sox9-dependent acinar-to-ductal reprogramming as the principal mechanism for initiation of pancreatic ductal adenocarcinoma.* Cancer Cell, 2012. **22**(6): p. 737-50.
23. Solar, M., et al., *Pancreatic exocrine duct cells give rise to insulin-producing beta cells during embryogenesis but not after birth.* Dev Cell, 2009. **17**(6): p. 849-60.
24. Schaffer, A.E., et al., *Nkx6 transcription factors and Ptf1a function as antagonistic lineage determinants in multipotent pancreatic progenitors.* Dev Cell, 2010. **18**(6): p. 1022-9.
25. Zhou, Q., et al., *A multipotent progenitor domain guides pancreatic organogenesis.* Dev Cell, 2007. **13**(1): p. 103-14.
26. Esni, F., et al., *Notch inhibits Ptf1 function and acinar cell differentiation in developing mouse and zebrafish pancreas.* Development, 2004. **131**(17): p. 4213-24.
27. Jensen, J., et al., *Independent development of pancreatic alpha- and beta-cells from neurogenin3-expressing precursors: a role for the notch pathway in repression of premature differentiation.* Diabetes, 2000. **49**(2): p. 163-76.
28. Holmstrom, S.R., et al., *LRH-1 and PTF1-L coregulate an exocrine pancreas-specific transcriptional network for digestive function.* Genes Dev, 2011. **25**(16): p. 1674-9.
29. Jia, D., Y. Sun, and S.F. Konieczny, *Mist1 regulates pancreatic acinar cell proliferation through p21 CIP1/WAF1.* Gastroenterology, 2008. **135**(5): p. 1687-97.
30. Luo, X., et al., *Aberrant localization of intracellular organelles, Ca2+ signaling, and exocytosis in Mist1 null mice.* J Biol Chem, 2005. **280**(13): p. 12668-75.
31. Pin, C.L., A.C. Bonvissuto, and S.F. Konieczny, *Mist1 expression is a common link among serous exocrine cells exhibiting regulated exocytosis.* Anat Rec, 2000. **259**(2): p. 157-67.
32. Pin, C.L., et al., *The bHLH transcription factor Mist1 is required to maintain exocrine pancreas cell organization and acinar cell identity.* J Cell Biol, 2001. **155**(4): p. 519-30.
33. Miyamoto, Y., et al., *Notch mediates TGF alpha-induced changes in epithelial differentiation during pancreatic tumorigenesis.* Cancer Cell, 2003. **3**(6): p. 565-76.
34. Stanger, B.Z., et al., *Pten constrains centroacinar cell expansion and malignant transformation in the pancreas.* Cancer Cell, 2005. **8**(3): p. 185-95.
35. Kopinke, D., et al., *Ongoing Notch signaling maintains phenotypic fidelity in the adult exocrine pancreas.* Dev Biol, 2012. **362**(1): p. 57-64.
36. Jensen, J.N., et al., *Recapitulation of elements of embryonic development in adult mouse pancreatic regeneration.* Gastroenterology, 2005. **128**(3): p. 728-41.
37. Morris, J.P.t., et al., *Beta-catenin blocks Kras-dependent reprogramming of acini into pancreatic cancer precursor lesions in mice.* J Clin Invest, 2010. **120**(2): p. 508-20.
38. Siveke, J.T., et al., *Notch signaling is required for exocrine regeneration after acute pancreatitis.* Gastroenterology, 2008. **134**(2): p. 544-55.
39. Barker, N., M. van de Wetering, and H. Clevers, *The intestinal stem cell.* Genes Dev, 2008. **22**(14): p. 1856-64.
40. Barker, N., et al., *Identification of stem cells in small intestine and colon by marker gene Lgr5.* Nature, 2007. **449**(7165): p. 1003-7.
41. Bjerknes, M. and H. Cheng, *Clonal analysis of mouse intestinal epithelial progenitors.* Gastroenterology, 1999. **116**(1): p. 7-14.
42. Booth, C. and C.S. Potten, *Gut instincts: thoughts on intestinal epithelial stem cells.* J Clin Invest, 2000. **105**(11): p. 1493-9.
43. Merlos-Suarez, A., et al., *The intestinal stem cell signature identifies colorectal cancer stem cells and predicts disease relapse.* Cell Stem Cell, 2011. **8**(5): p. 511-24.
44. Reynolds, B.A. and S. Weiss, *Generation of neurons and astrocytes from isolated cells of the adult mammalian central nervous system.* Science, 1992. **255**(5052): p. 1707-10.
45. Sun, Y., et al., *CD133 (Prominin) negative human neural stem cells are clonogenic and tripotent.* PLoS One, 2009. **4**(5): p. e5498.

46. Uchida, N., et al., *Direct isolation of human central nervous system stem cells.* Proc Natl Acad Sci U S A, 2000. **97**(26): p. 14720-5.
47. Becker, A.J., C.E. Mc, and J.E. Till, *Cytological demonstration of the clonal nature of spleen colonies derived from transplanted mouse marrow cells.* Nature, 1963. **197**: p. 452-4.
48. Reya, T., et al., *Stem cells, cancer, and cancer stem cells.* Nature, 2001. **414**(6859): p. 105-11.
49. Till, J.E. and C.E. Mc, *A direct measurement of the radiation sensitivity of normal mouse bone marrow cells.* Radiat Res, 1961. **14**: p. 213-22.
50. Wu, A.M., et al., *Cytological evidence for a relationship between normal hemotopoietic colony-forming cells and cells of the lymphoid system.* J Exp Med, 1968. **127**(3): p. 455-64.
51. Siegel, R., D. Naishadham, and A. Jemal, *Cancer statistics, 2013.* CA Cancer J Clin, 2013. **63**(1): p. 11-30.
52. Moore, M.J., et al., *Erlotinib plus gemcitabine compared with gemcitabine alone in patients with advanced pancreatic cancer: a phase III trial of the National Cancer Institute of Canada Clinical Trials Group.* J Clin Oncol, 2007. **25**(15): p. 1960-6.
53. Ahlgren, J.D., *Chemotherapy for pancreatic carcinoma.* Cancer, 1996. **78**(3 Suppl): p. 654-63.
54. Rosenberg, L., *Treatment of pancreatic cancer. Promises and problems of tamoxifen, somatostatin analogs, and gemcitabine.* Int J Pancreatol, 1997. **22**(2): p. 81-93.
55. Rothenberg, M.L., et al., *A rationale for expanding the endpoints for clinical trials in advanced pancreatic carcinoma.* Cancer, 1996. **78**(3 Suppl): p. 627-32.
56. Warshaw, A.L. and C. Fernandez-del Castillo, *Pancreatic carcinoma.* N Engl J Med, 1992. **326**(7): p. 455-65.
57. Xu, Q., T.P. Zhang, and Y.P. Zhao, *Advances in early diagnosis and therapy of pancreatic cancer.* Hepatobiliary Pancreat Dis Int, 2011. **10**(2): p. 128-35.
58. Collins, M.A., et al., *Oncogenic Kras is required for both the initiation and maintenance of pancreatic cancer in mice.* J Clin Invest, 2012. **122**(2): p. 639-53.
59. Collins, M.A., et al., *Metastatic pancreatic cancer is dependent on oncogenic Kras in mice.* PLoS One, 2012. **7**(12): p. e49707.
60. Hezel, A.F., et al., *Genetics and biology of pancreatic ductal adenocarcinoma.* Genes Dev, 2006. **20**(10): p. 1218-49.
61. Iacobuzio-Donahue, C.A., et al., *Genetic basis of pancreas cancer development and progression: insights from whole-exome and whole-genome sequencing.* Clin Cancer Res, 2012. **18**(16): p. 4257-65.
62. Moskaluk, C.A., R.H. Hruban, and S.E. Kern, *p16 and K-ras gene mutations in the intraductal precursors of human pancreatic adenocarcinoma.* Cancer Res, 1997. **57**(11): p. 2140-3.
63. Ying, H., et al., *Oncogenic Kras maintains pancreatic tumors through regulation of anabolic glucose metabolism.* Cell, 2012. **149**(3): p. 656-70.
64. Caldas, C. and S.E. Kern, *K-ras mutation and pancreatic adenocarcinoma.* Int J Pancreatol, 1995. **18**(1): p. 1-6.
65. Aguirre, A.J., et al., *High-resolution characterization of the pancreatic adenocarcinoma genome.* Proc Natl Acad Sci U S A, 2004. **101**(24): p. 9067-72.
66. Hingorani, S.R. and D.A. Tuveson, *Ras redux: rethinking how and where Ras acts.* Curr Opin Genet Dev, 2003. **13**(1): p. 6-13.
67. Maitra, A. and R.H. Hruban, *Pancreatic cancer.* Annu Rev Pathol, 2008. **3**: p. 157-88.
68. Ardito, C.M., et al., *EGF receptor is required for KRAS-induced pancreatic tumorigenesis.* Cancer Cell, 2012. **22**(3): p. 304-17.
69. Jones, S., et al., *Core signaling pathways in human pancreatic cancers revealed by global genomic analyses.* Science, 2008. **321**(5897): p. 1801-6.
70. Yachida, S. and C.A. Iacobuzio-Donahue, *Evolution and dynamics of pancreatic cancer progression.* Oncogene, 2013.

71. De La, O.J., et al., *Notch and Kras reprogram pancreatic acinar cells to ductal intraepithelial neoplasia.* Proc Natl Acad Sci U S A, 2008. **105**(48): p. 18907-12.
72. Guerra, C., et al., *Chronic pancreatitis is essential for induction of pancreatic ductal adenocarcinoma by K-Ras oncogenes in adult mice.* Cancer Cell, 2007. **11**(3): p. 291-302.
73. Habbe, N., et al., *Spontaneous induction of murine pancreatic intraepithelial neoplasia (mPanIN) by acinar cell targeting of oncogenic Kras in adult mice.* Proc Natl Acad Sci U S A, 2008. **105**(48): p. 18913-8.
74. Shi, G., et al., *Loss of the acinar-restricted transcription factor Mist1 accelerates Kras-induced pancreatic intraepithelial neoplasia.* Gastroenterology, 2009. **136**(4): p. 1368-78.
75. Zhu, L., et al., *Acinar cells contribute to the molecular heterogeneity of pancreatic intraepithelial neoplasia.* Am J Pathol, 2007. **171**(1): p. 263-73.
76. Lowenfels, A.B., et al., *Pancreatitis and the risk of pancreatic cancer. International Pancreatitis Study Group.* N Engl J Med, 1993. **328**(20): p. 1433-7.
77. Malka, D., et al., *Risk of pancreatic adenocarcinoma in chronic pancreatitis.* Gut, 2002. **51**(6): p. 849-52.
78. Carriere, C., et al., *Acute pancreatitis markedly accelerates pancreatic cancer progression in mice expressing oncogenic Kras.* Biochem Biophys Res Commun, 2009. **382**(3): p. 561-5.
79. Maitra, A., et al., *Precursors to invasive pancreatic cancer.* Adv Anat Pathol, 2005. **12**(2): p. 81-91.
80. Yachida, S., et al., *Distant metastasis occurs late during the genetic evolution of pancreatic cancer.* Nature, 2010. **467**(7319): p. 1114-7.
81. Kloppel, G., et al., *Histological and fine structural features of pancreatic ductal adenocarcinomas in relation to growth and prognosis: studies in xenografted tumours and clinico-histopathological correlation in a series of 75 cases.* Histopathology, 1985. **9**(8): p. 841-56.
82. Korc, M., *Pancreatic cancer-associated stroma production.* Am J Surg, 2007. **194**(4 Suppl): p. S84-6.
83. Mollenhauer, J., I. Roether, and H.F. Kern, *Distribution of extracellular matrix proteins in pancreatic ductal adenocarcinoma and its influence on tumor cell proliferation in vitro.* Pancreas, 1987. **2**(1): p. 14-24.
84. Apte, M.V., et al., *Desmoplastic reaction in pancreatic cancer: role of pancreatic stellate cells.* Pancreas, 2004. **29**(3): p. 179-87.
85. Bachem, M.G., et al., *Pancreatic stellate cells--role in pancreas cancer.* Langenbecks Arch Surg, 2008. **393**(6): p. 891-900.
86. Yen, T.W., et al., *Myofibroblasts are responsible for the desmoplastic reaction surrounding human pancreatic carcinomas.* Surgery, 2002. **131**(2): p. 129-34.
87. Hwang, R.F., et al., *Cancer-associated stromal fibroblasts promote pancreatic tumor progression.* Cancer Res, 2008. **68**(3): p. 918-26.
88. Bachem, M.G., et al., *Pancreatic carcinoma cells induce fibrosis by stimulating proliferation and matrix synthesis of stellate cells.* Gastroenterology, 2005. **128**(4): p. 907-21.
89. Farrow, B., D.H. Berger, and D. Rowley, *Tumor-derived pancreatic stellate cells promote pancreatic cancer cell invasion through release of thrombospondin-2.* J Surg Res, 2009. **156**(1): p. 155-60.
90. Froeling, F.E., et al., *Organotypic culture model of pancreatic cancer demonstrates that stromal cells modulate E-cadherin, beta-catenin, and Ezrin expression in tumor cells.* Am J Pathol, 2009. **175**(2): p. 636-48.
91. Mahadevan, D. and D.D. Von Hoff, *Tumor-stroma interactions in pancreatic ductal adenocarcinoma.* Mol Cancer Ther, 2007. **6**(4): p. 1186-97.
92. Muerkoster, S.S., et al., *Role of myofibroblasts in innate chemoresistance of pancreatic carcinoma--epigenetic downregulation of caspases.* Int J Cancer, 2008. **123**(8): p. 1751-60.

93. Qian, L.W., et al., *Co-cultivation of pancreatic cancer cells with orthotopic tumor-derived fibroblasts: fibroblasts stimulate tumor cell invasion via HGF secretion whereas cancer cells exert a minor regulative effect on fibroblasts HGF production.* Cancer Lett, 2003. **190**(1): p. 105-12.
94. Schneiderhan, W., et al., *Pancreatic stellate cells are an important source of MMP-2 in human pancreatic cancer and accelerate tumor progression in a murine xenograft model and CAM assay.* J Cell Sci, 2007. **120**(Pt 3): p. 512-9.
95. Tian, H., et al., *Hedgehog signaling is restricted to the stromal compartment during pancreatic carcinogenesis.* Proc Natl Acad Sci U S A, 2009. **106**(11): p. 4254-9.
96. Yoshida, S., et al., *Pancreatic cancer stimulates pancreatic stellate cell proliferation and TIMP-1 production through the MAP kinase pathway.* Biochem Biophys Res Commun, 2004. **323**(4): p. 1241-5.
97. Luttenberger, T., et al., *Platelet-derived growth factors stimulate proliferation and extracellular matrix synthesis of pancreatic stellate cells: implications in pathogenesis of pancreas fibrosis.* Lab Invest, 2000. **80**(1): p. 47-55.
98. Mews, P., et al., *Pancreatic stellate cells respond to inflammatory cytokines: potential role in chronic pancreatitis.* Gut, 2002. **50**(4): p. 535-41.
99. Apte, M.V., et al., *Pancreatic stellate cells are activated by proinflammatory cytokines: implications for pancreatic fibrogenesis.* Gut, 1999. **44**(4): p. 534-41.
100. Fujita, H., et al., *Tumor-stromal interactions with direct cell contacts enhance proliferation of human pancreatic carcinoma cells.* Cancer Sci, 2009. **100**(12): p. 2309-17.
101. Farrow, B., et al., *Characterization of tumor-derived pancreatic stellate cells.* J Surg Res, 2009. **157**(1): p. 96-102.
102. Tien, Y.W., et al., *Pancreatic carcinoma cells stimulate proliferation and matrix synthesis of hepatic stellate cells.* J Hepatol, 2009. **51**(2): p. 307-14.
103. Grunert, S., M. Jechlinger, and H. Beug, *Diverse cellular and molecular mechanisms contribute to epithelial plasticity and metastasis.* Nat Rev Mol Cell Biol, 2003. **4**(8): p. 657-65.
104. Petersen, O.W., et al., *Epithelial to mesenchymal transition in human breast cancer can provide a nonmalignant stroma.* Am J Pathol, 2003. **162**(2): p. 391-402.
105. Potenta, S., E. Zeisberg, and R. Kalluri, *The role of endothelial-to-mesenchymal transition in cancer progression.* Br J Cancer, 2008. **99**(9): p. 1375-9.
106. Zeisberg, E.M., et al., *Discovery of endothelial to mesenchymal transition as a source for carcinoma-associated fibroblasts.* Cancer Res, 2007. **67**(21): p. 10123-8.
107. Jungert, K., et al., *Sp1 is required for transforming growth factor-beta-induced mesenchymal transition and migration in pancreatic cancer cells.* Cancer Res, 2007. **67**(4): p. 1563-70.
108. Watanabe, S., et al., *HMGA2 maintains oncogenic RAS-induced epithelial-mesenchymal transition in human pancreatic cancer cells.* Am J Pathol, 2009. **174**(3): p. 854-68.
109. Bonnet, D. and J.E. Dick, *Human acute myeloid leukemia is organized as a hierarchy that originates from a primitive hematopoietic cell.* Nat Med, 1997. **3**(7): p. 730-7.
110. Kamel-Reid, S., et al., *A model of human acute lymphoblastic leukemia in immune-deficient SCID mice.* Science, 1989. **246**(4937): p. 1597-600.
111. Lapidot, T., et al., *A cell initiating human acute myeloid leukaemia after transplantation into SCID mice.* Nature, 1994. **367**(6464): p. 645-8.
112. Shultz, L.D. and C.L. Sidman, *Genetically determined murine models of immunodeficiency.* Annu Rev Immunol, 1987. **5**: p. 367-403.
113. Dieter, S.M., et al., *Distinct types of tumor-initiating cells form human colon cancer tumors and metastases.* Cell Stem Cell, 2011. **9**(4): p. 357-65.
114. Dick, J.E., *Stem cell concepts renew cancer research.* Blood, 2008. **112**(13): p. 4793-807.
115. Nguyen, L.V., et al., *Cancer stem cells: an evolving concept.* Nat Rev Cancer, 2012. **12**(2): p. 133-43.

116. Bechhoefer, J. and N. Rhind, *Replication timing and its emergence from stochastic processes.* Trends Genet, 2012. **28**(8): p. 374-81.
117. Dingli, D., A. Traulsen, and J.M. Pacheco, *Stochastic dynamics of hematopoietic tumor stem cells.* Cell Cycle, 2007. **6**(4): p. 461-6.
118. Greaves, M. and C.C. Maley, *Clonal evolution in cancer.* Nature, 2012. **481**(7381): p. 306-13.
119. Nowell, P.C., *The clonal evolution of tumor cell populations.* Science, 1976. **194**(4260): p. 23-8.
120. Shackleton, M., et al., *Heterogeneity in cancer: cancer stem cells versus clonal evolution.* Cell, 2009. **138**(5): p. 822-9.
121. Asknazy, M., *Die Teratome nach ihrem Bau, ihrem Verlauf, ihrer Genese und im Vergleich zum experimentellen Teratoid.* Verhandl. Deutsch. Pathol., 1907. **11**: p. 39-82.
122. Kleinsmith, L.J. and G.B. Pierce, Jr., *Multipotentiality of Single Embryonal Carcinoma Cells.* Cancer Res, 1964. **24**: p. 1544-51.
123. Pierce, G.B., Jr., F.J. Dixon, Jr., and E.L. Verney, *Teratocarcinogenic and tissue-forming potentials of the cell types comprising neoplastic embryoid bodies.* Lab Invest, 1960. **9**: p. 583-602.
124. Pierce, G.B. and L.D. Johnson, *Differentiation and cancer.* In Vitro, 1971. **7**(3): p. 140-5.
125. Pierce, G.B. and W.C. Speers, *Tumors as caricatures of the process of tissue renewal: prospects for therapy by directing differentiation.* Cancer Res, 1988. **48**(8): p. 1996-2004.
126. Pierce, G.B. and C. Wallace, *Differentiation of malignant to benign cells.* Cancer Res, 1971. **31**(2): p. 127-34.
127. Hope, K.J., L. Jin, and J.E. Dick, *Acute myeloid leukemia originates from a hierarchy of leukemic stem cell classes that differ in self-renewal capacity.* Nat Immunol, 2004. **5**(7): p. 738-43.
128. Jamieson, C.H., et al., *Granulocyte-macrophage progenitors as candidate leukemic stem cells in blast-crisis CML.* N Engl J Med, 2004. **351**(7): p. 657-67.
129. Neering, S.J., et al., *Leukemia stem cells in a genetically defined murine model of blast-crisis CML.* Blood, 2007. **110**(7): p. 2578-85.
130. Oravecz-Wilson, K.I., et al., *Persistence of leukemia-initiating cells in a conditional knockin model of an imatinib-responsive myeloproliferative disorder.* Cancer Cell, 2009. **16**(2): p. 137-48.
131. Miraglia, S., et al., *A novel five-transmembrane hematopoietic stem cell antigen: isolation, characterization, and molecular cloning.* Blood, 1997. **90**(12): p. 5013-21.
132. Yin, A.H., et al., *AC133, a novel marker for human hematopoietic stem and progenitor cells.* Blood, 1997. **90**(12): p. 5002-12.
133. Richardson, G.D., et al., *CD133, a novel marker for human prostatic epithelial stem cells.* J Cell Sci, 2004. **117**(Pt 16): p. 3539-45.
134. Alessandri, G., et al., *Isolation and culture of human muscle-derived stem cells able to differentiate into myogenic and neurogenic cell lineages.* Lancet, 2004. **364**(9448): p. 1872-83.
135. Singh, S.K., et al., *Identification of a cancer stem cell in human brain tumors.* Cancer Res, 2003. **63**(18): p. 5821-8.
136. Singh, S.K., et al., *Identification of human brain tumour initiating cells.* Nature, 2004. **432**(7015): p. 396-401.
137. Ricci-Vitiani, L., et al., *Identification and expansion of human colon-cancer-initiating cells.* Nature, 2007. **445**(7123): p. 111-5.
138. Suva, M.L., et al., *Identification of cancer stem cells in Ewing's sarcoma.* Cancer Res, 2009. **69**(5): p. 1776-81.
139. Al-Hajj, M., et al., *Prospective identification of tumorigenic breast cancer cells.* Proc Natl Acad Sci U S A, 2003. **100**(7): p. 3983-8.

140. Beier, D., et al., *CD133(+) and CD133(-) glioblastoma-derived cancer stem cells show differential growth characteristics and molecular profiles.* Cancer Res, 2007. **67**(9): p. 4010-5.
141. Shmelkov, S.V., et al., *CD133 expression is not restricted to stem cells, and both CD133+ and CD133- metastatic colon cancer cells initiate tumors.* J Clin Invest, 2008. **118**(6): p. 2111-20.
142. Penchev, V.R., et al., *Heterogeneity and targeting of pancreatic cancer stem cells.* Clin Cancer Res, 2012. **18**(16): p. 4277-84.
143. Li, C., et al., *Identification of pancreatic cancer stem cells.* Cancer Res, 2007. **67**(3): p. 1030-7.
144. Hermann, P.C., et al., *Distinct populations of cancer stem cells determine tumor growth and metastatic activity in human pancreatic cancer.* Cell Stem Cell, 2007. **1**(3): p. 313-23.
145. Lonardo, E., et al., *Nodal/Activin signaling drives self-renewal and tumorigenicity of pancreatic cancer stem cells and provides a target for combined drug therapy.* Cell Stem Cell, 2011. **9**(5): p. 433-46.
146. Ginestier, C., et al., *ALDH1 is a marker of normal and malignant human mammary stem cells and a predictor of poor clinical outcome.* Cell Stem Cell, 2007. **1**(5): p. 555-67.
147. Ishizawa, K., et al., *Tumor-initiating cells are rare in many human tumors.* Cell Stem Cell, 2010. **7**(3): p. 279-82.
148. Rasheed, Z.A., et al., *Prognostic significance of tumorigenic cells with mesenchymal features in pancreatic adenocarcinoma.* J Natl Cancer Inst, 2010. **102**(5): p. 340-51.
149. Ma, I. and A.L. Allan, *The role of human aldehyde dehydrogenase in normal and cancer stem cells.* Stem Cell Rev, 2011. **7**(2): p. 292-306.
150. Chute, J.P., et al., *Inhibition of aldehyde dehydrogenase and retinoid signaling induces the expansion of human hematopoietic stem cells.* Proc Natl Acad Sci U S A, 2006. **103**(31): p. 11707-12.
151. Muramoto, G.G., et al., *Inhibition of aldehyde dehydrogenase expands hematopoietic stem cells with radioprotective capacity.* Stem Cells, 2010. **28**(3): p. 523-34.
152. Kastan, M.B., et al., *Direct demonstration of elevated aldehyde dehydrogenase in human hematopoietic progenitor cells.* Blood, 1990. **75**(10): p. 1947-50.
153. Jean, E., et al., *Aldehyde dehydrogenase activity promotes survival of human muscle precursor cells.* J Cell Mol Med, 2011. **15**(1): p. 119-33.
154. Vauchez, K., et al., *Aldehyde dehydrogenase activity identifies a population of human skeletal muscle cells with high myogenic capacities.* Mol Ther, 2009. **17**(11): p. 1948-58.
155. Burger, P.E., et al., *High aldehyde dehydrogenase activity: a novel functional marker of murine prostate stem/progenitor cells.* Stem Cells, 2009. **27**(9): p. 2220-8.
156. Brabletz, T., et al., *Opinion: migrating cancer stem cells - an integrated concept of malignant tumour progression.* Nat Rev Cancer, 2005. **5**(9): p. 744-9.
157. Barrallo-Gimeno, A. and M.A. Nieto, *The Snail genes as inducers of cell movement and survival: implications in development and cancer.* Development, 2005. **132**(14): p. 3151-61.
158. Berx, G., et al., *Pre-EMTing metastasis? Recapitulation of morphogenetic processes in cancer.* Clin Exp Metastasis, 2007. **24**(8): p. 587-97.
159. Peinado, H., D. Olmeda, and A. Cano, *Snail, Zeb and bHLH factors in tumour progression: an alliance against the epithelial phenotype?* Nat Rev Cancer, 2007. **7**(6): p. 415-28.
160. Sanchez-Tillo, E., et al., *EMT-activating transcription factors in cancer: beyond EMT and tumor invasiveness.* Cell Mol Life Sci, 2012. **69**(20): p. 3429-56.
161. Wellner, U., et al., *The EMT-activator ZEB1 promotes tumorigenicity by repressing stemness-inhibiting microRNAs.* Nat Cell Biol, 2009. **11**(12): p. 1487-95.
162. Takahashi, K. and S. Yamanaka, *Induction of pluripotent stem cells from mouse embryonic and adult fibroblast cultures by defined factors.* Cell, 2006. **126**(4): p. 663-76.
163. Adachi, K. and H.R. Scholer, *Directing reprogramming to pluripotency by transcription factors.* Curr Opin Genet Dev, 2012. **22**(5): p. 416-22.

164. Di Renzo, M.F., et al., *Expression of the Met/hepatocyte growth factor receptor in human pancreatic cancer.* Cancer Res, 1995. **55**(5): p. 1129-38.
165. Ebert, M., et al., *Coexpression of the c-met proto-oncogene and hepatocyte growth factor in human pancreatic cancer.* Cancer Res, 1994. **54**(22): p. 5775-8.
166. Furukawa, T., et al., *Hepatocyte growth factor and Met receptor expression in human pancreatic carcinogenesis.* Am J Pathol, 1995. **147**(4): p. 889-95.
167. Li, C., et al., *c-Met is a marker of pancreatic cancer stem cells and therapeutic target.* Gastroenterology, 2011. **141**(6): p. 2218-2227 e5.
168. Schmidt, M., et al., *High-resolution insertion-site analysis by linear amplification-mediated PCR (LAM-PCR).* Nat Methods, 2007. **4**(12): p. 1051-7.
169. Schmidt, M., et al., *Detection and direct genomic sequencing of multiple rare unknown flanking DNA in highly complex samples.* Hum Gene Ther, 2001. **12**(7): p. 743-9.
170. Naldini, L., et al., *Efficient transfer, integration, and sustained long-term expression of the transgene in adult rat brains injected with a lentiviral vector.* Proc Natl Acad Sci U S A, 1996. **93**(21): p. 11382-8.
171. Naldini, L., et al., *In vivo gene delivery and stable transduction of nondividing cells by a lentiviral vector.* Science, 1996. **272**(5259): p. 263-7.
172. Case, S.S., et al., *Stable transduction of quiescent CD34(+)CD38(-) human hematopoietic cells by HIV-1-based lentiviral vectors.* Proc Natl Acad Sci U S A, 1999. **96**(6): p. 2988-93.
173. Uchida, N., et al., *HIV, but not murine leukemia virus, vectors mediate high efficiency gene transfer into freshly isolated G0/G1 human hematopoietic stem cells.* Proc Natl Acad Sci U S A, 1998. **95**(20): p. 11939-44.
174. Kallio, M.A., et al., *Chipster: user-friendly analysis software for microarray and other high-throughput data.* BMC Genomics, 2011. **12**: p. 507.
175. Bachem, M.G., et al., *Identification, culture, and characterization of pancreatic stellate cells in rats and humans.* Gastroenterology, 1998. **115**(2): p. 421-32.
176. Dull, T., et al., *A third-generation lentivirus vector with a conditional packaging system.* J Virol, 1998. **72**(11): p. 8463-71.
177. Oppel, F., et al., *SOX2-RNAi attenuates S-phase entry and induces RhoA-dependent switch to protease-independent amoeboid migration in human glioma cells.* Mol Cancer, 2011. **10**: p. 137.
178. Zavidij, O., et al., *Stable long-term blood formation by stem cells in murine steady-state hematopoiesis.* Stem Cells, 2012. **30**(9): p. 1961-70.
179. Oppel, F.B., C. R.; Dubash, T. D.; Hoffmann, C. M.; Abel, U.; Dieter, S. M.; Koch, M.; Weitz, J.; Werner, J.; Bergmann, F.; Weichert, W.; Schmidt, M.; von Kalle, C.; Glimm, H., *Succession Of Transiently Active Tumour-Initiating Cell Clones in Human Pancreatic Cancer* in submission, 2013.
180. Pollard, S.M., et al., *Glioma stem cell lines expanded in adherent culture have tumor-specific phenotypes and are suitable for chemical and genetic screens.* Cell Stem Cell, 2009. **4**(6): p. 568-80.
181. Lee, J., et al., *Tumor stem cells derived from glioblastomas cultured in bFGF and EGF more closely mirror the phenotype and genotype of primary tumors than do serum-cultured cell lines.* Cancer Cell, 2006. **9**(5): p. 391-403.
182. Beres, T.M., et al., *PTF1 is an organ-specific and Notch-independent basic helix-loop-helix complex containing the mammalian Suppressor of Hairless (RBP-J) or its paralogue, RBP-L.* Mol Cell Biol, 2006. **26**(1): p. 117-30.
183. Jorgensen, M.C., et al., *An illustrated review of early pancreas development in the mouse.* Endocr Rev, 2007. **28**(6): p. 685-705.
184. Masui, T., et al., *Early pancreatic development requires the vertebrate Suppressor of Hairless (RBPJ) in the PTF1 bHLH complex.* Genes Dev, 2007. **21**(20): p. 2629-43.

185. Rutter, W.J., et al., *Regulation of specific protein synthesis in cytodifferentiation.* J Cell Physiol, 1968. **72**(2): p. Suppl 1:1-18.
186. Hald, J., et al., *Pancreatic islet and progenitor cell surface markers with cell sorting potential.* Diabetologia, 2012. **55**(1): p. 154-65.
187. Portela-Gomes, G.M., G.W. Hacker, and R. Weitgasser, *Neuroendocrine cell markers for pancreatic islets and tumors.* Appl Immunohistochem Mol Morphol, 2004. **12**(3): p. 183-92.
188. Rizzino, A., *Sox2 and Oct-3/4: a versatile pair of master regulators that orchestrate the self-renewal and pluripotency of embryonic stem cells.* Wiley Interdiscip Rev Syst Biol Med, 2009. **1**(2): p. 228-36.
189. Paruzynski, A., et al., *Genome-wide high-throughput integrome analyses by nrLAM-PCR and next-generation sequencing.* Nat Protoc, 2010. **5**(8): p. 1379-95.
190. Kent, W.J., *BLAT--the BLAST-like alignment tool.* Genome Res, 2002. **12**(4): p. 656-64.
191. Hecht, B.K., et al., *Cytogenetics of malignant gliomas: I. The autosomes with reference to rearrangements.* Cancer Genet Cytogenet, 1995. **84**(1): p. 1-8.
192. Kubota, H., et al., *Identification of recurrent chromosomal rearrangements and the unique relationship between low-level amplification and translocation in glioblastoma.* Genes Chromosomes Cancer, 2001. **31**(2): p. 125-33.
193. Wiltshire, R.N., et al., *Comparative genetic patterns of glioblastoma multiforme: potential diagnostic tool for tumor classification.* Neuro Oncol, 2000. **2**(3): p. 164-73.
194. Jimeno, A., et al., *A direct pancreatic cancer xenograft model as a platform for cancer stem cell therapeutic development.* Mol Cancer Ther, 2009. **8**(2): p. 310-4.
195. Rubio-Viqueira, B., et al., *An in vivo platform for translational drug development in pancreatic cancer.* Clin Cancer Res, 2006. **12**(15): p. 4652-61.
196. Immervoll, H., et al., *Expression of the "stem cell marker" CD133 in pancreas and pancreatic ductal adenocarcinomas.* BMC Cancer, 2008. **8**: p. 48.
197. Lonardo, E., P.C. Hermann, and C. Heeschen, *Pancreatic cancer stem cells - update and future perspectives.* Mol Oncol, 2010. **4**(5): p. 431-42.
198. Taussig, D.C., et al., *Anti-CD38 antibody-mediated clearance of human repopulating cells masks the heterogeneity of leukemia-initiating cells.* Blood, 2008. **112**(3): p. 568-75.
199. Taussig, D.C., et al., *Leukemia-initiating cells from some acute myeloid leukemia patients with mutated nucleophosmin reside in the CD34(-) fraction.* Blood, 2010. **115**(10): p. 1976-84.
200. Quintana, E., et al., *Phenotypic heterogeneity among tumorigenic melanoma cells from patients that is reversible and not hierarchically organized.* Cancer Cell, 2010. **18**(5): p. 510-23.
201. Eisterer, W., et al., *Different subsets of primary chronic myeloid leukemia stem cells engraft immunodeficient mice and produce a model of the human disease.* Leukemia, 2005. **19**(3): p. 435-41.
202. Wilson, A., et al., *Hematopoietic stem cells reversibly switch from dormancy to self-renewal during homeostasis and repair.* Cell, 2008. **135**(6): p. 1118-29.
203. Wilson, A., E. Laurenti, and A. Trumpp, *Balancing dormant and self-renewing hematopoietic stem cells.* Curr Opin Genet Dev, 2009. **19**(5): p. 461-8.
204. Wilson, A., et al., *Dormant and self-renewing hematopoietic stem cells and their niches.* Ann N Y Acad Sci, 2007. **1106**: p. 64-75.
205. van der Wath, R.C., et al., *Estimating dormant and active hematopoietic stem cell kinetics through extensive modeling of bromodeoxyuridine label-retaining cell dynamics.* PLoS One, 2009. **4**(9): p. e6972.
206. Essers, M.A., et al., *IFNalpha activates dormant haematopoietic stem cells in vivo.* Nature, 2009. **458**(7240): p. 904-8.
207. Essers, M.A. and A. Trumpp, *Targeting leukemic stem cells by breaking their dormancy.* Mol Oncol, 2010. **4**(5): p. 443-50.

208. Trumpp, A., M. Essers, and A. Wilson, *Awakening dormant haematopoietic stem cells.* Nat Rev Immunol, 2010. **10**(3): p. 201-9.
209. Guan, Y., B. Gerhard, and D.E. Hogge, *Detection, isolation, and stimulation of quiescent primitive leukemic progenitor cells from patients with acute myeloid leukemia (AML).* Blood, 2003. **101**(8): p. 3142-9.
210. Holyoake, T., et al., *Isolation of a highly quiescent subpopulation of primitive leukemic cells in chronic myeloid leukemia.* Blood, 1999. **94**(6): p. 2056-64.
211. Saito, Y., et al., *Induction of cell cycle entry eliminates human leukemia stem cells in a mouse model of AML.* Nat Biotechnol, 2010. **28**(3): p. 275-80.
212. Trumpp, A. and O.D. Wiestler, *Mechanisms of Disease: cancer stem cells--targeting the evil twin.* Nat Clin Pract Oncol, 2008. **5**(6): p. 337-47.
213. Copland, M., et al., *Dasatinib (BMS-354825) targets an earlier progenitor population than imatinib in primary CML but does not eliminate the quiescent fraction.* Blood, 2006. **107**(11): p. 4532-9.
214. Glauche, I., et al., *Therapy of chronic myeloid leukaemia can benefit from the activation of stem cells: simulation studies of different treatment combinations.* Br J Cancer, 2012. **106**(11): p. 1742-52.
215. Roesch, A., et al., *A temporarily distinct subpopulation of slow-cycling melanoma cells is required for continuous tumor growth.* Cell, 2010. **141**(4): p. 583-94.
216. Sharma, S.V., et al., *A chromatin-mediated reversible drug-tolerant state in cancer cell subpopulations.* Cell, 2010. **141**(1): p. 69-80.
217. Chu, P., E. Wu, and L.M. Weiss, *Cytokeratin 7 and cytokeratin 20 expression in epithelial neoplasms: a survey of 435 cases.* Mod Pathol, 2000. **13**(9): p. 962-72.
218. Mertens, J.C., et al., *Therapeutic effects of deleting cancer-associated fibroblasts in cholangiocarcinoma.* Cancer Res, 2013. **73**(2): p. 897-907.
219. Andrae, J., R. Gallini, and C. Betsholtz, *Role of platelet-derived growth factors in physiology and medicine.* Genes Dev, 2008. **22**(10): p. 1276-312.
220. Blau, H.E., *AID Dependent DNA demethylation in reprogramming to pluripotency.* Stem cells and cancer, 6th international Heinrich F.C. Behr symposium, German Cancer Research Center, Heidelberg, 2010.
221. Wang, R., et al., *Spontaneous cancer-stromal cell fusion as a mechanism of prostate cancer androgen-independent progression.* PLoS One, 2012. **7**(8): p. e42653.
222. Berger, R.L. and D.D. Boos, *P-Values Maximized over a Confidence Set for the Nuisance Parameter.* Journal of the American Statistical Association, 1994. **89**(427): p. 1012-1016.
223. Barnard, G.A., *Significance tests for 2 X 2 tables.* Biometrika, 1947. **34**(1-2): p. 123-38.
224. Berger, R.L., *More powerful tests from confidence interval p values.* American Statistician, 1996. **50**(4): p. 314-318.
225. Lin, C.Y. and M.C. Yang, *Improved p-Value Tests for Comparing Two Independent Binomial Proportions.* Communications in Statistics-Simulation and Computation, 2009. **38**(1): p. 78-91.
226. Baker, C.T., et al., *Modelling and analysis of time-lags in some basic patterns of cell proliferation.* J Math Biol, 1998. **37**(4): p. 341-71.
227. Banks, H.T. and W.C. Thompson, *Mathematical Models of Dividing Cell Populations: Application to CFSE Data.* Mathematical Modelling of Natural Phenomena, 2012. **7**(5): p. 24-52.

Appendix A: Comparative gene expression profiling of serum-treated and serum-free control cells reveals altered expression of markers associated with undifferentiated cell populations or mature pancreas cells.

	Patient 1								Patient 2							
	3Pa, serum-free	3Pa, 10% FBS	fold change	fold expression	8Pa, serum-free	8Pa, 10% FBS	fold change	fold expression	3Pa, serum-free	3Pa, 10% FBS	fold change	fold expression	8Pa, serum-free	8Pa, 10% FBS	fold change	fold expression
TIC or stem cell associated markers																
ALDH1a1	10.04	8.11	1.93	0.26	9.06	7.46	1.6	0.33	7.7	7.07	0.63	0.65	8.63	6.56	2.07	0.24
ALDH1a2	6.79	6.56	0.23	0.85	6.5	6.93	-0.43	1.35	6.83	6.43	0.4	0.76	6.76	6.71	0.05	0.97
ALDH1a3	9.19	13.11	-3.92	15.14	8.41	13.29	-4.88	29.45	12.22	13	-0.78	1.72	11.21	13.49	-2.28	4.86
CD24	8.38	8.65	-0.27	1.21	7.81	9.58	-1.77	3.41	8.46	9.33	-0.87	1.83	8.82	8.31	0.51	0.70
CD44	6.71	6.65	0.06	0.96	6.68	6.7	-0.02	1.01	8.74	8.48	0.26	0.84	8	7.57	0.43	0.74
CXCR4	6.45	6.3	0.15	0.90	6.48	6.4	0.08	0.95	6.52	6.39	0.13	0.91	6.5	6.47	0.03	0.98
KLF4	9.08	8.47	0.61	0.66	9.73	8.73	1	0.50	9.4	8.31	1.09	0.47	8.85	9.57	-0.72	1.65
OCT4	6.54	6.62	-0.08	1.06	6.6	6.51	0.09	0.94	6.48	6.53	-0.05	1.04	6.49	6.58	-0.09	1.06
PROM1	8.75	7.77	0.98	0.51	8.37	7.01	1.36	0.39	9.2	6.46	2.74	0.15	8.45	6.49	1.96	0.26
SOX2	6.82	6.36	0.46	0.73	6.44	7.12	-0.68	1.60	7.76	6.72	1.04	0.49	7.19	6.62	0.57	0.67
Panreatic progenitors associated markers																
SOX9	10.69	9.78	0.91	0.53	11.07	10.27	0.8	0.57	8.72	7.77	0.95	0.52	9.15	7.88	1.27	0.41
CLU	6.5	6.51	-0.01	1.01	6.41	6.36	0.05	0.97	6.32	6.29	0.03	0.98	6.4	6.35	0.05	0.97
HES1	10.23	9.36	0.87	0.55	11.28	10.55	0.73	0.60	9.53	8.32	1.21	0.43	9.89	11.43	-1.54	2.91
NOTCH1	8.03	6.99	1.04	0.49	7.04	8.04	-1	2.00	9.8	8.78	1.02	0.49	10.3	8.62	1.68	0.31
PDX1	6.83	6.51	0.32	0.80	6.8	6.58	0.22	0.86	6.54	6.51	0.03	0.98	6.56	6.61	-0.05	1.04
Duct associated markers																
CA2	11.43	8.38	3.05	0.12	11.67	8.73	2.94	0.13	9.25	10.18	-0.93	1.91	10.1	9.2	0.9	0.54
EPCAM	9.17	8.9	0.27	0.83	9.58	8.54	1.04	0.49	11.92	11.07	0.85	0.55	11.14	10.82	0.32	0.80
HNF1B	6.32	6.32	0	1.00	6.24	6.35	-0.11	1.08	7.19	7.34	-0.15	1.11	6.74	7.11	-0.37	1.29
HNF6α	6.46	6.48	-0.02	1.01	6.47	6.49	-0.02	1.01	6.62	6.53	0.09	0.94	6.47	6.48	-0.01	1.01
HNF6β	8.86	7.49	1.37	0.39	8.74	6.5	2.24	0.21	6.42	6.67	-0.25	1.19	6.46	6.33	0.13	0.91
KRT19	13.81	13.21	0.6	0.66	14.05	12.96	1.09	0.47	13.13	13.5	-0.37	1.29	13.01	12.99	0.02	0.99
KRT7	11.36	11.77	-0.41	1.33	10.98	11.37	-0.39	1.31	9.47	12.28	-2.81	7.01	8.7	11.64	-2.94	7.67
MUC1	9.75	7.12	2.63	0.16	9.68	8.1	1.58	0.33	7.4	9.44	-2.04	4.11	7.05	8.8	-1.75	3.36
Acinar associated markers																
AMY2A	6.62	6.45	0.17	0.89	6.39	6.38	0.01	0.99	6.59	6.73	-0.14	1.10	6.6	6.52	0.08	0.95
BHLHA15	6.43	6.35	0.08	0.95	6.33	6.32	0.01	0.99	6.52	6.39	0.13	0.91	6.47	6.52	-0.05	1.04
CELA1	6.19	6.33	-0.14	1.10	6.13	6.29	-0.16	1.12	6.33	6.46	-0.13	1.09	6.43	6.41	0.02	0.99
CELA2A	6.34	6.44	-0.1	1.07	6.26	6.48	-0.22	1.16	6.5	6.73	-0.23	1.17	6.47	6.81	-0.34	1.27
CELA2B	6.45	6.42	0.03	0.98	6.45	6.42	0.03	0.98	6.42	6.46	-0.04	1.03	6.53	6.52	0.01	0.99
CELA3A	6.58	6.67	-0.09	1.06	6.58	6.51	0.07	0.95	6.63	6.66	-0.03	1.02	6.49	6.87	-0.38	1.30
CELA3B	6.49	6.44	0.05	0.97	6.3	6.4	-0.1	1.07	6.49	6.46	0.03	0.98	6.5	6.56	-0.06	1.04
CPA1	6.2	6.36	-0.16	1.12	6.53	6.26	0.27	0.83	6.45	6.43	0.02	0.99	6.43	6.41	0.02	0.99
CPA2	6.49	6.31	0.18	0.88	6.2	6.49	-0.29	1.22	6.34	6.31	0.03	0.98	6.48	6.47	0.01	0.99
CTRB2	6.55	6.56	-0.01	1.01	6.59	6.44	0.15	0.90	6.58	6.68	-0.1	1.07	6.54	7	-0.46	1.38
CTRC	6.53	6.75	-0.22	1.16	6.46	6.6	-0.14	1.10	6.55	6.8	-0.25	1.19	6.68	6.76	-0.08	1.06
PNLIP	6.45	6.3	0.15	0.90	6.07	6.41	-0.34	1.27	6.49	6.41	0.08	0.95	6.41	6.18	0.23	0.85
PRSS1	9.64	8.82	0.82	0.57	8.03	9.28	-1.25	2.38	7.43	8.01	-0.58	1.49	6.94	6.58	0.36	0.78
PRSS2	7.35	7.56	-0.21	1.16	7.69	7.84	-0.15	1.11	6.77	8.21	-1.44	2.71	6.83	7.2	-0.37	1.29
PRSS3	9.18	7.95	1.23	0.43	9.94	8.13	1.81	0.29	6.99	10	-3.01	8.06	7	8.75	-1.75	3.36
PTF1A	6.45	6.47	-0.02	1.01	6.34	6.59	-0.25	1.19	6.27	6.43	-0.16	1.12	6.54	6.41	0.13	0.91
RBPJL	6.58	6.41	0.17	0.89	6.39	6.61	-0.22	1.16	6.59	6.76	-0.17	1.13	6.59	6.61	-0.02	1.01
Islet associated markers																
CHGA	6.61	6.37	0.24	0.85	6.63	6.38	0.25	0.84	6.69	6.62	0.07	0.95	6.61	6.51	0.1	0.93
CHGB	6.51	6.57	-0.06	1.04	6.36	6.47	-0.11	1.08	6.41	6.59	-0.18	1.13	6.48	6.53	-0.05	1.04
DDR1	10.07	9.63	0.44	0.74	10.19	9.74	0.45	0.73	6.94	6.72	0.22	0.86	6.7	6.63	0.07	0.95
DISP2	6.51	6.59	-0.08	1.06	6.45	6.4	0.05	0.97	6.54	6.63	-0.09	1.06	6.88	6.65	0.23	0.85
DNER	6.31	6.52	-0.21	1.16	6.23	6.31	-0.08	1.06	7.17	7.04	0.13	0.91	6.89	6.85	0.04	0.97
FOXA1	10.1	10.67	-0.57	1.48	9.68	11.1	-1.42	2.68	9.62	9.72	-0.1	1.07	9.85	9.81	0.04	0.97
FOXA2	7.42	6.76	0.66	0.63	7.37	6.51	0.86	0.55	6.46	6.45	0.01	0.99	6.61	6.41	0.2	0.87
FOXA3	8.85	6.71	2.14	0.23	8.99	6.46	2.53	0.17	6.48	6.42	0.06	0.96	6.58	6.76	-0.18	1.13
GAD1	6.58	6.6	-0.02	1.01	6.58	6.74	-0.16	1.12	6.88	6.59	0.29	0.82	6.8	7.45	-0.65	1.57
GCG	6.34	6.41	-0.07	1.05	6.37	6.37	0	1.00	6.41	6.47	-0.06	1.04	6.45	6.56	-0.11	1.08
HEPACAM2	6.53	6.55	-0.02	1.01	6.59	6.51	0.08	0.95	6.49	6.64	-0.15	1.11	6.44	6.38	0.06	0.96
KCNK1	9.16	8.6	0.56	0.68	9.56	8.39	1.17	0.44	9.28	8.91	0.37	0.77	8.36	9.03	-0.67	1.59
EPHA7	6.25	6.51	-0.26	1.20	6.47	6.26	0.21	0.86	6.52	6.48	0.04	0.97	6.48	6.48	0	1.00
PTPRN	6.46	6.49	-0.03	1.02	6.42	6.44	-0.02	1.01	6.39	6.4	-0.01	1.01	6.5	6.58	-0.08	1.06
IAPP	6.42	6.45	-0.03	1.02	6.44	6.43	0.01	0.99	6.37	6.57	-0.2	1.15	6.32	6.63	-0.31	1.24
INS	6.61	6.6	0.01	0.99	6.51	6.45	0.06	0.96	6.51	6.55	-0.04	1.03	6.58	6.67	-0.09	1.06
ISL1	6.68	6.64	0.04	0.97	6.72	6.78	-0.06	1.04	7.3	7.48	-0.18	1.13	7.62	7.18	0.44	0.74
LRP11	8.6	8.34	0.26	0.84	8.8	8.51	0.29	0.82	9.11	8.26	0.85	0.55	8.44	8.8	-0.36	1.28
NEUROG3	6.59	6.42	0.17	0.89	6.47	6.55	-0.08	1.06	6.51	6.81	-0.3	1.23	6.51	6.58	-0.07	1.05
NKX6-1	6.31	6.33	-0.02	1.01	6.33	6.44	-0.11	1.08	6.44	6.37	0.07	0.95	6.55	6.58	-0.03	1.02
ENO2	7.73	7.6	0.13	0.91	7.92	7.25	0.67	0.63	6.83	7.28	-0.45	1.37	6.91	6.59	0.32	0.80
PAX4	6.42	6.24	0.18	0.88	6.46	6.24	0.22	0.86	6.45	6.53	-0.08	1.06	6.48	6.57	-0.09	1.06
PAX6	6.63	6.52	0.11	0.93	6.25	6.47	-0.22	1.16	6.55	6.48	0.07	0.95	6.52	6.53	-0.01	1.01
PPY	6.49	6.4	0.09	0.94	6.41	6.47	-0.06	1.04	6.39	6.62	-0.23	1.17	6.59	6.42	0.17	0.89
PPY2	6.5	6.5	0	1.00	6.31	6.55	-0.24	1.18	6.38	6.29	0.09	0.94	6.55	6.46	0.09	0.94
SEZ6L2	8.25	8.4	-0.15	1.11	8.67	7.93	0.74	0.60	9.82	9.95	-0.13	1.09	9.47	9.63	-0.16	1.12
SLC30A8	6.16	6.38	-0.22	1.16	6.34	6.38	-0.04	1.03	6.32	6.44	-0.12	1.09	6.32	6.42	-0.1	1.07
SST	6.42	6.46	-0.04	1.03	6.46	6.45	0.01	0.99	6.57	6.58	-0.01	1.01	6.48	6.41	0.07	0.95
TMEM27	6.75	6.43	0.32	0.80	6.62	6.73	-0.11	1.08	6.82	6.67	0.15	0.90	6.75	6.82	-0.07	1.05
TSPAN7	6.68	6.43	0.25	0.84	6.5	6.19	0.31	0.81	9.37	7.92	1.45	0.37	8.52	8.43	0.09	0.94

	Patient 3				Patient 4											
	3Pa, serum-free	3Pa, 10% FBS	fold change	fold expression	8Pa, serum-free	8Pa, 10% FBS	fold change	fold expression	3Pa, serum-free	3Pa, 10% FBS	fold change	fold expression	8Pa, serum-free	8Pa, 10% FBS	fold change	fold expression
TIC or stem cell associated markers																
ALDH1a1	8.62	7.92	0.7	0.62	9.5	9.19	0.31	0.81	9.07	8.56	0.51	0.70	9.2	9.18	0.02	0.99
ALDH1a2	6.71	6.72	-0.01	1.01	6.6	6.66	-0.06	1.04	6.29	6.26	0.03	0.98	6.4	6.49	-0.09	1.06
ALDH1a3	11.86	13.18	-1.32	2.50	10.71	13.34	-2.63	6.19	9.37	12.04	-2.67	6.36	9.4	9.94	-0.54	1.45
CD24	12.64	12.23	0.41	0.75	12.25	12.17	0.08	0.95	8.61	8.93	-0.32	1.25	12.93	12.8	0.13	0.91
CD44	6.79	6.59	0.2	0.87	7.04	7.02	0.02	0.99	11.37	10.68	0.69	0.62	8.44	8.75	-0.31	1.24
CXCR4	6.27	6.32	-0.05	1.04	6.93	6.45	0.48	0.72	6.43	6.4	0.03	0.98	6.35	6.4	-0.05	1.04
KLF4	8.71	8.37	0.34	0.79	9.65	8.3	1.35	0.39	8.26	7.23	1.03	0.49	8.25	8.69	-0.44	1.36
OCT4	6.57	6.55	0.02	0.99	6.74	6.6	0.14	0.91	6.22	6.35	-0.13	1.09	6.39	6.21	0.18	0.88
PROM1	6.72	7.4	-0.68	1.60	6.86	8.38	-1.52	2.87	9.94	8.46	1.48	0.36	6.83	7.1	-0.27	1.21
SOX2	8.04	6.98	1.06	0.48	9.5	7.86	1.64	0.32	6.39	6.4	-0.01	1.01	5.98	6.43	-0.45	1.37
Panreatic progenitors associated markers																
SOX9	9.48	7.71	1.77	0.29	9.11	9.16	-0.05	1.04	8.67	8.87	-0.2	1.15	8.53	9.35	-0.82	1.77
CLU	6.52	6.75	-0.23	1.17	6.22	6.3	-0.08	1.06	6.42	6.39	0.03	0.98	6.62	6.42	0.2	0.87
HES1	10.36	9.45	0.91	0.53	10.66	8.74	1.92	0.26	8.85	9.83	-0.98	1.97	9.78	10.09	-0.31	1.24
NOTCH1	7.92	7.28	0.64	0.64	8.84	8.3	0.54	0.69	8.41	8.65	-0.24	1.18	8.49	8.38	0.11	0.93
PDX1	7.28	7.09	0.19	0.88	7.01	7.53	-0.52	1.43	6.74	6.52	0.22	0.86	6.51	6.48	0.03	0.98
Duct associated markers																
CA2	6.65	7.42	-0.77	1.71	6.66	8.25	-1.59	3.01	8.44	6.91	1.53	0.35	9.34	6.77	2.57	0.17
EPCAM	11.32	11.53	-0.21	1.16	11.41	11.15	0.26	0.84	10.26	10.54	-0.28	1.21	9.72	10.18	-0.46	1.38
HNF1B	6.1	6.18	-0.08	1.06	6.25	6.18	0.07	0.95	6.18	6.05	0.13	0.91	6.4	6.2	0.2	0.87
HNF6α	6.29	6.21	0.08	0.95	6.3	6.24	0.06	0.96	6.43	6.4	0.03	0.98	6.44	6.3	0.14	0.91
HNF6β	6.17	6.08	0.09	0.94	6.12	6.27	-0.15	1.11	6.34	6.4	-0.06	1.04	6.6	6.52	0.08	0.95
KRT19	13.66	13.24	0.42	0.75	13.95	13.44	0.51	0.70	12.95	13.77	-0.82	1.77	13.75	13.75	0	1.00
KRT7	10.88	12.1	-1.22	2.33	8.77	10.67	-1.9	3.73	9.26	10.88	-1.62	3.07	9.69	9.98	-0.29	1.22
MUC1	10.51	8.69	1.82	0.28	10.35	10.25	0.1	0.93	6.23	6.78	-0.55	1.46	10.09	8.13	1.96	0.26
Acinar associated markers																
AMY2A	6.67	6.68	-0.01	1.01	6.66	6.67	-0.01	1.01	6.38	6.39	-0.01	1.01	6.57	6.51	0.06	0.96
BHLHA15	6.2	6.24	-0.04	1.03	6.41	6.26	0.15	0.90	6.09	6.21	-0.12	1.09	6.27	6.43	-0.16	1.12
CELA1	6.19	6.18	0.01	0.99	6.27	6.22	0.05	0.97	6.12	6.17	-0.05	1.04	6.35	6.34	0.01	0.99
CELA2A	6.39	6.47	-0.08	1.06	6.45	6.47	-0.02	1.01	6.24	6.43	-0.19	1.14	6.45	6.46	-0.01	1.01
CELA2B	6.4	6.34	0.06	0.96	6.24	6.43	-0.19	1.14	6.32	6.14	0.18	0.88	6.54	6.52	0.02	0.99
CELA3A	6.43	6.55	-0.12	1.09	6.74	6.6	0.14	0.91	6.48	6.51	-0.03	1.02	6.51	6.51	0	1.00
CELA3B	6.56	6.62	-0.06	1.04	6.35	6.33	0.02	0.99	6.64	6.56	0.08	0.95	6.32	6.52	-0.2	1.15
CPA1	6.34	6.27	0.07	0.95	6.11	6.33	-0.22	1.16	6.08	6.04	0.04	0.97	6.35	6.36	-0.01	1.01
CPA2	6.43	6.61	-0.18	1.13	6.38	6.48	-0.1	1.07	6.5	6.51	-0.01	1.01	6.61	6.42	0.19	0.88
CTRB2	6.53	6.52	0.01	0.99	6.52	6.26	0.26	0.84	6.28	6.64	-0.36	1.28	6.45	6.29	0.16	0.90
CTRC	6.68	6.56	0.12	0.92	6.57	6.29	0.28	0.82	6.63	6.56	0.07	0.95	6.57	7.11	-0.54	1.45
PNLIP	6.23	6.24	-0.01	1.01	6.31	6.38	-0.07	1.05	6.28	6.16	0.12	0.92	6.28	6.24	0.04	0.97
PRSS1	7.03	11.81	-4.78	27.47	6.42	10.22	-3.8	13.93	6.33	6.44	-0.11	1.08	6.39	6.6	-0.21	1.16
PRSS2	6.91	8.3	-1.39	2.62	6.82	7.21	-0.39	1.31	6.58	6.52	0.06	0.96	6.6	6.45	0.15	0.90
PRSS3	8.72	10.55	-1.83	3.56	7.33	8.75	-1.42	2.68	6.89	6.58	0.31	0.81	8.01	7.44	0.57	0.67
PTF1A	6.35	6.74	-0.39	1.31	6.26	6.14	0.12	0.92	6.34	6.4	-0.06	1.04	6.26	6.39	-0.13	1.09
RBPJL	6.54	6.47	0.07	0.95	6.78	6.67	0.11	0.93	6.48	6.53	-0.05	1.04	6.52	6.54	-0.02	1.01
Islet associated markers																
CHGA	6.64	6.47	0.17	0.89	6.67	6.65	0.02	0.99	6.49	6.41	0.08	0.95	6.5	6.51	-0.01	1.01
CHGB	6.35	6.45	-0.1	1.07	6.43	6.36	0.07	0.95	6.29	6.2	0.09	0.94	6.29	6.33	-0.04	1.03
DDR1	7.04	7.27	-0.23	1.17	6.6	7.06	-0.46	1.38	6.6	6.87	-0.27	1.21	6.59	6.78	-0.19	1.14
DISP2	6.5	6.56	-0.06	1.04	6.48	6.62	-0.14	1.10	6.4	6.46	-0.06	1.04	6.66	6.57	0.09	0.94
DNER	6.21	6.31	-0.1	1.07	6.54	6.42	0.12	0.92	6.65	6.37	0.28	0.82	6.53	6.35	0.18	0.88
FOXA1	8.59	9.37	-0.78	1.72	7.73	10.05	-2.32	4.99	6.68	8.42	-1.74	3.34	7.77	9.88	-2.11	4.32
FOXA2	6.13	6.29	-0.16	1.12	6.18	6.29	-0.11	1.08	6.07	6.2	-0.13	1.09	6.44	6.27	0.17	0.89
FOXA3	6.54	6.15	0.39	0.76	6.37	6.54	-0.17	1.13	6.58	6.31	0.27	0.83	6.71	6.46	0.25	0.84
GAD1	6.64	7.06	-0.42	1.34	6.71	6.7	0.01	0.99	6.56	6.86	-0.3	1.23	6.55	6.45	0.1	0.93
GCG	6.46	6.48	-0.02	1.01	6.57	6.44	0.13	0.91	6.24	6.31	-0.07	1.05	6.37	6.36	0.01	0.99
HEPACAM2	6.31	6.34	-0.03	1.02	6.38	6.21	0.17	0.89	6.4	6.25	0.15	0.90	6.27	6.4	-0.13	1.09
KCNK1	8	7.61	0.39	0.76	7.98	7.5	0.48	0.72	8.78	8.36	0.42	0.75	8.62	9.57	-0.95	1.93
EPHA7	6.16	6.32	-0.16	1.12	6.23	6.32	-0.09	1.06	6.16	6.28	-0.12	1.09	6.39	6.3	0.09	0.94
PTPRN	6.35	6.1	0.25	0.84	6.46	6.39	0.07	0.95	6.44	6.38	0.06	0.96	6.41	6.42	-0.01	1.01
IAPP	6.61	6.39	0.22	0.86	6.42	6.52	-0.1	1.07	6.33	6.22	0.11	0.93	6.32	6.56	-0.24	1.18
INS	6.65	6.68	-0.03	1.02	6.66	6.55	0.11	0.93	6.27	6.55	-0.28	1.21	6.27	6.4	-0.13	1.09
ISL1	7.69	7.85	-0.16	1.12	8.44	8.59	-0.15	1.11	7.02	7.19	-0.17	1.13	7.03	7.68	-0.65	1.57
LRP11	9.46	9.25	0.21	0.86	8.71	8.98	-0.27	1.21	9.03	9.35	-0.32	1.25	9.61	8.67	0.94	0.52
NEUROG3	6.44	6.66	-0.22	1.16	6.5	6.41	0.09	0.94	6.65	6.52	0.13	0.91	6.59	6.57	0.02	0.99
NKX6-1	6.26	6.25	0.01	0.99	6.06	6.2	-0.14	1.10	6.24	6.23	0.01	0.99	6.37	6.32	0.05	0.97
ENO2	7.16	7.25	-0.09	1.06	7.02	7.32	-0.3	1.23	6.58	6.49	0.09	0.94	6.87	6.56	0.31	0.81
PAX4	6.12	6.42	-0.3	1.23	6.34	6.48	-0.14	1.10	6.3	6.27	0.03	0.98	6.39	6.21	0.18	0.88
PAX6	6.52	6.41	0.11	0.93	6.43	6.51	-0.08	1.06	6.68	6.73	-0.05	1.04	6.44	6.33	0.11	0.93
PPY	6.63	6.55	0.08	0.95	6.51	6.52	-0.01	1.01	6.27	6.19	0.08	0.95	6.39	6.41	-0.02	1.01
PPY2	6.31	6.25	0.06	0.96	6.16	6.26	-0.1	1.07	6.27	6.19	0.08	0.95	6.32	6.2	0.12	0.92
SEZ6L2	6.55	6.7	-0.15	1.11	6.73	6.56	0.17	0.89	6.62	6.22	0.4	0.76	6.7	6.6	0.1	0.93
SLC30A8	6.17	6.42	-0.25	1.19	6.35	6.39	-0.04	1.03	6.22	6.23	-0.01	1.01	6.33	6.3	0.03	0.98
SST	6.44	6.46	-0.02	1.01	6.47	6.36	0.11	0.93	6.15	6.37	-0.22	1.16	6.38	6.24	0.14	0.91
TMEM27	6.85	6.55	0.3	0.81	6.87	6.51	0.36	0.78	6.48	6.81	-0.33	1.26	6.56	6.53	0.03	0.98
TSPAN7	6.65	6.82	-0.17	1.13	6.77	7.28	-0.51	1.42	8.2	6.64	1.56	0.34	8.15	6.79	1.36	0.39

Absolute expression values are indicated by green to red color code. Fold change (FC) is calculated by substraction of absolute gene expression values measured for control cultures (serum-free) from the values obtained for serum-treated cultures (10% FBS). Fold expression (FE) indicates the ratio of gene expression after serum treatment compared to serum-free controls and is calculated by $FE=2^{FC}$. FE is highlighted in light red when expression was ≥2 representing up-regulation and highlighted in light blue when expression was ≤0.5 representing down-regulation of this marker. Analysis was performed in culture passage 3 (3Pa) and 8 (8Pa). Appendix modified from [187].

Appendix B: Lentiviral integration sites identified in the genome of serially transplanted pancreatic xenograft tumors.

Chromosome	Integration locus	Sequence Orientation	Upstream of TSS (bp)	In Gene, distance to TSS (bp)	Intron/Exon	Downstream of Gene	RefSeq Gene
1	1329293	+	0			0	
1	8257858	+	126532			0	SLC45A1
1	10791545	-	0	65162	In2	0	CASZ1
1	45231061	-	0	25571	In19	0	KIF2C
1	100491634	+	0			2628	SLC35A3
1	101256690	+	0			52091	VCAM1
1	110101504	+	0	10318	In1	0	GNAI3
1	154953330	-	0			1606	CKS1B
1	168909832	-	0			0	
1	169943362	-	0	100517	In16	0	KIFAP3
1	182477665	-	0	58409	In9	0	RGSL1
1	204476156	+	0			0	
1	215533018	-	0			122583	KCNK2
1	226331003	+	0			1379	ACBD3
2	28690039	+	0			0	
2	28992434	+	0	17820	In2	0	PPP1CB
2	53661698	+	0			235420	ASB3
2	55475232	-	0	21152	In9	0	MTIF2
2	62322164	-	0	189361	In2	0	COMMD1
2	64795287	-	0	43822	In3	0	AFTPH
2	75928395	+	0	9927	Ex4	0	C2orf3
2	118980760	-	0			113164	INSIG2
2	161339209	-	0	11109	In1	0	RBMS1
2	173562383	+	38142			0	RAPGEF4
2	187447445	+	7345			0	ITGAV
2	203608196	-	0	107985	In4	0	FAM117B
2	219367930	-	0	65154	In11	0	USP37
3	4582201	+	0			0	
3	17443681	+	0	338718	In8	0	TBC1D5
3	93770222	+	0	71240	In7	0	ARL13B
3	128837134	-	0	3485	In1	0	RAB43
3	144863512	+	0			923716	PLOD2
3	167704730	-	0			22924	GOLIM4
3	183717969		0			0	
3	195066475	-	0	97342	In4	0	ACAP2
4	73149820	-	0	284696	In21	0	ADAMTS3
4	95439852	-	0	66814	In2	0	PDLIM5
4	125132609	+	0			452859	ANKRD50
5	5275927	+	0	135484	In18	0	ADAMTS16
5	14667690	-	0			0	
5	18008665	+	0			731730	BASP1
5	24167549	-	0			319661	CDH10
5	34458904	-	197529			0	RAI14
5	36239974	+	0	1926	In1	0	C5orf33
5	37064508	+	0	187647	Ex46	0	NIPBL
5	39071098	-	0	3403	In2	0	RICTOR
5	57237298	-	458662			0	ACTBL2
5	58942558	-	0	247063	In1	0	PDE4D
5	64999040	+	0	18901	In5	0	SGTB
5	83036660	-	19764			0	HAPLN1
5	138197426	-	0	108319	In7	0	CTNNA1
5	139006337	+	0	65586	In6	0	UBE2D2
6	30703118	+	0	7335	In8	0	FLOT1
6	32913970	-	0			2421	HLA-DMA
6	36427824	+	0	17280	In1	0	KCTD20
6	90958501	-	0	48061	In3	0	BACH2
6	130241258	-	58842			0	C6orf191
7	42396054	-	0			0	
7	74257829	+	0			0	
7	85011774	-	260527			0	SEMA3D
7	123348078	-	0	41038	In2	0	WASL
7	135189767	-	0	5084	In1	0	CNOT4
7	158613293	+	0	9026	In1	0	FAM62B
8	24039400	+	0			0	
8	39639341	+	0	56438	In10	0	ADAM2
8	41667105	+	0			0	
8	54958990	+	0			0	
8	63917239	-	0			10404	GGH
8	90652495	+	117480			0	RIPK2
8	91533561	-	0			100662	TMEM64
8	133810659	+	0	23055	In4	0	PHF20L1

Chromosome	Integration locus	Sequence Orientation	Upstream of TSS (bp)	In Gene, distance to TSS (bp)	Intron/Exon	Downstream of Gene	RefSeq Gene
9	14107155	-	0	206790	In8	0	NFIB
9	111844293	-	0	37932	In6	0	C9orf5
9	115810273	-	0	8723	In3	0	ZFP37
9	126475924	-	0	216493	In5	0	DENND1A
9	127645822	-	0	57564	In19	0	GOLGA1
9	129829259	-	0	152206	In7	0	RALGPS1
9	131348541	+	0	33675	In19	0	SPTAN1
9	134565403	+	0	47522	In1	0	RAPGEF1
10	32162644	-	0	55126	In3	0	ARHGAP12
10	42396904	-	0			687651	ZNF33B
10	54742020	-	0			0	
10	74407227	-	0			0	
10	76701079	+	0	114700	In3	0	MYST4
10	93700427	-	0	16691	In3	0	BTAF1
10	105762912	+	0	35442	Ex9	0	SLK
11	1465549	-	0	54420	In8	0	BRSK2
11	56646719	-	109670			0	OR5AK2
11	62029660	+	7970			0	SCGB2A2
11	65159269	+	0	5228	In3	0	FRMD8
11	66082227	-	0	2288	Ex1	0	CD248
11	66922843	-	0	36103	In2	0	KDM2A
11	67947516	-	0	33268	In4	0	SUV420H1
11	74149628	-	0			16260	KCNE3
11	77082053	-	0	103055	In5	0	PAK1
12	6476233	-	0	8672	In2	0	SCNN1A
12	6597195	-	0			4121	MRPL51
12	14948802	-	0	7599	In5	0	WBP11
12	15888231	-	0	54279	In1	0	EPS8
12	46762763	+	0	3882	In4	0	SLC38A2
12	82509970	+	0			236120	CCDC59
12	110586867	+	0	24727	In10	0	IFT81
12	122263577	-	0	20939	In13	0	SETD1B
12	133763800	-	0	5805		0	ZNF268
13	32918151	+	0	28534	In11	0	BRCA2
13	45929590	+	14293			0	TPT1
13	97294990	+	0	551897	In1	0	HS6ST3
14	27993304	-	926344			0	NOVA1
14	28147200	+	1080240			0	NOVA1
14	35660285	+	0	68509	In5	0	KIAA0391
14	74370485	+	0	16899	In5	0	ZNF410
14	92475844	+	0	30973	In9	0	TRIP11
14	103125719	+	0	66486	In2	0	RCOR1
14	103896014	+	0	44313	In3	0	MARK3
14	104484030	+	0	89213	In22	0	TDRD9
15	42882720	+	0			20532	HAUS2
15	52898770	-	0	72050	In6	0	KIAA1370
15	62246148	-	0	106499	In36	0	VPS13C
15	66609809	+	0	24176	In7	0	DIS3L
15	72415626	-	0	4872	In1	0	SENP8
15	74860057	-	0	26509	In2	0	ARID3B
15	84224228	-	0	108137	In1	0	SH3GL3
16	2494598	+	0	15203	In9	0	CCNF
16	24779530	-	0	38481	In4	0	TNRC6A
16	50129776	+	0	29895	In12	0	HEATR3
16	73040211	-	0	42063	In1	0	ZFHX3
16	89579202	-	0	4397	In2	0	SPG7
17	860089	-	0	22921	In1	0	NXN
17	7149773	+	0	5222	In4	0	DULLARD
17	8022549	-	689			0	ALOXE3
17	9315391	-	0	163884	In6	0	STX8
17	15611694	+	0	8803	In5	0	ZNF286A
17	18446086	-	0			40636	CCDC144B
17	29821625	+	0	102983	In3	0	RAB11FIP4
17	36931607	-	0	24551	In7	0	PIP4K2B
17	36951404	+	0	4754	In1	0	PIP4K2B
17	54898096	-	4846			0	C17orf67
17	61480018	+	0	393120	In17	0	TANC2
17	74344627	+	0	5603	Ex2	0	PRPSAP1
17	81000905	-	0	8781	In3	0	B3GNTL1
18	24753543	-	0	11746	In1	0	CHST9
18	47315949	+	0	24302	In7	0	ACAA2
18	60202233	+	0	11575	In1	0	ZCCHC2
19	5709698	+	0	10478	In4	0	LONP1
19	6107091	+	0			0	
19	6760255	+	0	7268	In3	0	SH2D3A
19	8526061	-	0	16258	In2	0	HNRNPM
19	9539366	-	0	6868	In4	0	ZNF266
19	9924000	-	0	5731	In2	0	FBXL12
19	13236758	+	0	7649	In1	0	NACC1
19	13287786	+	0			22070	IER2
19	15095593	-	11863			0	SLC1A6

Chromosome	Integration locus	Sequence Orientation	Upstream of TSS (bp)	In Gene, distance to TSS (bp)	Intron/Exon	Downstream of Gene	RefSeq Gene
19	16534450	-	0	48312	In9	0	EPS15L1
19	19399928	-	0	31379	In8	0	SF4
19	45483969	+	0	25331	In5	0	CLPTM1
19	56157726	-	0			0	
19	58024410	+	0			0	
19	58996092	+	0			3496	ZNF446
20	478723	-	0	45759	In6	0	CSNK2A1
20	21321202	+	0	37260	In14	0	XRN2
20	25618627	-	13979			0	NANP
20	33322989	-	0	90444	In12	0	NCOA6
20	61845914	-	0	1624	In2	0	YTHDF1
21	42591020	-	0			0	
22	29982623	+	5479			0	NIPSNAP1
22	44397443	-	0	2270	In2	0	PARVB
22	50975416	-	4408			0	ODF3B
23	31388197	+	0			0	
23	35715311	+	101148			0	MAGEB16
23	45510729	+	0			0	
23	51619875	-	0	73720	In1	0	MAGED1
23	93308941	+	0			341680	FAM133A
23	94965853		0			0	
23	129374599	+	0	28274	In5	0	ZNF280C
23	143781956	+	547151			0	SPANXN1
24	21632540		0			0	
24	22970081	+	0			0	

Integration sites in human tumor cells were analysed by LAM-PCR and subsequent 454-seqencing. Sequenced DNA-molecules were mapped in the human genome using BLAT. The integration site locus indicates the exact position of the vector in the host cell genome. Genome distances are depicted in base pairs (bp); TSS=Transcription start site; RefSeq: NCBI Reference Sequence Database. Appendix B was taken from [187].

Appendix C: Statistical analysis of data presented in chapter 3.3.

This appendix was written by Prof. Dr. Dr. Ulrich Abel (National Center for Tumor Diseases, Heidelberg). Text was taken literally from [187].

"General Remarks

The statistical analysis focused exclusively on transduced cells; i.e., in what follows the terms "tumour", "sample", and "clone" solely refer to transduced cells. Statistical analyses essentially consisted of "theory-based worst case analyses". The special techniques employed were as follows:

1. Confidence interval p-values: This is an important tool for worst-case analyses. The concept was developed by Berger and Boos [222], and in some way constitutes an improvement over the old idea of supremum p-values originally formulated by Barnard [223], which stated that when using a statistical test involving a nuisance parameter Θ, a valid p-value can be obtained by maximizing the conditional p-values $p(\Theta)$ over the parameter space of Θ. Berger and Boos showed that restricting the maximization of the conditional p-values to a 1-β confidence C_β set for Θ (obtained when the null hypothesis is true), and adding ß to this maximum, also results in a valid p-value (the "confidence interval p-value" see also [224, 225]). Thus, when using confidence interval p-values the probabilities of error add up. This remains true when the principle is applied several times in a chain of arguments. Thus, e.g. confidence interval p-values can be used to calculate test-based confidence intervals for a nuisance parameter of another test.

2. Confidence intervals for the parameter n of a binomial distribution B(n,p). While this situation is rarely considered in the biostatistical literature, it is what was needed for calculating confidence interval p-values in several situations, where the unknown n was a nuisance parameter of the test to be performed.

3. Confidence rectangles for two nuisance parameters using the well-known principle that, if C_1,C_2 are level (1-β) confidence intervals for two nuisance parameters Θ_1, Θ_2, respectively, then C_1 x C_2 is a level (1-2β) confidence region for (Θ_1,Θ_2), even if the

two pairs of confidence bounds are not statistically independent [222]. This principle was sufficient to reach conclusions when used in connection with an extension of confidence interval p-values. The result still holds true when Θ is an n-dimensional parameter with a corresponding n-dimensional confidence region C_β.

4. Supremum p-values over possible constellations of unobservable count data. This is a special case of supremum p-values, the missing numbers being regarded as nuisance parameters.

For the analysis of proliferation rates we modeled the cell growth process by means of a birth process (a Yule process, i.e. a Poisson process for the number of divisions a single cell) with an identical growth parameter for all cells of a clone (Model 1). The model accommodated a "time-lag", or "delay" Δ, in cell proliferation [226, 227]. Within this model, null hypotheses regarding proliferation rates can be expressed in terms of the growth parameters λ, i.e. the rate of the Poisson process. E.g., the null hypothesis of homogeneity of proliferation rates states that the parameters λ_i of the processes are the same for each clone i. In case of no time lag, clone size distributions were obtained by using known formulas for the Yule process [222], which imply that cell numbers after a fixed time follow a negative binomial distribution NB(r,p), with r=number of cells at t=0 and p=exp(-λt). For Δ>0 no mathematical formulas are available, so that computer simulations emulating the entire cell growth process of a clone were used to obtain clone size distributions. The homogeneity of rates across the clones could then tested by comparing the observed clone sizes with the calculated or simulated distribution, the growth parameter λ being a nuisance parameter in this analysis (see below for the details of this procedure). We chose a particular value (8 hours) to delimit the potential influence of a time lag on the results. A simpler model (Model 2) assumes that the growth process can be described by a growth curve (as may result, e.g., from a nonstochastic differential equation) and that the entire variability in the observed clone sized is solely due to the sampling process from the tumour. The null hypothesis H_0 of homogeneity of the growth rates then states that the clone sizes in the tumour are all identical, implying that for a given cell the probability to fall into any clone is the same across all clones of the tumour. This

can be tested using a chi-squared goodness-of-fit test based on the observed clone sizes in S_i (Undetected clones with a size of zero in the samples increase the heterogeneity, as is easily checked; i.e., ignoring them produces an upper bound for the p-value). We based our analyses on Model 1. In one instance, an additional analysis was done using Model 2 to illustrate the differences in the approaches.

In addition to the special tools described above, standard methods, such as tests for equality of proportions (Fisher's exact test), were used. Throughout the analyses, only upper bounds for p-values could be calculated. All confidence intervals for single parameters were two-sided and of a Clopper-Pearson type, i.e., based on two exact one-sided binomial tests. Two approximations were used throughout the analysis: 1, the number of transduced cells (among all cells of a tumour or a sample hereof) was set to be equal to the expected value calculated as the total cell number in the tumour or sample multiplied with the proportion of transduced cells, the latter having been determined in a separate analysis based on about 10,000 cells; 2, in order to describe sampling from a clone the binominal distribution was used when, in fact, the sampling depended on the total complex clone structure of a tumour, i.e. followed a multivariate hypergeometric distribution. The approximation was justified by the low probabilities of selection (ranging from 1.92% to 10% in primary or secondary mice). Adjustment for multiplicity was restricted to situations where several results (e.g., inferences for each clone in a tumour) were used in the same analysis, i.e. for testing the same hypothesis. No adjustment for multiple testing was done regarding the multiplicity of different hypotheses or experiments conducted.

Details of the analysis

Notation: Let (for i=1,…,3) M_i designate primary, secondary, and tertiary mice (respectively), T_i the tumours of these mice, S_i the samples taken from these tumours and analyzed for clonality, CS_i the clones detected in S_i, CNS_i the clones present in T_i but not detected in S_i, and CNS_i* the subset of the latter which were detected in samples of later mouse generations. Letters a,b,c (e.g. T_{2a},T_{2b}) will be used to differentiate between tumours and samples taken from several secondary mice (and analogously for tertiary mice). Let k(…) and n(…) denote the numbers clones and cells (respectively) in a sample of cells or a set of clones. If not stated differently, cell numbers will refer to tumours, not samples taken from tumours; thus, e.g. n(CNS_1)

designates the number of cells in T_1 contained in clones that were not detected in the sample S_1.

Upper bounds for the number of clones in a tumour

Upper confidence limits for the number of clones in a tumour were test-based and calculated as the sum of the number of clones contained in the sample (i.e., "detected" in the sample) plus a test-based upper confidence limit for the number of clones not contained in the sample. We describe the procedure for T_1: Let H_0 be the null hypothesis that all tumour cells in T_1 have the same probability *s* (*s* = sampling fraction) of being sampled in S_1, and assume H_0 to hold true. Then, for a given total number $n(CNS_1)$ of cells in CNS_1, the possible number of clones in CNS_1 is maximal if all clones in CNS_1 are of size 1, and the probability that, given this cell number, no clone in CNS_1 is detected is equal to the probability that none out of a given set of $n(CNS_1)$ cells is contained in S_1. The upper bound of a two-sided test-based level $(1-\beta)$ confidence interval for $n(CNS_1)$ can thus be determined using a binomially distributed variable $X \sim B(n,s)$, X being the number of cells out of *n* detected in S_1, and is calculated as the highest number *n* of cells such $P(X=0) \geq \beta/2$. The upper bound is given by $[\log(\gamma)/\log(1-s)]$.

Heterogeneity of proliferation rates

The statistical analysis made use of clone size distributions generated by the stochastic process of cell growth (birth process with or without a time-lag). If clones are generated from single cells without a time-lag (i.e., $\Delta=0$), the standard deviation of the clone sizes after time t is equal to the mean, namely $\exp(\lambda t)$, in contrast to a Poisson process growth model with synchronized cell divisions, where $\log_2$(clone size(t))) - which is equal to the number of cell divisions of the clone in the time interval [0,t] - follows a Poisson distribution with parameter $t\lambda$ and thus has standard deviation of $(t\lambda)^{0.5}$. I.e., the assumption of synchronized cell divisions would imply that the standard deviation of the clone numbers is vastly higher than the mean clone sizes.

In order to ascertain the heterogeneity of proliferation rates in T_1 we first determined an upper confidence bound, λ_u, for the parameter of the process under the

assumption of H_0 that all clones in T_1 had the same growth parameter. The upper bound was test-based. The idea underlying the procedure was that once the common growth parameter λ (and thus the expected clone size at time t_s of sampling) exceeded a certain level, this would no longer be statistically compatible with the rather high number of clones (namely, at least $k(CNS_1^*)$ many) not present in the sample. In case of no time lag λ_u was calculated using exact probabilities p_0 that a particular clone is undetected in S_1, which is given by

$$p_0(\lambda, s) = \sum_{i=0}^{\infty} P(X(t) = i) P(Y_i = 0)$$

where X(t) is size of this clone in T_1 after time t and starting with a single cell at t=0 (i.e., X(t) follows a negative binomial distribution NB(1,exp(-λt))), and Y_i describes the sampling from this clone. Hence, Y_i is binomially distributed as $Y_i \sim B(i,s)$, s being the proportion of cells analyzed for clonality (the "sampling fraction"), which is the ratio of the cell numbers in S_1 to those in T_1. Thus, a valid test-based level (1-β) confidence bound λ_u is given by the lowest value (of all discrete values examined) such that high observed ratio of undetected clones, namely,

$$R = \frac{k(CNS_1^*)}{k(CNS_1^*) + k(CS_1)}$$

is statistically "incompatible" with the probability $p_{\square}(\lambda,s)$, meaning that $P(Z \geq CNS^*_1) < \beta/2$, where $Z \sim B(k(CNS_1^*) + k(CS_1), p_0(\lambda,s))$.

The ratio R ratio is not equal to the exact proportion of clones not present in the S_1, because neither the nominator nor the denominator includes unobserved clones contained in $CNS_1 \backslash CNS_1^*$. However, each of these clones would increase both the nominator and denominator by 1 and thus increase the proportion. Thus, a statistical test taken this modification into account would have an even lower p-value.

In case of a positive time lag, the exact probability $p_0(\lambda,s)$ was replaced with a ratio R' obtained from simulated clone size distributions. The nominator of R' equals the number of random clone sizes clones generated but not present in a random sample of cells with given sampling fraction s; the denominator of R is the number of clones generated in the simulations.

The time interval from transplantation (t=0) to sampling (t_s) was rescaled to one time unit. The growth parameter λ then is the mean number of cell divisions until t_s. For each of the growth parameter values λ=1, 2,….13, we generated 100,000 clone sizes. The lowest value of λ, λ_υ, no longer compatible with the minimum number of undetected clones (i.e. clones in CNS_1*) at the $1\text{-}10^{-5}$ confidence level was then investigated to determine whether, conversely, it was statistically compatible with the very high observed clone sizes in CS_1. To obtain p-values we considered the maximum observed clone size, c_{max}. While the true number $k(S_1)$ was unknown, for any assumed number $k:=k(S_1)$, given growth rate, and time lag Δ=0, the probability distribution function $F_\lambda(x)$ of the maximum clone size could be calculated using elementary results from extreme-value theory, viz. $F_\lambda(x) = G_\lambda(x)^k$, where $G_\lambda(x)$ is the distribution function of the cell number of a clone after time t_s. Here, the value of k used for the analysis was the sum of clones observed plus the upper $(1\text{-}10^{-5})$ confidence bounds for the number of unobserved clones (calculated as outlined in paragraph 1). Finally, following the confidence interval p-value principle, we added 1- the confidence levels used for the nuisance parameters, i.e. $2*10^{-5}$.

The distribution function $G_\lambda(x)$ was known, mathematically, if no time-lag was assumed. If Δ>0 the clone-size distribution is shifted to smaller values. Thus, the minimum growth rate λ_u' statistically incompatible with the number of undetected clones in CNS_1* will be (slightly) higher than the value λ_u obtained without a time-tag. On the other hand, due to the negative shift of the clone size distribution, the p-value calculated as outlined above (with Δ=0 but using this higher value λ_u') is a valid upper bound for the true p-value in case of a time lag. Therefore, the negative binomial (valid only if Δ=0) can be used to determine upper bounds for the p-value if Δ>0.

Changes in proliferation rates

The analysis focused on an observed increase of proliferation rates for clones in CNS_1*, i.e. on clones in $CNS_1^* \cap CS_2$. It aimed at showing that there was at least one clone in CNS_1* whose proliferation rate increased in T_2. In view of the fact that the true proliferation rate acted as a nuisance parameter which could be different for each clone, we based our analysis on a single pair, namely the clone in CNS_1* that

was largest in CS_2, along with a Bonferroni adjustment for the multiple testing implicitly involved in this particular choice.

The analysis was based on clone size distributions generated either by means of the formulas for birth processes or computer simulation. In this analysis (and in the formulas) T_2, in contrast to T_1, originated from more than one transplanted cell. The number of cells transplanted into the secondary mice and starting the growth process was itself a random variable, namely the result of a sampling process in the primary tumour. The analysis exploited the fact that the growth processes in T_1 and T_2 were independent, following from the known property of Poisson processes of being memory less.

The null hypotheses tested was a joint hypothesis, stating that sampling from tumours was random and the proliferation rates of each clone in T_1 were unchanged in T_2. We chose a statistical test based on the pair (X_1, X_2) of the observed sizes X_i of the same clone in S_1 and S_2, respectively. The rejection region was such that it simultaneously reflected the fact that (under H_0) at least one of the two clone sizes was too extreme to be compatible with any assumed proliferation rate λ (resp.). Since we used only a single two-dimensional test statistic this was not a union-intersection test. In view of the independence of the growth processes in T_1 and T_2, the p-value was calculated as a product of probabilities namely p_1*p_2, where $p_1=P(X_1\leq c_1|H_0)$ and $p_2=P(X_2\geq c_2|H_0)$. Both p_1 and p_2 were calculated form identical clone size distributions, i.e. assuming identical growth rates and growth times (see the remarks below). The rejection region was defined by one-sided probabilities taken from the cumulative distribution of X_i under H_0. The particular definition of the test statistic implies that only increases in clone sizes were considered when calculating p-values. The single p-values $p_1=P(X_1\leq c_1)$ and $p_2=P(X_1\geq c_2)$ were then determined using the clone size distribution in S_1 and S_2, again either based on the negative binomial distribution or on computer simulations. From the definition of CNS_1* it follows that $c_1=0$, while c_2 was obtained by multiplying $n(S_2)$ with the observed proportion of the clone in S_2. By construction p_1 will be small for high growth rates $_l$, while p_2 will be small for low growth rates of a clone. Therefore, the product p_1p_2 as a function of the growth rate λ has a maximum. This maximal value was determined and used as an upper bound for the p-value. The result was then adjusted for multiplicity, using the upper

confidence bounds for the number of clones in CNS_1 (see point 1 above). In this context, to mitigate the effect of the adjustment, we selected the lowest confidence level of those presented in table C1 (namely, 99%) allowing a statistically significant result when used to calculate the confidence interval p-values.

The analysis was restricted to P1-1, P2-1, P3-1, and P3-2, where the time interval from transplantation to purification in secondary mice was at most as long as in primary mice. Note that the shorter this interval the smaller the clones. This implies that the probability p_2 calculated under the assumption of identical clone size distributions in T_1 and T_2 is an upper bound for the true value of p_2 if proliferation time in T_2 is shorter than in T_1.

Heterogeneity of the seeding efficiency (SE)

We defined seeding efficiency at the clone level. The following definition was used: Seeding efficiency = probability that a randomly chosen cell of a clone that is transplanted into a mouse proliferates or survives until the time t_s when the tumour is examined for clonality.

All inferences regarding the SE of a clone had to be deduced from two data points, namely the estimated clone sizes at times t_0 (transplantation) and t_s (cell sampling from the tumour).

We focused the analysis on T_2, and, more specifically, on the first secondary mouse M_{2a}. The analysis was aimed at showing that a lower bound for the seeding efficiencies (in T_{2a}) of cells in clones contained CNS_1 was significantly higher than an upper bound for the seeding efficiencies of at least one clone in CS_1 (while adjusting for multiplicity of testing).

A lower bound for the seeding efficiency of cells in CNS_1 was obtained by observing that the nominator, i.e., the number of cells in (clones of) CNS_1 successfully transplanted into M_{2a} was at least as large as the number clones in CNS_1 observed either in M_{2a} or its corresponding tertiary mice. Let n_A denote this number. To obtain an upper bound d_A for the denominator we replaced the number of cells in CNS_1 with their upper 99.9% confidence bound (see point 1 above). Thus, at the 99.9% confidence level for the denominator the seeding efficiency of cells in CNS_1 was at least n_A/d_A.

The clone selected for comparison was the largest clone C in $CS_1 \cap CNS_2$. We calculated a lower 99.9% confidence bound, p, for its clone proportion of C in T_1 based on the observed proportion of C in S_1. Multiplying p with the number of cells of T_1 transplanted into the secondary mouse yielded a lower 99.9% confidence bound, d_B, for the number of cells in C transplanted into the secondary mouse. This number served as the denominator for calculating an upper bound for the seeding efficiency of C. Since C was undetected in T_2, an upper 99.9% confidence bound for the size of C in T_2 was obtained as described above. This yielded an upper bound for the number of cells in C successfully seeded and was used as the nominator for the seeding efficiency of C in M_{2a}. The ratios d_A/n_A and d_B/n_B were then compared using an exact test, and the p-value was adjusted for multiplicity involved in the particular selection of C (a Bonferroni adjustment with the total number of clones in CS_1 being the adjustment factor).

Results

Upper bounds for the number of clones in a tumour

Upper confidence bounds, N_u^-, for the number of cells, N^-, in clones present, but not detected in the tumour T_1 and T_{2a}, T_{2b}, T_{2c} of primary and secondary mice, respectively, are given in table C1.

Table C1: Upper bounds N_u^- of level (1-β) confidence intervals for N^- (*).

a) Primary mice

Experiment	N_u^- (1-β)=99%	99.9%	99.99%	99.999
P1-1	149	214	275	344
P2-1	205	295	384	474
P3-1	262	376	490	604
P3-2	50	72	93	115
P3-3	67	96	125	154

(*) Test-based, Clopper-Pearson type, two-sided. The sampling fractions, i.e. the proportions of cells in the tumours whose DNA was analyzed for clonality, in the 5 experiments and used in the calculation were: s=3.48%, 2.54%, 2.0%, 10%, 7.6% (resp.).

b) Secondary mice 1 (*)

Experiment	N_u^- (1-β)=99%	99.9%	99.99%	99.999%
P1-1	191	274	357	440
P2-1	243	349	455	561
P3-1	273	392	510	629
P3-2	100	144	188	232
P3-3	74	107	139	172

(*)Sampling fractions: s=2.73%, 2.15%, 1.92%, 5.12%, 6.85% (resp.)

c) Secondary mice 2 (*)

Experiment	(1-β)=99%	N_u^- 99.9%	99.99%	99.999%
P1-1	167	239	312	385
P2-1	203	291	380	468
P3-1	114	163	213	262
P3-2	93	134	175	215
P3-3	138	198	259	319

(*)Sampling fractions: s=3.12%, 2.57%, 4.54%, 5.50%, 3.75% (resp.)

d) Secondary mouse 3 (*)

Experiment	(1-β)=99%	N_u^- 99.9%	99.99%	99.999%
P1-1	134	192	250	309

(*)Sampling fraction: s=3.87%

At the same time, the numbers given in table C1 may be viewed as upper bounds for the total number of clones contained in CNS (assuming the worst case that each of these clones consist of a single cell).

In contrast to CNS_i, CNS_i* (i=1,…, 3) was observable. In case of P1-1, e.g., CNS_1* contained 30 clones. The numbers given in table C1 impose upper limits to the (mean) size of clones in CNS_i*, which are obtained by dividing these by the number of clones in CNS_i*, yielding, e.g., at level 99.9% a mean size of about 7 in case of the primary mouse of P1-1. In other words, clones that were definitely present, but undetected were few and mostly extremely small.

Clone sizes within a tumour were very heterogeneous. Table C2 shows the estimated sizes (cell numbers) of the largest and smallest clones detected in S_1 as well as an upper bound for the smallest clone in CNS_1. For clones observed in S_1, the numbers were obtained by multiplying the clone size proportions in S_1 with the number of cells in T_1. For clones in CNS_1, the upper confidence bounds from table

C1 were used and divided by the minimum number of clones contained in CNS_1, viz. the number of clones in CNS_1*.

Table C2: Range of clone sizes in T_1 (estimated cell numbers).

	Cell number per clone		
Experiment	min (obs.)	max (obs.)	min (present, but non-obs.)(*)
P1-1	4,401	509,095	≤ 11
P2-1	10,566	1,013,328	≤ 20
P3-1	75,918	4,357,437	≤ 20
P3-2	20,885	1,946,043	≤ 2
P3-3	378	94,871	≤ 11

(*) Upper bounds based on level 99.999 confidence bounds of table C1. Since the minimum sizes multiplied with the number of clones must not exceed the values in table C1, the results were rounded off to the next lower number.

Heterogeneity of proliferation rates

Based on the minimum number of unobserved clones, a value of λ=5 (the rate of the process with time interval from transplantation to sampling rescaled to length 1) was obtained as an upper bound at the $(1\text{-}10^{-5})$ confidence level for each experiment. However, using the extreme-value distribution with the total number of clones being limited by the observed clones plus the values in table C1 (again at the $(1\text{-}10^{-5})$ confidence level), λ=5 was not compatible with the size of the largest clone T_1 ($p<10^{-8}$ based on the negative binomial distribution). Adding 1-confidence levels of the nuisance parameters (twice 10-5), the result remained highly significant (confidence interval p-value $<10^{-4}$) for each experiment.

With a time lag of 8 hours, the lowest growth rate λ incompatible with the undetected clones in CNS_1* (again at the $(1\text{-}10^{-5})$ confidence level) increased slightly to λ=7. Again, however, this was too low to accommodate the high observed clone sizes ($p<10^{-4}$ for each experiment after adjustment). Thus, the results are firm evidence for the heterogeneity of proliferation rates.

Changes in proliferation rates

As for changes of proliferation rates, the Model 2 applied to clones in $CNS_1^* \cap CS_2$ led to a rejection of the null hypothesis of constant proliferation rates, owing to the fact that clones in CNS_1^* were necessarily very small (see tables C1 and C2), while those in CS_2 were large. The nominal p-value, calculated as a confidence interval p-value, the true unknown clone size in T_1 (and thus also in T_2) being the nuisance parameter) was $<10^{-6}$ in each case and remained significant at the 0.001 level after adjustment for the multiplicity of tests.

Under Model 1, which implies a high variability of clone sizes, the analysis was more complex. Carrying out the procedure as described above, the upper bounds for the nominal p-values obtained for P1-1, P2-1, P3-1, P3-2 were 0.00033, 0.000056, 0.000034, and $3.8 \cdot 10^{-6}$, respectively. Except for P1-1 they remained significant at the α=0.05 level after adjusting for multiplicity and the use of confidence interval p-values. This was also true if a time-lag was introduced, as described above. Upper bounds for the p-values (derived from the simulations) did not exceed $1.2 \cdot 10^{-5}$, regardless of the growth rate, and again remained statistically significant after adjustment.

Analysis of seeding efficiency

As described above, the analysis of the heterogeneity of clones with respect to seeding efficiency focused on seeding efficiency in M2a. A statistical comparison between a lower bound for the seeding efficiency (in M2a) of clones in CNS1 versus an upper bound for the largest clone (largest with respect to T1) in CS1∩CNS2 was performed for the first 4 experiments. It yielded nominal p-values of p=1.0·10-4 in case of P1-1, and p<10-6 in case P2-1, P3-1, and P3-2, and thus remained significant (p< 10-2) after adjusting for the use of confidence interval p-values and multiplicity of testing. This demonstrates that transplanted clones were heterogeneous with respect to seeding efficiency in the secondary mice."

Appendix C references

222. Berger, R.L. and D.D. Boos, *P-Values Maximized over a Confidence Set for the Nuisance Parameter.* Journal of the American Statistical Association, 1994. **89**(427): p. 1012-1016.
223. Barnard, G.A., *Significance tests for 2 X 2 tables.* Biometrika, 1947. **34**(1-2): p. 123-38.
224. Berger, R.L., *More powerful tests from confidence interval p values.* American Statistician, 1996. **50**(4): p. 314-318.
225. Lin, C.Y. and M.C. Yang, *Improved p-Value Tests for Comparing Two Independent Binomial Proportions.* Communications in Statistics-Simulation and Computation, 2009. **38**(1): p. 78-91.
226. Baker, C.T., et al., *Modelling and analysis of time-lags in some basic patterns of cell proliferation.* J Math Biol, 1998. **37**(4): p. 341-71.
227. Banks, H.T. and W.C. Thompson, *Mathematical Models of Dividing Cell Populations: Application to CFSE Data.* Mathematical Modelling of Natural Phenomena, 2012. **7**(5): p. 24-52.

Publications and Conferences

Publications

Succession Of Transiently Active Tumour-Initiating Cell Clones in Human Pancreatic Cancer

Felix Oppel, Claudia R. Ball*, Taronish D. Dubash, Christopher M. Hoffmann, Ulrich Abel, Sebastian M. Dieter, Moritz Koch, Jürgen Weitz, Jens Werner, Frank Bergmann, Wilko Weichert, Manfred Schmidt, Christof von Kalle, Hanno Glimm*

In submission, 2013

* *These authors equally contributed to this work*

Stable Long-term Blood Formation by Stem Cells in Murine Steadystate Hematopoiesis

Oksana Zavidij, Claudia R. Ball,* Friederike Herbst, Felix Oppel, Sylvia Fessler, Manfred Schmidt, Christof von Kalle, and Hanno Glimm*

Stem Cells, 2012 Sep; 30(9):1961-70

* *These authors equally contributed to this work*

Oral Presentations

Succession Of Transiently Active TIC Clones Drives Long-term Human Pancreatic Cancer Progression

Felix Oppel, Claudia R. Ball, Christopher M. Hoffmann, Sebastian M. Dieter, Taronish Dubash, Moritz Koch, Jürgen Weitz, Frank Bergmann, Manfred Schmidt, Ulrich Abel, Christof von Kalle, Hanno Glimm

AACR 104th Annual Meeting 2013, April 2013, Washington D.C., USA

Clonal Composition of the Pancreatic Tumor Initiating Compartment

Felix Oppel, Claudia Ball, Christopher Hoffman, Sebastian Dieter, Jürgen Weitz, Frank Bergmann, Manfred Schmidt, Christof von Kalle, Hanno Glimm

DKFZ PhD Student Retreat 2011, July 2011, Weil der Stadt, Germany

Poster Presentations:

Human Long-Term Pancreatic Cancer Progression Is Driven By A Succession Of Transiently Active TIC Clones

Felix Oppel, Claudia R. Ball, Christopher M. Hoffmann, Sebastian M. Dieter, Taronish Dubash, Moritz Koch, Jürgen Weitz, Jens Werner, Frank Bergmann, Wilko Weichert, Manfred Schmidt, Ulrich Abel, Christof von Kalle, Hanno Glimm

Accepted for DGHO Jahrestagung, October 2013, Vienna, Austria

Manipulation of Tumor-Initiating Cells in Human Pancreatic Cancer

Felix Oppel, Claudia R. Ball, Christopher M. Hoffmann, Sebastian M. Dieter, Moritz Koch, Jürgen Weitz, Frank Bergmann, Manfred Schmidt, Christof von Kalle, Hanno Glimm

DKFZ PhD Student Poster Presentation 2011, December 2011, Heidelberg, Germany

Declaration of academic honesty

Hereby I declare that this thesis is my work and all other sources of information used have been cited or announced explicitly. Moreover, the content of this thesis has not been submitted previously to this or any other Faculty.

Hiermit erkläre ich, dass diese Arbeit von mir selbst verfasst wurde und dass alle Quellen und Hilfsmittel explizit kenntlich gemacht wurden. Diese Arbeit oder Bestandteile davon, wurden noch nicht im Rahmen einer Dissertation an dieser oder einer anderen Fakultät eingereicht.

Heidelberg, ……

Felix Oppel

Acknowledgements

Hereby I thank all people who have supported me and my thesis throughout the last four years.

First, I would like to express my deepest gratitude to my supervisors Prof. Dr. Hanno Glimm, Dr. Claudia Ball and Prof. Dr. Christof von Kalle for their excellent supervision, guidance through my project and for the lively discussions.

I thank Prof. Dr. Hanno Glimm for the opportunities to work on this exciting project and present my data to the international science community at high-ranking meetings. Dr. Hanno`s lab has provided an outstanding environment for scientific work with nearly unlimited possibilities to expand data and follow new ideas.

I acknowledge Dr. Claudia Ball for the correction and improvement of all my work throughout my time as a PhD student. I strongly appreciated her advice and ideas regarding my project, also in cases where we had different opinions.

I want to thank Prof. Dr. Christof von Kalle for his comments and advice as a TAC-member and the inspiring, motivating atmosphere in the G100 department, especially at the annual retreats.

Moreover, I thank Prof. Dr. Andreas Trumpp for being first referee of my thesis and supervising me as a TAC-member. His ideas substantially improved my work by unraveling weak points of my data and giving suggestions how to overcome them.

I further acknowledge Prof. Dr. Dirk Jäger for accepting to be my third TAC-member and the discussion along the TAC-committee-meetings.

I thank Prof. Dr. Elisabeth Schwarz and PD Dr. Suat Özbek for being examiners of my thesis defense. Thank you to PD Dr. Suat Özbek for chairing my examination-committee.

Thanks go to Prof. Dr. Dr. Ulrich Abel for his incomparable work using my data and the perfect cooperation, Dr. Frank Bergmann for the outstanding histopathology

analysis, and Prof. Dr. Jürgen Weitz, Prof. Dr. Moritz Koch and Prof. Dr. Jens Werner for providing primary tumor material.

I also thank Galina Dornhof, Sabrina Hettinger, Stefanie Wenzel, Annika Mengering and Sylvia Fessler for their excellent work on my project. Thank you to Sebastian Dieter and Christopher Hoffmann for their help at the beginning of my work that was crucial for my technical and scientific development within my thesis project.

At the end of this thesis my thank you also goes to Silke Hamsoui-Nord, Martin Friedel and the entire IVC-crew for the outstanding work on my experimental mice. I thank Felix Bestvater and Manuela Brom for their help with all imaging tasks and the team of the Core Facility for Genomics and Proteomics for their work.

Thanks go to AG Schmidt, AG Zenz, AG Ungerechts and AG Fröhling for all advice and project discussions at scientific presentations.

A special thank you goes to Eva-Maria Hartinger for the great atmosphere and the fun time we shared throughout our PhD thesis time. You have been an important support when going through hard times.

Thank you also Taro, Bela, Shayda, Tati, Klara, Fee, Oksana, Jenny, Alex (Alles Ex), Caro, Chris and Annika for all the joking and the amusing time that made hard work easier. I acknowledge the “Colon-People” for deep analysis.

I thank Marge and Seth very much for their help. Moreover, loving thanks go to Solvejg Raabe for her continuous help and emotional assistance that strongly supported my work as a PhD student.

Finally, I especially thank my parents Irene and Falk Oppel for their never ending love and support throughout my life, this thesis and my previous studies.